INFORMATION TO USERS

This manuscript has been reproduced from the microfilm master. UMI films the text directly from the original or copy submitted. Thus, some thesis and dissertation copies are in typewriter face, while others may be from any type of computer printer.

The quality of this reproduction is dependent upon the quality of the copy submitted. Broken or indistinct print, colored or poor quality illustrations and photographs, print bleedthrough, substandard margins, and improper alignment can adversely affect reproduction.

In the unlikely event that the author did not send UMI a complete manuscript and there are missing pages, these will be noted. Also, if unauthorized copyright material had to be removed, a note will indicate the deletion.

Oversize materials (e.g., maps, drawings, charts) are reproduced by sectioning the original, beginning at the upper left-hand corner and continuing from left to right in equal sections with small overlaps. Each original is also photographed in one exposure and is included in reduced form at the back of the book.

Photographs included in the original manuscript have been reproduced xerographically in this copy. Higher quality 6" x 9" black and white photographic prints are available for any photographs or illustrations appearing in this copy for an additional charge. Contact UMI directly to order.

UMI

AN INVESTIGATION OF CUSP LATITUDE MAGNETOSPHERE-IONOSPHERE PHYSICS: A TIME SERIES ANALYSIS APPROACH

A

THESIS

Presented to the Faculty

of the University of Alaska Fairbanks

in Partial Fulfillment of the Requirements

for the Degree of

DOCTOR OF PHILOSOPHY

By

Curt A. L. Szuberla, B.S.

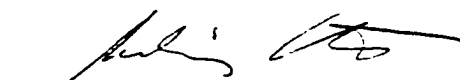Fairbanks, Alaska

December 1997

UMI Number: 9816412

UMI
300 North Zeeb Road
Ann Arbor, MI 48103

AN INVESTIGATION OF CUSP LATITUDE
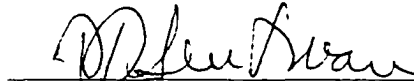# MAGNETOSPHERE-IONOSPHERE PHYSICS: A TIME SERIES ANALYSIS
APPROACH

By

Curt A. L. Szuberla

RECOMMENDED:

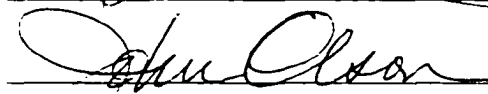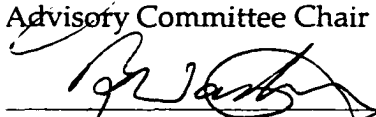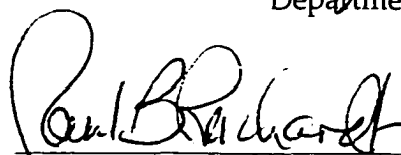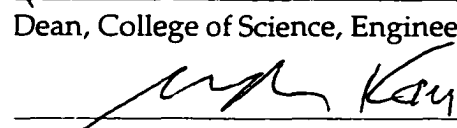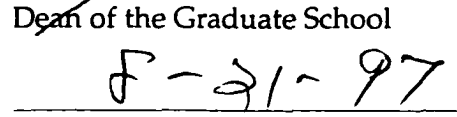Advisory Committee Chair

Department Head

APPROVED:

Dean, College of Science, Engineering and Mathematics

Dean of the Graduate School

$f - 3/ - 97$

Date

Abstract

The shocked solar wind plasma of the magnetosheath has direct access to the Earth's high-latitude ionosphere and upper atmosphere only through the magnetospheric cusps. The interaction of solar and terrestrial plasmas and fields in these regions has made them an obvious choice for the study of coupling processes in the geospace environment. Some of the information regarding these processes is manifest in the transmission and generation of wave energy, a portion of which can be detected by ground-based magnetometers. In the present day, records of the magnetic field are stored in a digital format; therefore, some form of signal processing is required to extract meaningful physical information from them. This thesis is aimed at the physical characterization of the cusp region through the careful application of digital time series analysis techniques to ground-based magnetometer records. It is demonstrated that judicious application of signal processing techniques can yield new, physically meaningful results from ground-based magnetometer records, and aid in the understanding of disparate reports from groups using different analysis techniques on like data.

Characterization of the cusp region is couched in terms of three specific, open problems of the physics of magnetic perturbations in the cusp: 1) the coherence of localized pulsations, 2) the spatiotemporal nature of the cusp magnetic spectrum, and 3) the ground-based magnetic determination of the separatrix. The first problem is addressed by assuming that localized pulsations are coherent only over some finite spatial extent. A statistical measure of interstation coherence is developed to estimate an upper bound of $\mathcal{O}(200 \text{ km})$ for the coherence length of this class of pulsations. The second problem is addressed by examining the ultra low frequency polarization spectrum. An information theoretic measure is established as a quantitative means of discriminating the spatial passage of the cusp by ground-based magnetic means. This procedure replaces previous determinations which were made "by-eye." Finally, separatrix identification is addressed by applying the statistical interstation coherence measure to pulsations presumably representative of a magnetic field line resonance. The analysis indicates that a determination is not possible to a resolution better than $\mathcal{O}(300 \text{ km})$.

Contents

iv

.i

λ

List of Figures

List of Tables

Acknowledgements

I wish to thank Colonel Raymond Winkel, of the United States Military Academy, for first sparking within me the curiosity of a physicist. To my thesis advisor, Professor John Olson, I am deeply indebted for rekindling that flame, years after I thought it had burnt out. In the time we have worked together, John has proved himself a rare combination of mentor, colleague and friend. Without his patient guidance, this work would never have come to fruition. I thank John for granting me license to come to know space physics on my own terms, even when my path diverged from the well-worn track. Our discussions concerning all areas of physics, fly fishing and fountain pens made my work both profitable and enjoyable.

I thank the members of my advisory committee for their unique contributions to my development as a physicist. My research greatly benefited from their combined, encyclopedic knowledge of physics. Professor Channon Price re-taught me virtually all of classical physics; his example in the classroom is one I hope to emulate. Professor Davis Sentman, without knowing it, taught me the value of persistence in following my intuition regarding the data. To Professors Antonius Otto and Hans Stenbaek-Nielsen I owe a special thanks for agreeing to serve on my committee rather late in the game.

Professors Mark Engebretson and Brian Fraser deserve special thanks for the numerous discussions we have had at various meetings. I greatly appreciate that they have treated me as a colleague during my apprenticeship. Mark made a significant contribution to this thesis by graciously opening the doors of his facilities at Augsburg College while he was working abroad; his data comprise the bulk of that which I examine herein.

I am grateful for the many friendships I have made during the course of my thesis research, especially that of my officemates Don Hampton and Peter Delamere. In the same breath, I thank the greater Szuberla and Johnson families (as well as all subsidiary

branches) for their concern, support, encouragement and interest. For countless hours spent discussing physics, computers and/or zymurgy, I also thank Dean Prichard, Geoff McHarg, John Williams, Tom Immel, Matt Heavner and Laura Peticolas. Jen Simmons, Carolyn Talus and Anne Ruggles offered a view of life and fulfillment outside physics, one that surely helped me maintain some semblance of sanity. Nettie La Belle-Hamer, Jim Conner and Gerard Fasel, some of the "old ones," merit comment as they helped talk me into entering graduate school in the first place. Among the Geophysical Institute staff, I thank Dave Covey and Anne Trent for their service with a smile, always above and beyond the call of duty. My canine friends deserve more than a passing mention, of course. For patiently sleeping by my feet — while I typed away into the small hours of the morning — I thank Cosmos; a more loyal companion I could not hope to find. Wrangell and Adirondac helped me keep my perspective and kept me running during the course of this work.

Finally, I thank my best friend, Alice, for seeing me through this endeavor. It was with her encouragement that I undertook the effort; without her unflagging support I could never have completed it. When I found myself struggling, she saw within me not only the desire to pursue physics, but the ability to realize my dreams. Would that I were able to fully express the gratitude and love I feel toward her. I owe her a debt that will take a lifetime to repay; fortunately, we have that time ahead of us together.

When the Lady smiles she holds me in Her hand;
  as a matter of fact, She can always let me down.
But, when the Lady smiles I cannot resist Her call;
  as a matter of fact, I do not resist at all.
Because I am walking on clouds She is leading with.
— Barry Hay & George Koomans, 1984

Chapter 1

Introduction

A topological consequence of the interaction of the solar wind with the Earth's dipolar magnetic field is the existence of the polar magnetic cusps. These features are important to space physics research because they represent a portal through which solar wind plasma may eventually pass. Some of the plasma ejected from the Sun impinges upon the Earth's magnetic field, forming a standing bow shock in the solar wind. The region of shocked solar wind plasma that forms between the bow shock and the magnetosphere is known as the magnetosheath. Magnetosheath plasma has direct access to the high-latitude ionosphere and upper atmosphere only through the cusps. The interaction of solar and terrestrial plasmas, as well as the transmission and generation of wave energy, in the vicinity of the cusps has made them an obvious choice for the study of coupling processes in the solar wind-magnetosphere-ionosphere system.

Each cusp is bounded above by the magnetosheath and below by the high-latitude ionosphere. The "sides" of the cusps are enveloped by the low-latitude boundary layer (LLBL) and the plasma mantle. Both of these latter boundary regions are important because they lie along the magnetopause, the demarcation between the shocked solar wind of the magnetosheath and the Earth's magnetospheric cavity. Processes which occur here — in the solar wind, magnetosheath, LLBL, mantle and along the magnetopause — all convey information down the throat of the cusp to ionospheric heights.

Information transmitted from the varied regions associated with the cusp typically manifests itself in the high-latitude ionosphere as either precipitating particles or ultra

1

low frequency (ULF) wave phenomena. A ground-based magnetometer at high latitude is capable of receiving this information via the magnetic perturbations caused by either of these manifestations. In the present day, records of the magnetic field are stored in a digital format; therefore, some form of signal processing is required to extract meaningful physical information from them. This thesis is aimed at the physical characterization of the cusp region through the careful application of digital time series analysis techniques to ground-based magnetometer records.

1.1   ULF studies of the cusp: A historical perspective

The existence of the magnetospheric cusps was first postulated by *Chapman and Ferraro* [1931], although at the time they used the term "horns." The solar wind was then unknown, but they reasoned that the sun might occasionally eject a quasi-neutral stream of charged particles (what we term a plasma today). They modeled this stream as a planar front impinging upon the dipolar magnetic field of the Earth, simplifying the former to be a perfectly conducting plane. In this simple geometry, the method of images was used to deduce the existence of two magnetic horns (null points) across which solar wind plasma would have access to the region dominated by the Earth's magnetic field. In this manner *Chapman and Ferraro* [1931] were the first to show that the solar wind confines the Earth's dipole field, implicitly giving rise to the concept of the magnetosphere [*Smith and Lockwood*, 1996].

The horns of *Chapman and Ferraro* [1931] eventually became known as the magnetospheric cusps. Some four decades later, satellite observations made by *Heikkila and Winningham* [1971] and *Frank* [1971] gave the first direct evidence for the existence of the cusps. *Heikkila and Winningham* [1971] found that the shocked solar wind plasma of the magnetosheath had unimpeded access to the cusp regions, well inside the magnetopause. Although the simple geometry of *Chapman and Ferraro* [1931] indicated the existence of two singular points of plasma entry, it was soon found that particles had access across much broader regions. When both linear and funnel-shaped access were observed (see the review by *Smith and Lockwood* [1996]), the concept (and jargon) of the cusp became somewhat confusing. The linear region of plasma entry across the magnetopause is termed the

cleft, whereas the funnel-shaped region is called the cusp proper. Today the term cleft has fallen into disuse, although some investigators still use the term cusp/cleft when referring to the cusp region. In Figure 1.1 we present a cartoon representation of various dayside magnetospheric regions as they might be seen in a noon-midnight meridional slice.

Today the standard definition of high-latitude magnetospheric regions, including the cusp and boundary regions, stems from the statistical work of *Newell and Meng* [1988, 1992]. They made a survey of roughly 60,000 passes of the low-altitude Defense Meteorological Satellite Program (DMSP) satellites and arrived at operational definitions for the various regions based on statistical particle precipitation patterns. They then mapped these regions to the ionosphere; a summary of this work is shown in Figure 1.2. As *Newell and Meng* [1992] state, "[Figure 1.2] is less than reality, but more than a cartoon." Their work in defining these regions has been confirmed by other workers using Viking data [*Lundin*, 1988; *Aparicio et al.*, 1991], and recent high-altitude data from POLAR further confirms their statistical picture [*Zhou and Russell*, 1997; *Zhou et al.*, 1997].

Throughout this work, we refer to high-latitude magnetospheric regions variously as the cusp and boundary regions. We take these terms to be consistent with those shown in Figures 1.1 and 1.2 as the low-latitude boundary layer, mantle and cusp. The former two border the latter on the equatorward and poleward edges, respectively. We typically refer to the cusp and boundary regions as a single unit; however, when we reference one in isolation, the distinction is made clear.

One cannot get far through the current literature of geomagnetic pulsations without encountering the Pc/Pi terminology; this was not always the case. Prior to the work of *Jacobs et al.* [1964] pulsations were given ad hoc names by the investigator discovering them (e.g., whistlers, pearls, ipcl or ipdp). As the satellite era began in earnest, the catalog of observed pulsation types was growing steadily. Lacking a recognized standard, an international committee was formed and *Jacobs et al.* [1964] produced the currently accepted classification system; Table 1.1 summarizes this work. Pulsations were termed either continuous (Pc) or irregular (Pi)[1], with a number designator depending upon the frequency

---

[1]Not all authors agree on what constitutes a continuous or irregular pulsation. Event-oriented researchers tend to make the distinction between Pc and Pi more frequently [e.g., *Engebretson et al.*, 1990]. We generally prefer not to select individual events from the data, thus we use the term Pc broadly to mean any pulsations within the frequency range indicated.
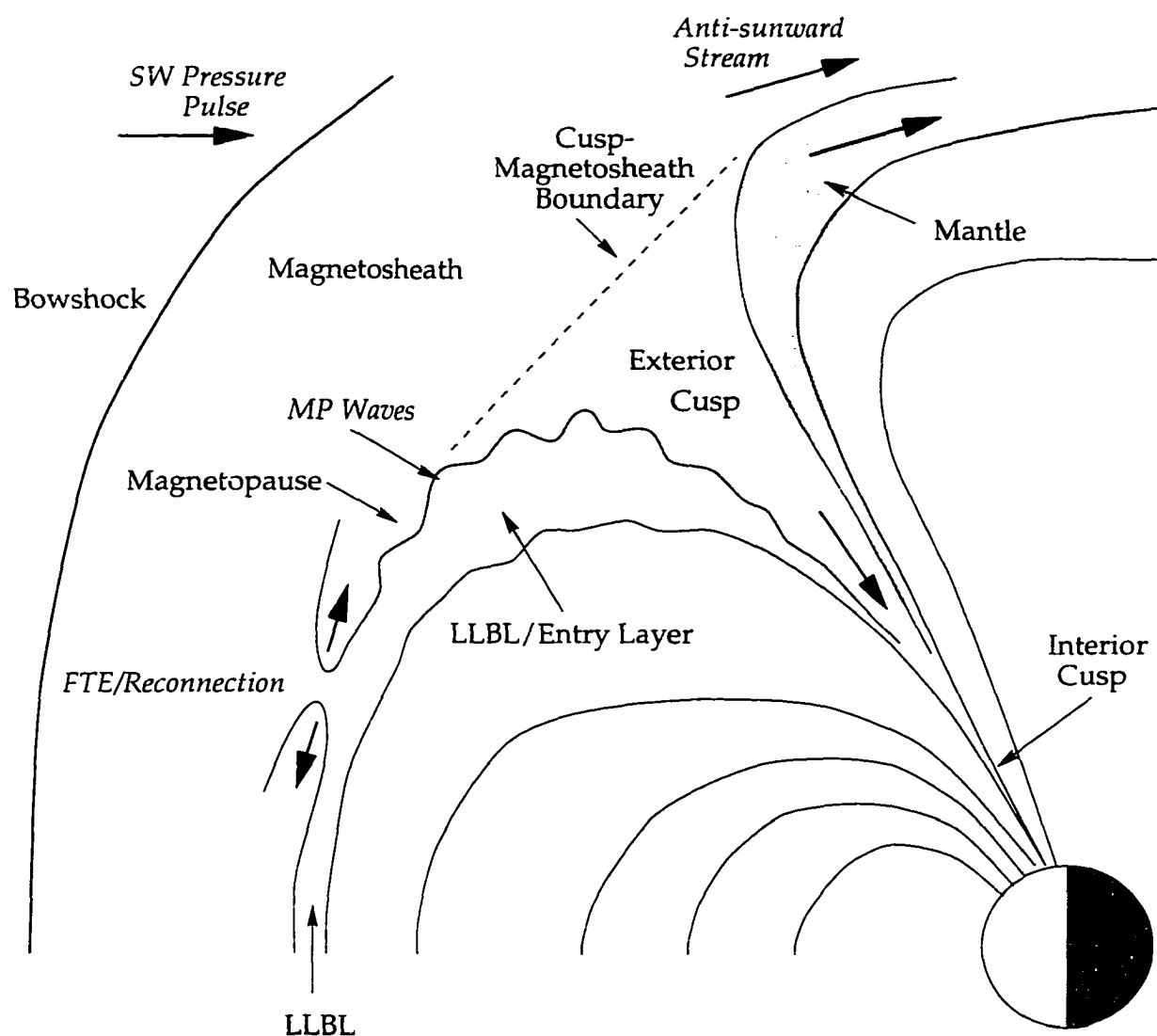
Figure 1.1. Cartoon meridional view of the salient features of the boreal magnetospheric cusp and boundary regions. Shown in the figure (adapted from *Glassmeier* [1989]) are the major plasma flows (bold arrows) and processes (italics) thought to take place in the cusp and boundary regions. Waves may be generated at the equatorward face of the magnetopause by several processes, including: reconnection-driven flux transfer events (FTE), solar wind pressure pulses buffeting the magnetopause, or the anti-sunward streaming of magnetosheath plasma giving rise to the Kelvin-Helmholtz instability.
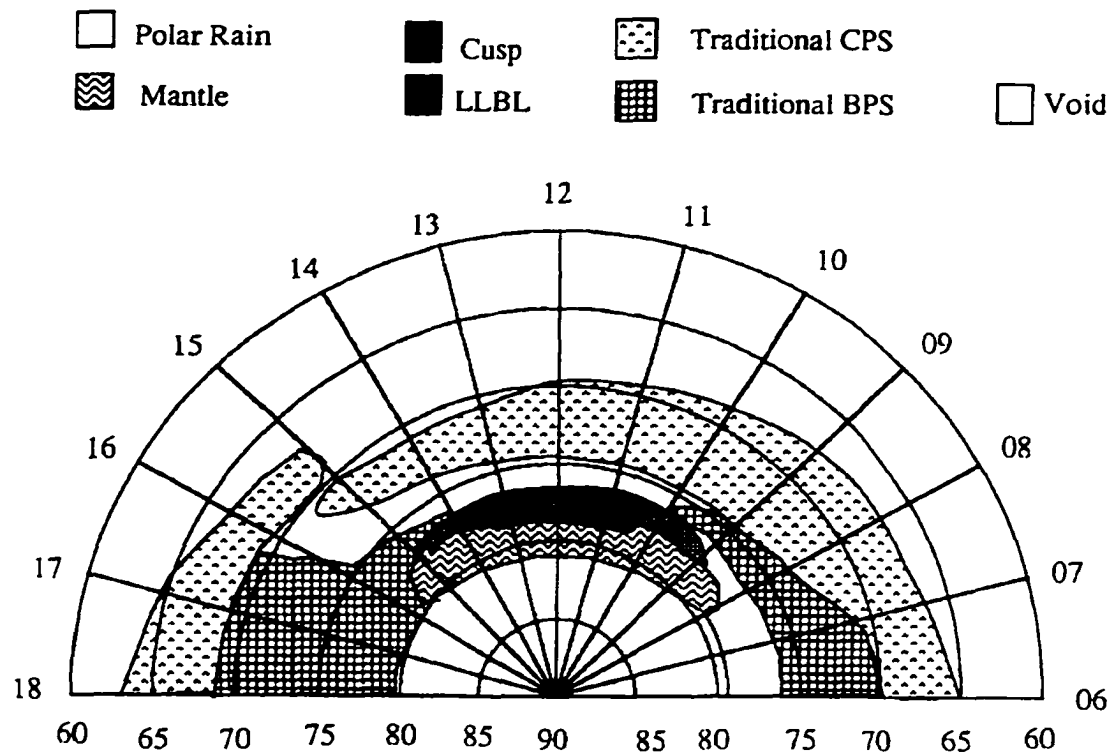
Figure 1.2. Statistical mapping of high-latitude particle precipitation regions to the iono-sphere. *Newell and Meng* [1992] generated this map using particle data from ~60,000 passes of the DMSP satellites. Note the latitudinal extent of the cusp and boundary regions, as well as their spread in local time.

band of each type. The system is in wide use today, although the exact frequency bands are sometimes modified for convenience.

In the remainder of this section, we present a brief review of observational and theoretical work germane to ground-based magnetic signals received at cusp latitude stations.[2] This review serves to outline the historical development of our present understanding of the magnetic observations associated with the cusp and boundary regions. We leave the discussion of more recent theoretical and observational work for the chapters that follow. We conclude this section by noting a few of the outstanding problems in cusp latitude

---

[2]For additional references concerning observational and theoretical treatments of the sources of ULF pulsations in the cusp, boundary regions and magnetosheath, see the reviews by *Hughes* [1994], *Sibeck* [1994], *Schwartz et al.* [1996] and *Smith and Lockwood* [1996].

Class	Period (s)	Frequency (mHz)
Pc 1	0.2 – 5	5000 – 200
Pc 2	5 – 10	200 – 100
Pc 3	10 – 45	100 – 22
Pc 4	45 – 150	22 – 6.7
Pc 5	150 – 600	6.7 – 1.7
Pi 1	1 – 40	1000 – 25
Pi 2	40 – 150	25 – 6.7

Table 1.1. ULF pulsation classification by frequency band.

research, problems which this thesis addresses.

1.1.1 Ground-based magnetic observations at cusp latitudes

The study of geomagnetic pulsations as a discipline began with the first reported observation of a ULF wave by *Stewart* [1861]. Although observations have continued through to the present day, we omit the observations prior to the Pc 5 observations of *Samson et al.* [1971]. These observations of the latitudinal and local time variation of polarization at high latitude led to perhaps the first genuine physical understanding of a class of ULF pulsations. The observations of *Samson et al.* [1971] were explained in terms of the magnetic field line resonance and the Kelvin-Helmholtz instability occurring at the magnetopause (see Section 1.1.2).

Olson and Rostoker [1978] later reported further evidence of the Kelvin-Helmholtz instability related to Pc 5 pulsations at a pair of cusp latitude stations. The observations of *Olson* [1989] showed a sense of poleward propagation of Pc 5 wave packets across the two sites. *Friis-Christensen et al.* [1988] and *Glassmeier et al.* [1989] gave further evidence of traveling Pc 5 signatures, this time across a large chain of magnetometers. This form of wave-packet, lasting only one or two cycles at a single station, has been shown to be related to a large scale, $\mathcal{O}(1000 \text{ km})$ horizontally, ionospheric vortical disturbance, the traveling convection vortex (TCV).

In separate work using a meridional chain of magnetometers in the then Soviet Union,

j

Troitskaya and Bol'shakova [1977] derived a method of locating the nominal cusp latitude via irregular, long-period pulsations (ipcl in her nomenclature, Pc 5 in current parlance). They found the cusp location to be $\lambda \in [77°, 83°]$, where λ is the geomagnetic latitude. If we consider that they may have actually been locating the broader expanse of the cusp and boundary regions, their ground-based results completely agree with the satellite-based statistical mapping of *Newell and Meng* [1992]. Continued observations across their array led *Bol'shakova and Troitskaya* [1984] and *Troitskaya* [1985] to suggest that it might be possible to track the cusp in local time via the character of Pc 3 pulsations at a single station.

With the advent of the computer age and digital recording techniques, inspection of individual time series gave way gradually to spectral analysis of magnetometer records. Investigators found that the cusp spectrum was quite variable, although repeatable features were commonly observed uniform in both the Pc 3 and Pc 5 frequency bands. Several workers have focused on observations of the cusp spectrum [e.g., *Troitskaya*, 1985; *Kato et al.*, 1985; *Olson*, 1986; *Engebretson et al.*, 1986]; others on the likely source mechanisms [e.g., *Tonegawa et al.*, 1985; *Engebretson et al.*, 1987]. They have all shown that the cusp ULF spectrum is composed of a broadband background of wave energy which has embedded within it short-lived wave packets. The wave packets are typically narrowband features that exhibit spatiotemporal correlation between nearby and conjugate stations; the broadband Pc 3 pulsations exhibit little interstation coherence or correlation, either in the local or conjugate sense [*Engebretson et al.*, 1990; *Olson and Fraser*, 1994].

The reviews of Pc 3 pulsations given by *Odera* [1986] and *Yumoto* [1986] summarize the solar wind control of Pc 3 detected on the ground. There are two chief correlations between solar wind and Pc 3 parameters, each first established by *Troitskaya et al.* [1971] in the former Soviet Union, and first confirmed in the west by *Greenstadt and Olson* [1977]. First is the magnitude of the solar wind magnetic field and the frequency of Pc 3 pulsations observed at the cusp, $f \, (\text{mHz}) \approx 5.6 \, B_{IMF} \, (\text{nT})$. Second is dependence of Pc 3 occurrence on the interplanetary magnetic field cone angle: as the bow shock becomes quasi-parallel Pc 3 power increases, while for the quasi-perpendicular shock Pc 3 power is minimized. *Engebretson et al.* [1986, 1989] noted correlations with observations taken near the austral polar cusp and upstream in the solar wind, deducing that the wave energy generated in the Earth's foreshock may be the source of Pc 3 observed on the ground. The recent refine-

ments to correlations between upstream (in the ion foreshock) wave frequency and solar wind parameters of *Le and Russell* [1996] are consistent with the ground-based correlations.

1.1.2 Cusp region electrodynamics

The first physical understanding of the source of ULF magnetic pulsations came about as an indirect result of the work of *Storey* [1953] in explaining the dispersion characteristics of whistlers. He showed that the waves were guided between the hemispheres along the geomagnetic field lines, which accounted for the observed dispersion. This led *Dungey* [1954] to his theory of magnetic field line resonances (FLR) [*Hughes*, 1994], in which the hydromagnetic wave equations for the field lines at each latitude decouple. In essence, each magnetic field line is free to oscillate at its own particular set of frequencies. The complete set of oscillatory modes in the magnetosphere make up a continuum of FLR frequencies. Early observations of the FLR continuum came from high latitudes, with pulsations in the Pc 5 range [e.g. *Jacobs*, 1970, sec. 2.4]. At mid-latitude, *Orr and Matthew* [1971] successfully predicted the dependence of FLR frequency on L-shell[3] in the Pc 3 range. Convincing satellite evidence of the FLR continuum in the magnetosphere, including higher order harmonics, was seen in the ATS 6 satellite magnetometer data reported by *Takahashi and McPherron* [1982].

An observation of *Samson et al.* [1971] led theorists to refine the original work of *Dungey* [1954] and to develop what is now the accepted physical explanation of the FLR. *Samson et al.* [1971] found that the polarization, or sense of ellipticity [e.g., *Fowler et al.*, 1967], of the high-latitude FLR changed sense as a function of both L-shell and local time. *Chen and Hasegawa* [1974a,b] and *Southwood* [1974] each separately advanced a theory which invoked the Kelvin-Helmholtz instability along the magnetopause, caused by the anti-sunward streaming of the magnetosheath. Essentially, the Kelvin-Helmholtz surface wave is excited at a frequency such that it couples strongly to the FLR. Dissipation via joule heating at the ionospheric ends of the FLR is required for the coupling, which then accounts for the observed changes in polarization.

An offshoot of Dungey's theory of the FLR is that the entire magnetospheric cavity may oscillate as a unit. *Kivelson et al.* [1984] were the first to show that such cavity modes

---

[3]The *McIlwain* [1961] L-shell is related to the magnetic latitude λ by: $L = \cos^{-2} \lambda$.

existed in the magnetic pulsation record and developed the model. For ground-based magnetometers the cavity modes will exhibit a different characteristic signature than the continuum FLR. The cavity mode frequency is not a function of latitude, whereas the fundamental mode of the FLR will exhibit a frequency dependence on L-shell. It was *Samson et al.* [1971] who gave the first evidence that these two modes couple at latitudes where the cavity mode frequency matches the FLR frequency fundamental mode. Two decades later, *Samson et al.* [1991] gave an alternative description of the cavity modes using a WKB approximation. Their work showed that cavity mode was likely only to exist in the Pc 5 frequency range, which would couple with the FLR mode at cusp latitudes. Theory regarding the FLR and cavity modes serve as an exemplar in the field of ULF magnetic pulsation research; they represent one of the few phenomena that are well understood. Unfortunately, these modes contribute only a fraction of the information content in the cusp spectrum.

Dungey's work in developing the FLR concept was of paramount interest to pulsation workers attempting to explain cusp latitude magnetic observations in the Pc 5 frequency band. Of broader importance however, was his development of the initial theory of magnetic merging, or reconnection [*Dungey*, 1958, 1961]. This work led *Russell and Elphic* [1978] to examine ISEE 2 satellite magnetometer data, whereupon they found a characteristic bipolar signature (presumably owing to reconnection) in the component of the magnetic field normal to the magnetopause. They termed this signature a "flux transfer event" (FTE), now widely considered a major mechanism for the transport of information (wave energy) and momentum (particles) across the magnetopause into the magnetosphere. The reconnection/FTE concept is not universally embraced, however. *Sibeck* [1990, 1992] and *Heikkila* [1997] have found both observational and theoretical evidence that presumed FTE signatures are actually mistaken characteristics of other processes, notably solar wind pressure pulses. It is quite likely that a combination of mechanisms is at play along the magnetopause, giving rise to the rich variety of pulsations received on the ground [e.g., *Yagodkina and Vorobjev*, 1997].

Magnetic pulsations in the magnetosphere must pass through the ionosphere before they can be observed at the ground. The problem of ionospheric transmission was first studied analytically by *Field and Greifinger* [1965] and *Greifinger and Greifinger* [1973] for short-period (Pc 1) pulsations, where they found that the ionosphere acted as a waveguide.
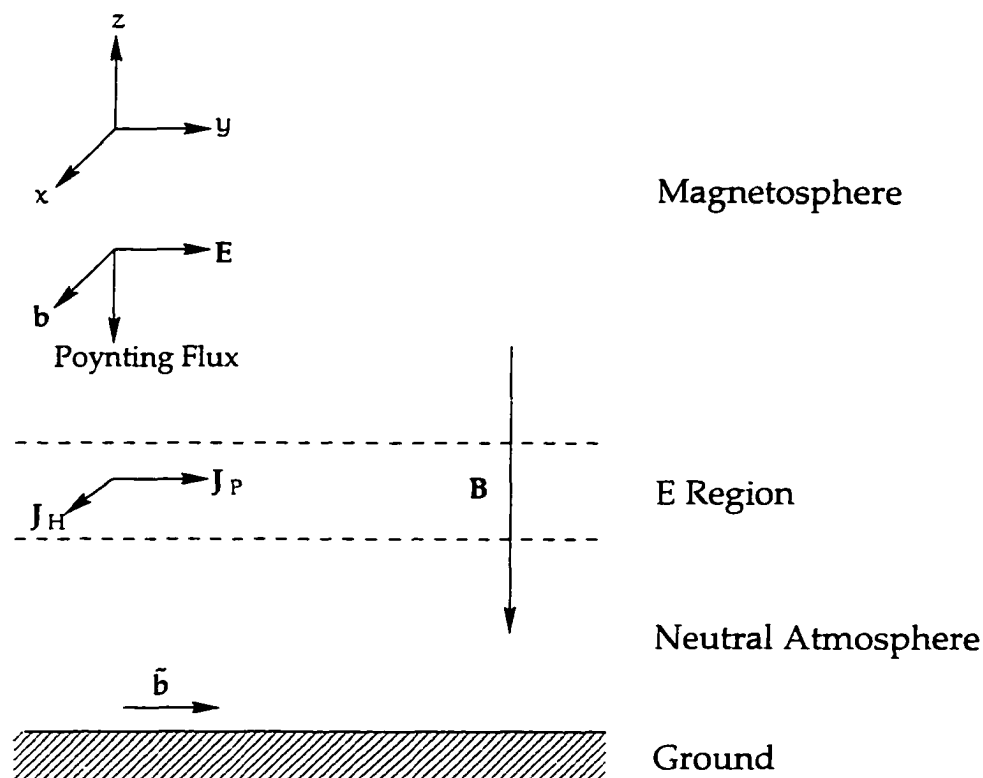
Figure 1.3. Cartoon of the ionospheric rotation of ULF waves. *Hughes* [1974] developed this scenario modeling a horizontally uniform ionosphere. An incident ULF wave generates Hall J_H and Pedersen J_P currents in the ionosphere. As a result, the magnetic perturbation **b** is effectively canceled out by the magnetic perturbation associated with J_P. What we observe on the ground is $\tilde{b}$, the result of J_H. Thus the ionosphere serves to rotate signals on the ground through 90°; this rotation occurs in the opposite sense in the southern hemisphere.

The scale size of the ionosphere is such that it is not an effective waveguide for long-period (Pc 5) pulsations. The transmission of long-period pulsations was qualitatively explained by *Nishida* [1964] and *Inoue* [1973] as an ionospheric rotation of the pulsations between the magnetosphere and the ground. In the course of his doctoral research, *Hughes* [1974] developed a theoretical treatment of this effect. Under the simple assumption of a horizontally uniform ionosphere, he showed that the magnetic perturbation of an incident magnetospheric ULF wave is rotated 90° by the ionosphere (see Figure 1.3). Effectively, the ionospheric Pedersen currents shield the ground-based observer; only the Hall currents transmit the magnetic disturbance. Extending the work of *Hughes* [1974], *Glassmeier* [1983,

1984] showed that horizontal conductivity gradients in the ionosphere were important and allowed both the effects of the Hall and Pedersen currents to be observed at a ground station.

Dungey [1963] argued heuristically that the magnetic perturbation of a current vertically incident on the upper ionosphere is completely shielded from the ground. *Fukushima* [1976] later developed a generalized theorem for currents with oblique incidence; thus, according to the Maxwell equations, only the component of the current with $(\nabla \times \mathbf{b})_z = 0$ is observed on the ground. *Hughes and Southwood* [1976] extended this concept to make a determination of the screening effect of the ionosphere in terms of the horizontal extent of a magnetic disturbance. They found that perturbations with a scale size $\lesssim 50$ km would be strongly attenuated at a ground station. As in the case of ionospheric rotation, *Glassmeier* [1984] showed that this screening effect was mitigated by horizontal conductivity gradients in the ionosphere. For the ground-based magnetic observer, these theoretical results are important considerations when proposing the deployment of a magnetometer array.

Another major source of wave energy lies along the boundary between the shocked solar wind and the magnetosphere. Since the magnetosheath plasma must flow past the obstacle of the magnetopause, it stands to reason that the interface should be susceptible to the Kelvin-Helmholtz instability (see Figure 1.1). In the incompressible limit, *Chandrasekhar* [1961] showed that the Kelvin-Helmholtz instability can lead to growth in a magnetofluid even for arbitrarily small velocity gradients. *Southwood* [1968], and later *Lee et al.* [1981], developed the theory of the instability along magnetopause and found it satisfied when

$$\mu_0 \rho_s \rho_p \left(\mathbf{V} \cdot \mathbf{k}_t\right)^2 > \left(\rho_s + \rho_p\right) \left(\left(\mathbf{B}_s \cdot \mathbf{k}_t\right)^2 + \left(\mathbf{B}_p \cdot \mathbf{k}_t\right)^2\right) \tag{1.1}$$

where the subscript "s" indicates the magnetosheath and "p" the magnetopause for the magnetic field $\mathbf{B}$ and density ρ; $\mathbf{k}_t$ is the tangential wavevector and $\mathbf{V}$ is the velocity of the magnetosheath relative to the magnetopause; μ_0 is the permittivity of free space. From this instability criterion, we can see that it is satisfied under three general conditions: 1) the waves move parallel to the magnetosheath flow, 2) the magnetosheath and magnetopause densities are both large, and 3) the waves move perpendicular to both the magnetosheath and magnetopause magnetic field. These criteria are most easily satisfied on the magnetospheric flanks, leading to surface wave generation along the magnetopause [*Sibeck*, 1994].

Correlating ground-based magnetic Pc 3-4 pulsations with solar wind velocity, *Greenstadt et al.* [1979] found a velocity threshold consistent with (1.1). *Lee et al.* [1981] showed that the LLBL is particularly unstable, and that Kelvin-Helmholtz waves induced there should switch polarity around local noon, explaining the high-latitude observations of *Samson et al.* [1971] and *Olson and Rostoker* [1978].

1.1.3 Outstanding problems

The Geospace Environment Modeling (GEM) effort of the National Science Foundation terminated its boundary layer campaign at the 1997 GEM Workshops. This decision was a programmatic one (owing to the vagaries of funding), not a scientific one. Although the past three decades have shown a great deal of progress in ascertaining the physics of the cusp, a great number of issues remain unresolved. Of the many open problems concerning the physics of the cusp and boundary regions, we find three that pertain generally to magnetic observations. The first concerns the scale size of localized pulsations; the second, the spatiotemporal nature of the cusp magnetic spectrum; and the third, the ground-based determination of the separatrix.

The work of *Engebretson et al.* [1990] provided the first conclusive evidence of a localized, ionospheric source of magnetic pulsations at cusp latitudes. His work left open the question of what scale size the ionospheric source regions occupy. *Olson and Szuberla* [1997] examined magnetometer records taken simultaneously at two stations to develop a preliminary determination of the coherence length of such pulsations. We greatly extend this study with an examination of station pairs of variable separation, in both hemispheres.

Yamauchi [1997] reported from the 1996 European Geophysical Society Alfvén Conference that spatial identifications of the cusp and boundary regions at low-altitude bore an ambiguous relationship to high-altitude regions. A panel discussion at the conference left the issue as an open topic warranting further research. In this light, the work of *Engebretson et al.* [1995] and *McHarg et al.* [1995] sparked a debate over the spatiotemporal nature of the cusp latitude spectrum. The former group argued that the events they recorded across the MACCS array were temporal in nature, while the latter reported that the cusp spectrum seen at Longyearbyen appeared to indicate spatial information, ie., the passage of certain regions nearby the magnetometer station. We examine both data sets in order to resolve

this issue.

A major goal of the GEM boundary layer campaign has been to identify the separatrix between open and and closed field lines. The dominant identification process rests with synoptic maps of DMSP polar over-flights and empirically derived Assimilative Mapping of Ionospheric Electrodynamics (AMIE) circulation patterns [*Lyons et al.*, 1996, also talks given at the 1995–1997 GEM Workshops]. At best, these separatrix identifications are unreliable; the question is clearly not yet resolved. An investigation of pulsations in the Pc 5 frequency range (those possibly associated with resonances of closed field lines at high-latitude) allows us to comment on the reliability of any ground-based magnetic determination of the separatrix.

1.2 Purpose

The principle aim of this thesis can be phrased as a single question: *How well can the cusp region be characterized through the analysis of ground-based magnetometer records?*

To achieve this characterization, we consider separately pulsations which are thought to have local source mechanisms and those which are thought to be indicative of particular regions associated with the cusp. At each stage, we reconcile the results of our time series analysis with physical processes that may take place anywhere between the distant magnetopause and the local ionosphere. An overview of this effort is given in Section 1.4.

1.3 Instrumentation

In this thesis we make use of ground magnetometer data taken in both hemispheres (see Figures 1.4 through 1.5). In the northern hemisphere, we have analyzed data from five of the nine Magnetometer Array for Cusp and Cleft Studies (MACCS) stations; two of the five University of Alaska (UA) pulsation stations; and the single station, Nordlysstasjonen, near Longyearbyen (LY) in the Norwegian Svalbard archipelago. In the southern hemisphere, we have analyzed data from two of the five Australian National Antarctic Research Expeditions (ANARE) stations. All of these stations are geomagnetically situated such that they span the statistical latitudinal extent of the cusp and boundary regions.

	Geographic		Geomagnetic			
	Latitude	Longitude	Latitude	Longitude	L	MLN (UT)
Sachs Harbor	72.0	235.0	76.1	273.0	17.3	2205
Cape Parry	70.2	235.3	74.6	276.6	14.2	2156
Gjoa Haven	68.6	264.1	78.5	320.1	25.2	1902
Pelly Bay	68.5	270.3	79.1	332.5	28.0	1821
Repulse Bay	66.5	273.8	77.5	340.7	21.3	1755
Coral Harbor	64.1	276.8	75.4	347.0	15.7	1735
Cape Dorset	64.2	283.4	75.4	359.6	15.7	1655
Longyearbyen	78.2	15.4	75.0	114.6	14.9	0902
Davis	-68.6	78.0	-74.3	101.5	13.7	0920
Zhong Shan	-69.4	76.4	-74.4	98.0	13.8	0928

Table 1.2. Magnetometer station parameters. Geomagnetic coordinates and L-shell values are given according to the PACE coordinate system of *Baker and Wing* [1989]. Magnetic local noon (MLN) is an annual average calculated via the dipole tilt angle.

Each array is equipped variously with ring-core fluxgate magnetometers, which record the magnitude of the magnetic field, or induction coil magnetometers, which record the time-rate-of-change of the magnetic field. Individual sensors are oriented to record the geomagnetic x-, y- and z-components after the standard fashion [*Knecht and Shuman*, 1985].[4] A summary of relevant station parameters is given in Table 1.2.

The MACCS array is operated by Mark Engebretson of Augsburg College and Jeff Hughes of Boston University. The array spans most of northern Canada at cusp/cleft geomagnetic latitudes. The geometry of the portion of the array used in this study is shown in Figure 1.5. Each station is equipped with a Narod ring-core fluxgate magnetometer, the analog output of which is sampled (after anti-aliasing filtration) at 2 Hz, giving a Nyquist frequency of 1 Hz. Signal correlations are made possible by computer-card crystal clocks which are synchronized between stations with a 1-s signal from an Omega band receiver, limiting timing errors at each station to better than ±0.05 s [*Engebretson et al.*, 1995]. As is

---

[4] In this study we examine only the horizontal (x and y) components of the magnetic field. As it turns out, the vertical (z) component is most susceptible to local, subsurface conductivity anomalies peculiar to each station [*Jacobs*, 1970; *McPherron*, 1995].
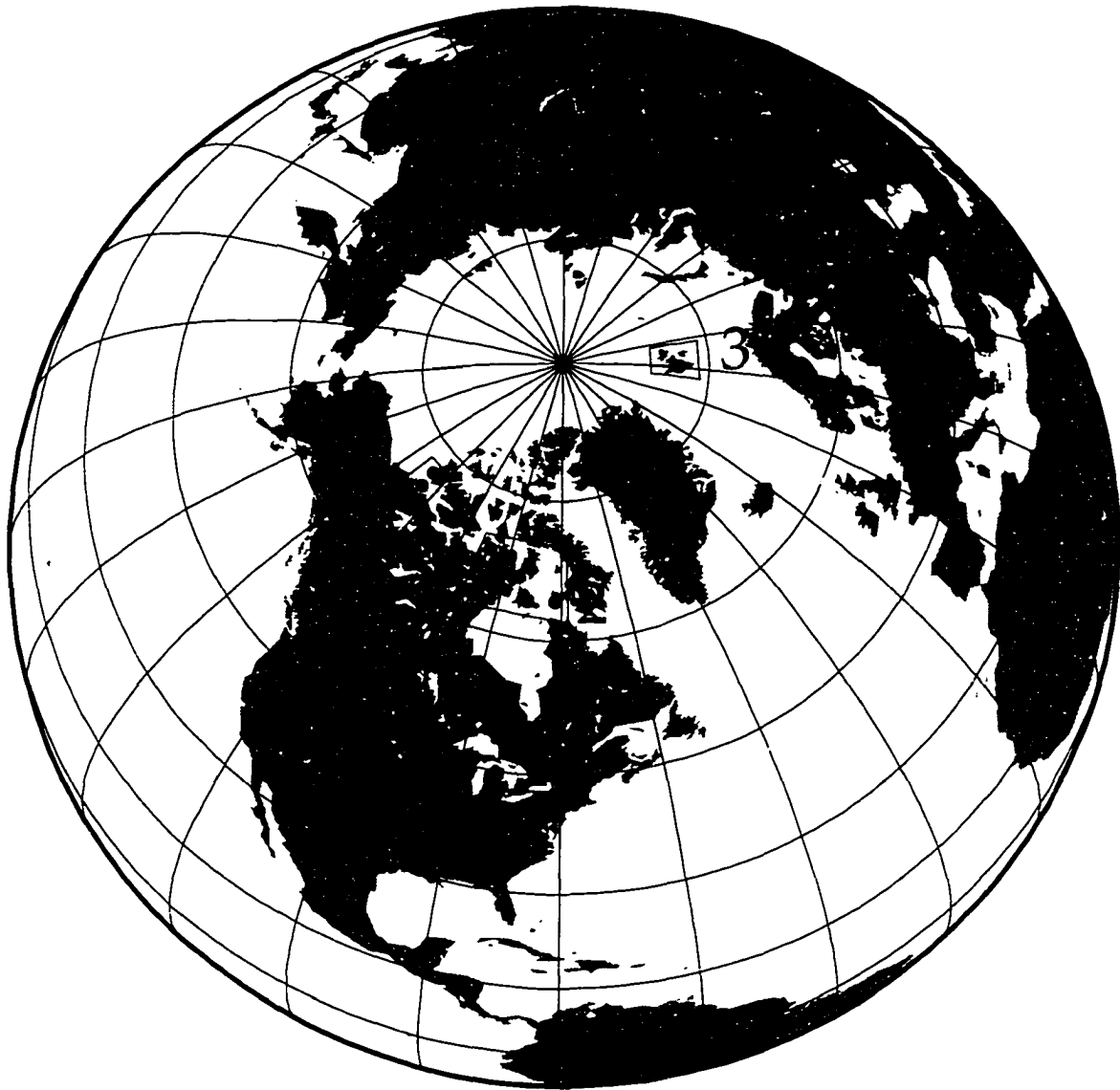
Figure 1.4. Geographic location of northern hemisphere magnetometer stations. Shown are portions of the UA pulsation network (1), portions of the MACCS array (2), and the single station near Longyearbyen (3). Detail maps are given in Figure 1.5.
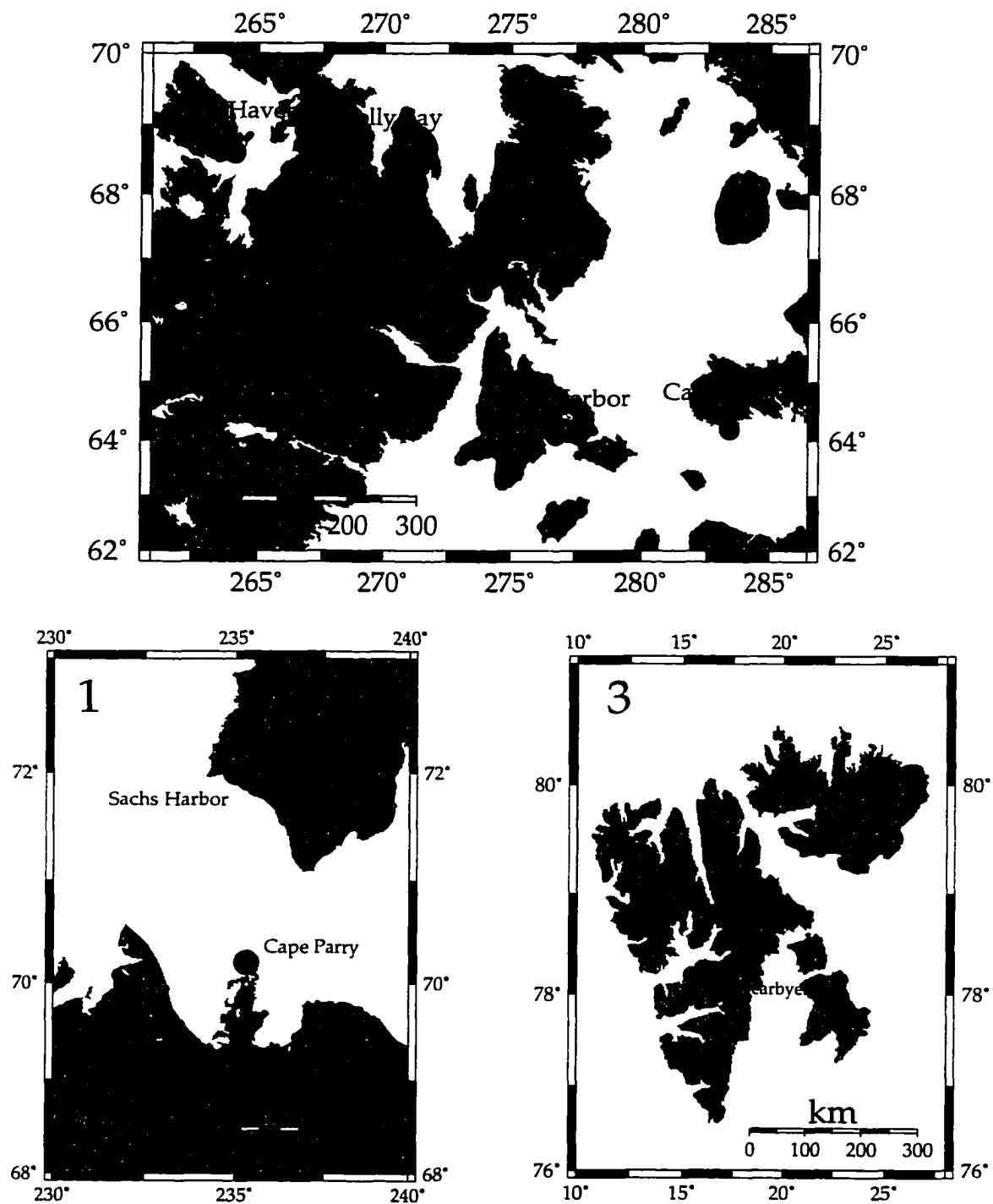
Figure 1.5. Detail maps of northern hemisphere magnetometer stations. Shown are portions of the MACCS array (top), the UA network (bottom, left) and the station near Longyearbyen (bottom, right).
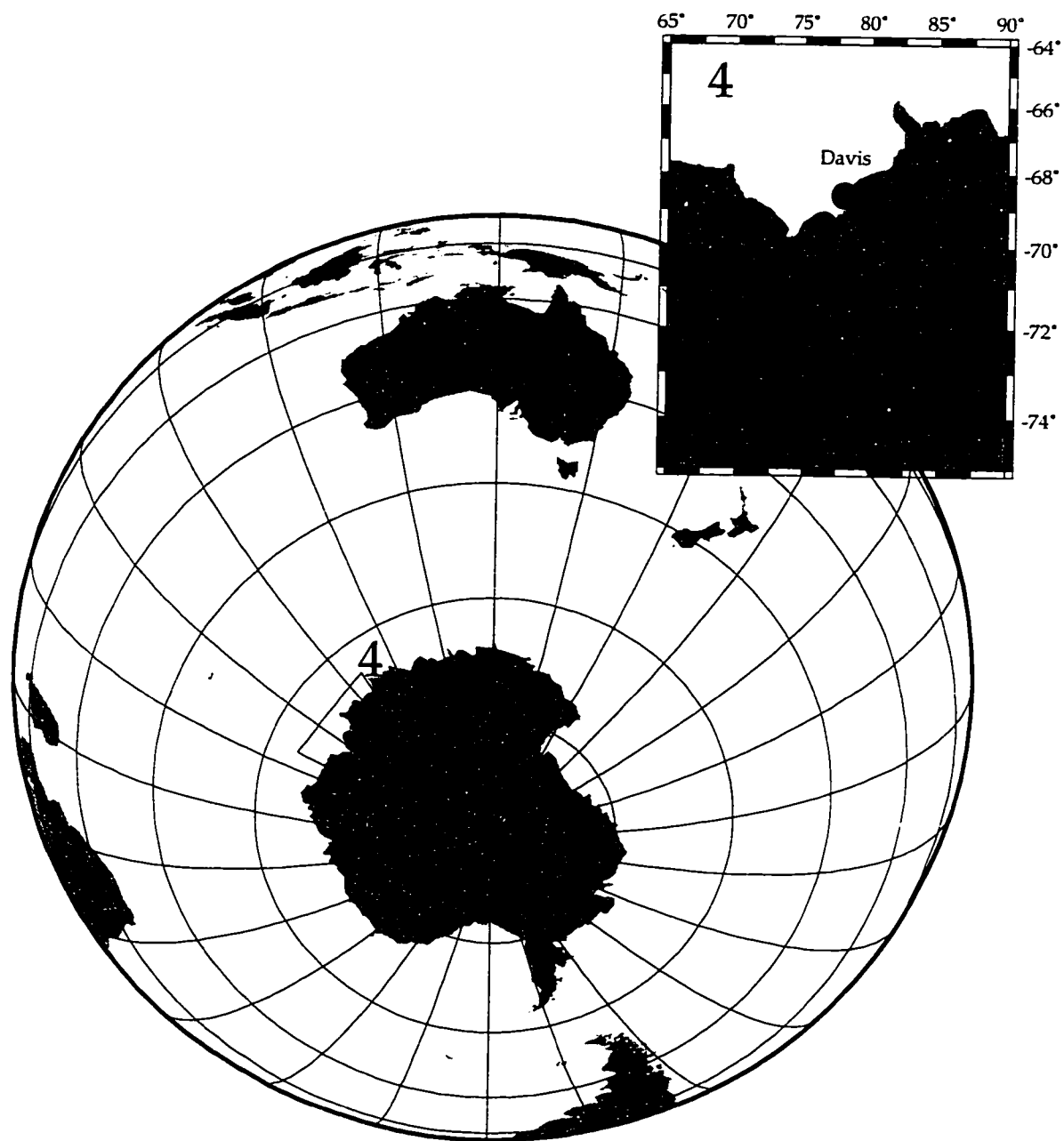
Figure 1.6. Geographic location of southern hemisphere magnetometer stations. Shown is a portion of the ANARE array (4, and inset).

	1993	1994
Gjoa Haven	5°53′ W	6°00′ W
Pelly Bay	25°49′ W	25°34′ W
Repulse Bay	27°51′ W	27°36′ W
Coral Harbor	27°10′ W	26°57′ W
Cape Dorset	35°22′ W	35°05′ W

Table 1.3. Declination corrections for the MACCS stations. Corrections shown for the years 1993 and 1994 are based on the 1995 Canadian Geomagnetic Reference Field.

the case for all the stations used in this study, the x-component was oriented to magnetic north; the y-component to magnetic east; and the z-component vertically downward. The actual MACCS data provided for use in this thesis were archival 5-s averages (prepared after the data were first Fourier lowpass filtered at 0.1 Hz), giving an effective Nyquist frequency of 0.1 Hz. The data were from 1993 and 1994. Since the archival records are stored in geographic coordinates, we have rotated them back into geomagnetic coordinates according to the declination corrections given in Table 1.3. These corrections are based on the Canadian Geomagnetic Reference Field and were provided by Larry Newitt of the National Geomagnetism Program of the Geological Survey of Canada.

Data taken from the MACCS array were invaluable resources in the production of this thesis. They comprise the bulk of our data, more than 800 days worth of station data. The magnitude of this contribution warrants its mention here, apart from the usual acknowledgements. The data, as well as processing facilities at Augsburg College, were generously provided by Mark Engebretson. The author is indebted to him for his unselfish cooperation in this research endeavor.

The University of Alaska pulsation stations are operated by John Olson of the University of Alaska Fairbanks. The two stations at cusp latitude used were Cape Parry and Sachs Harbor (see detail map in Figure 1.5). These stations operated simultaneously for a brief part of the 1985 summer season. Each station is equipped with induction coil magnetometers, the analog output of which is sampled (after anti-aliasing filtration) at 0.1 Hz, giving a Nyquist frequency of 0.05 Hz. The use of GEOS satellite time codes at each site synchronizes the time base to within ±1 s, allowing for interstation signal correlations [*Olson*,

1986]. At this site only the x- and y-components are recorded.

The Nordlysstasjonen magnetometer, near (hereinafter) Longyearbyen, is also operated by John Olson. This station is equipped with both 3-component fluxgate magnetometer and 2-component (x and y) induction coil magnetometer, both sampled (after anti-aliasing filtration) at 0.1 Hz, giving a Nyquist frequency of 0.05 Hz. The time code, not critical here for any interstation correlations, is kept on a computer-card crystal clock. Optical instruments at the same station, run by Chuck Deehr and Roger Smith of the University of Alaska Fairbanks, have been used to correlate optical and magnetic data at low frequencies (nominally in the Pc 5 frequency band) [*McHarg and Olson*, 1992; *McHarg et al.*, 1995].

Brian Fraser of the University of Newcastle operates the two ANARE stations used in this study, Davis and Zhong Shan. The site at Davis is located nearby the Australian Antarctic Division supply base; the site at Zhong Shan is about 5 km from the Chinese national base. The sites are equipped with induction coil magnetometers, the analog output of which is sampled (after anti-aliasing filtration) at 1 Hz, giving a Nyquist frequency of 0.5 Hz. Signal correlations between these stations are made possible by IRIGb serial time code modulated onto a 1-kHz carrier and transmitted to each site, giving time synchronization to better than ± 0.05 s [*Symons*, 1996]. The data used in this study were taken during the 1996 austral winter season. Again, at this site only the x- and y-components are recorded.

1.4   Thesis organization

Following this general introductory chapter, we give an overview of the tools of time series analysis in Chapter 2. These tools are used throughout the thesis. Given the present state of signal processing in the pulsation community, we find such a second introduction necessary. It is our experience that the basic techniques of digital time series analysis are not uniformly well-understood among the groups doing pulsation work at high latitudes. Since virtually all of our current observational evidence comes from the analysis of digital archives, a thorough understanding of these basic processing techniques is a requisite skill for extracting meaningful physical information from them. Beyond the traditional techniques, we present two that, while not new in and of themselves, are somewhat novel

in their application to geomagnetic pulsations. These two techniques are the Hilbert and Karhunen-Loéve transforms. As a companion paper to Chapter 2, we present a full development of the discrete Karhunen-Loéve transform in Appendix A.[5]

In Chapter 3 we begin our characterization of the cusp region with a focus on the interstation coherence of magnetic pulsation activity in the Pc 3 frequency range. A certain portion of this class of pulsations is thought to be generated via a localized source mechanism, most likely via modulated conductivities in the the overhead ionosphere. Based on the analysis of data taken from several station pairs in both hemispheres we develop a reliable measure of interstation coherence near the cusp. From this new measure we determine the coherence length of this type of pulsation and relate it to the future deployment of magnetometer stations at cusp latitudes.

Turning from localized sources, we examine long-period pulsations (nominally Pc 5) in Chapter 4. These pulsations are thought to be indicative of the passage of the cusp and boundary regions nearby the station. In an effort to develop a characteristic magnetic cusp signature we find an important phase property of one class of pulsations commonly used as a cusp discriminant. Using an information theoretic analysis of spectral records, we assess the spatiotemporal character of the cusp and boundary region spectrum. We find that there is both temporal and spatial information contained in the cusp latitude spectrum. Finally, we comment on the ability of any ground-based determination of the separatrix location via magnetometer records.

In Chapter 5 we conclude with a review of our findings, their importance to the research community and suggest further avenues of approach, ones which should assist us in our attempt to understand the physics of the cusp and boundary regions.

---

[5]Since the material of Appendix A is computationally motivated and algebraically detailed, we present it outside the main body of the thesis. Our twin-pronged eigensystem approach provides an efficient and effective means of calculating the basis functions and coefficients of the discrete Karhunen-Loéve expansion, one which avoids numerical difficulties and spurious results.

Chapter 2

Discrete time series analysis: An overview

We have asked how an analysis of magnetometer records enables us to characterize the cusp region. This characterization is greatly determined by the utility of any analysis technique brought to bear and our ability to interpret the results. In our exploration of the data, we found several discrete time series analysis techniques quite useful; this chapter is presented as an introduction to those techniques. It serves to familiarize the reader with the analytical methods and notational scheme used throughout this thesis. More than just a primer in signal processing, each section offers a physical motivation for the application of a particular technique or formalism to a given suite of data. Since the bulk of this thesis is concerned with the physical interpretation of ground-based magnetometer data, any such motivation stems from processes known to occur or thought to occur in the magnetosphere and ionosphere. While each technique is particularly suited to the analysis of the digital data stream derived from a magnetometer, the scope of its usefulness is not restricted to magnetometer data. The time series analysis techniques described herein are broadly applicable to many types of instrument data, geophysical and otherwise.

Since a comprehensive treatment of discrete time series analysis is beyond the scope of this thesis, some facility with statistical signal processing is assumed on the part of the reader. For a thorough introduction to the theoretical aspects of signal processing, several fine works are available and recommended [e.g., *Jenkins and Watts*, 1968; *Bracewell*,

21

Reproduced with permission of the copyright owner. Further reproduction prohibited without permission.

1978; *Press et al.*, 1992; *Therrien*, 1992]. What follows does, however, provide a sufficient overview for the space physicist interested in expanding his or her ability to gain physical insight through the analysis of instrument data. Our aim is to lay a foundation, one which enables the reader to follow our work. Moreover, considering our approach and examples provided in the ensuing chapters, the foundation should allow the reader to develop and build upon their own intuition, ultimately to pursue their own interests.

2.1 Traditional methods

Traditional approaches in physical signal processing are grounded in Fourier analysis. This is the case because the technique developed by J. Fourier nearly two centuries ago is widely applicable to both the description and analysis of physical systems whose nature is periodic. In addition, Fourier analysis is particularly useful in estimating the behavior of quasi- and non-periodic systems [*Jenkins and Watts*, 1968]. Both of these properties have direct bearing on the widespread use of Fourier theory in the analysis of geophysical data.

Consider the case of one of our ground-based fluxgate magnetometers. A typical example of the data sampled from such an instrument is shown in Figure 2.1. The data appear to be somewhat sinusoidal, or quasi-sinusoidal, in form; however, the dominant pulsations exist for only a portion of a full cycle. Quite clearly there are other components comprising the signal. Quasi-sinusoidal signals are characteristic of geomagnetic pulsations detected both at the ground and *in situ*. It is this characteristic which suggests the use of Fourier theory for their analysis.

Barring man-made perturbations, the currents we infer as the source of magnetometer signals are at least 90 km away in the overhead in the ionosphere. The information content of these current-carrying regions is conveyed to our instrument by the magnetic field as a wave phenomenon. Our fluxgate magnetometer is then essentially a current detector. In the magnetosphere-ionosphere system, wave interactions are described, to some approximation, by the equations of MHD theory.

Ultimately, it is the Maxwell equations which govern our understanding of how the magnetic field carries information from a distant current source to a local receiving station. In particular, in source-free regions we find generic wave solutions for the magnetic

.I
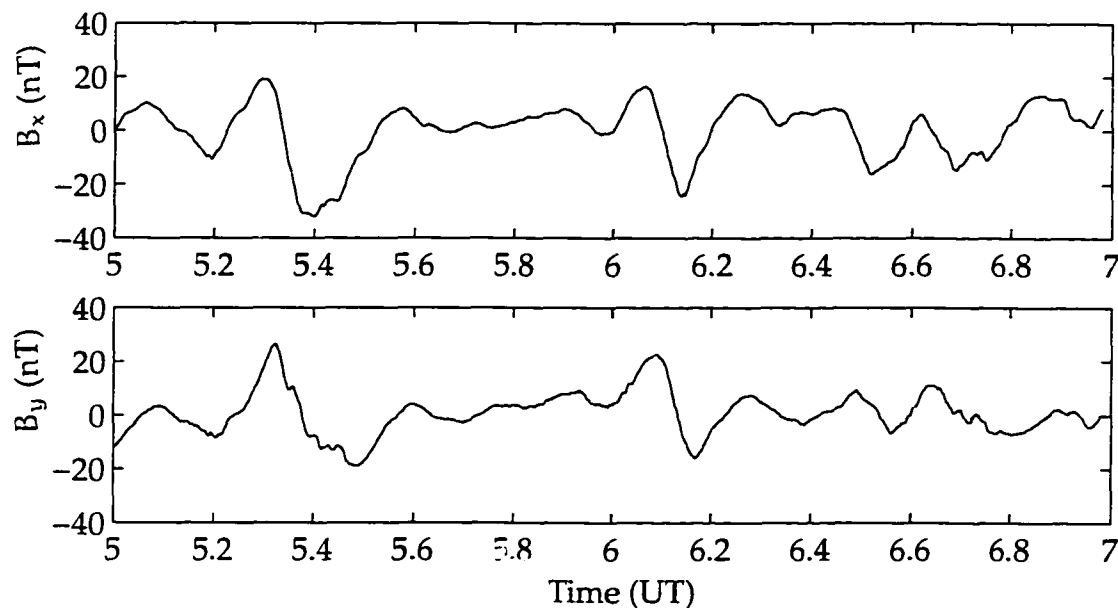
Figure 2.1. A typical example of fluxgate magnetometer data. These data were taken from the fluxgate magnetometer at Longyearbyen on 9 January 1991. The data are zero-mean detrended to show deviations from the background geomagnetic field. Shown in the panels are (top) the x and (bottom) y components of the magnetic field. Note the quasi-sinusoidal nature of the data.

field as $e^{i(k \cdot x - \omega t)}$, such that, given the appropriate boundary conditions, the following transformations hold:

$$\nabla \rightarrow ik \qquad (2.1)$$

$$\frac{\partial}{\partial t} \rightarrow -i\omega t \qquad (2.2)$$

where k is the wave vector. Solution of partial differential equations in this manner is identical to Fourier transforming in space and time.

The problem of cusp latitude magnetometer data is amenable to Fourier analysis on two levels. First, the data strike us visually, with the dominant waveforms appearing quasi-sinusoidal. Upon closer inspection, we find a rich variety of behaviors, from intervals of superposed sinusoids of differing frequency to intervals that are apparently completely stochastic. Second, our mathematical intuition concerning the source of the data lends itself to Fourier analysis. The physical, electrodynamical source of our data is fairly well described by a group of partial differential equations, the solution of which can be

had via Fourier transformation.

Both our visual and mathematical perception of the magnetometer data tend to suggest Fourier analysis for an increased understanding. Along with its many uses, Fourier theory does have its limitations; chiefly, its description of non-periodic data is only approximate at best. For that very reason Fourier theory is certainly not the last word in the analysis of geomagnetic signals; however, it is a natural starting point. For us, in presenting the thesis at hand, it is a point of departure.

2.1.1   The Fourier transform

Discrete signals, or time series, can be represented by a vector in bra-ket notation as $|x[t]\rangle$. This denotes a quantity x that is a function of a discrete variable t, or time. Each component of the vector is represented by $x[k]$. When the data are sampled at a regular frequency f_s, t and k are related by $t = k/f_s$. All Fourier theory applied to discrete signals implies the use of the discrete Fourier transform (DFT). In that vein, the DFT lies at the heart of virtually all the signal processing carried out in this thesis. Since it requires little by way of introduction, we merely define our convention here and offer a brief comment on numerical particulars.

Given a time series $|x[t]\rangle$ of T points, we define the forward and inverse transforms, respectively, as

$$X[q] = \frac{1}{T} \sum_{k=0}^{T-1} x[k] e^{-i2\pi kq/T} \tag{2.3a}$$

$$x[k] = \sum_{q=0}^{T-1} X[q] e^{i2\pi kq/T} \tag{2.3b}$$

Here f and q are related by $f = qf_s/T$.[1] These particular forms (2.3) are a modified and concatenated version of those given by *Jenkins and Watts* [1968] and *Press et al.* [1992]. Since the forward (2.3a) and inverse (2.3b) designation can be taken as a matter of convenience, ie. q and k are interchangeable in (2.3), we select our convention noting that our forward transform is consistent with a causal signal, and that the first Fourier component $X[0]$ is the mean of the times series $|x[t]\rangle$. The latter point is important in considering transient

---

[1]Note that the discrete indices of time k and frequency q are both integer-valued.

phenomenon, in which the mean, or dc component of the signal, is uninteresting and can be made to be zero.

Throughout this thesis, the following conventions hold: the time series data are real and T is even. While these specifications appear somewhat arbitrary, they are motivated by the fact that our magnetometer data are real, and it is computationally advantageous to consider an even number of samples.[2]

With real time series and T even, it is of numerical interest to note that $X[q] = X[T - q]^*$ for $q \in [0, T/2]$. Thus only $T/2 + 1$ of the T frequency estimates are independent; these are the so-called positive frequencies. Two of the Fourier components (2.3a) will be real: $X[0]$ and $X[T/2]$. The former is simply the mean of $|x[t]|$; the latter the Nyquist frequency component, or the highest frequency component of the time series which we may resolve. The Nyquist frequency is given by

$$f_N = f_s/2 \qquad (2.4)$$

where f_s is the sampling rate.

2.1.2   Spectrum estimation

Magnetometer output is sampled in time to provide a time series, here in the form of $|x[t]|$. This sampling provides us with one particular, and perhaps the most common, description of data, that in the time domain. Application of the forward Fourier transform (2.3a) takes us from the time domain to $|X[f]|$ in the spectral, or frequency domain.[3] Each domain is suited for certain types of analysis; however, the frequency domain often enables a simpler

---

[2]Some authors, notably *Press et al.* [1992], would argue that our restriction on T is too lax. Practically all computation of the DFT is carried out by a fast Fourier transform (FFT) algorithm based on those popularized by J. Cooley and J. Tukey in the mid-1960's [*Press et al.*, 1992]. The FFT is extremely efficient in that it requires only $\mathcal{O}(T \log_2 T)$ operations to compute the Fourier transform, whereas a brute force calculation of the sum (2.3) requires $\mathcal{O}(T^2)$ operations [*Brigham*, 1988]. The FFT is known as a radix-2 transform, and as such places a more stringent requirement on the number of samples; namely, $T = 2^m$ with $m \in [0, \infty)$. Owing to the great computational efficiency of the FFT, the use of anything other than power-of-two samples is often proscribed; such a requirement is no less arbitrary than our specification that number of samples be even.

While the radix-2 algorithm is certainly efficient, not all practical data lend themselves to division into power-of-two segments. Moreover, sophisticated algorithms exist that are computationally competitive with the FFT. These algorithms are known as mixed-radix transforms, and take advantage of the prime factorization of T to perform the calculation. For T prime, of course, the only available option is direct calculation via (2.3). All Fourier transforms in this thesis were computed by the mixed-radix routine of *Moler* [1992].

[3]From this point forward, we use $|x[t]|$ and $|x\rangle$ interchangeably; likewise with $|X[f]|$ and $|X\rangle$.

or reduced description of the data [*Samson*, 1983b]. Geomagnetic data, in particular, lends itself to spectral analysis.

Under the aegis of Fourier analysis, we find the most direct route into the spectral domain, particularly via computation of (2.3a); it is not, however, our only means of entry [*Press et al.*, 1992]. Other, non-Fourier, methods of spectral estimation have been developed, notably the maximum entropy (ME) method of *Burg* [1975]. The ME method assumes an autoregressive (AR) model of a certain order for the data, thus the spectra produced are model dependent [*Therrien*, 1992].

In choosing among various methods, we must ask what assumptions underlie our understanding of the physics governing the processes thought to give rise to the signals we receive at the magnetometer station. Too, we must recognize the limitations of each method — no one spectral technique is best for all data or situations. The method and assumptions used to estimate the spectrum have a marked influence on the result [*Lacoss*, 1971]. In this work we champion the use of Fourier methods to estimate the spectrum. Ostensibly, the data are quasi-periodic in nature, and the equations that govern our understanding of the processes involved may be solved, in principle, by Fourier methods.

A tempting advantage of the ME method is that it can provide arbitrary frequency resolution, as we need only consider an appropriately high order model of the data. Closely spaced spectral peaks that might otherwise evade Fourier methods may be resolvable in this manner. Unfortunately, the magnetometer signals we receive are not thought to be the result of an AR process — in some cases, we are unsure of their exact source mechanism. The ME method is well-suited for the detection and analysis of signals whose source or form is known *a priori* [*Lacoss*, 1971]. In the case of geophysical data, justification for the model order is marginal at best [*Bracalari and Salusti*, 1994], causing us to fall back on classical spectral analysis (J. C. Samson, private communication, 1994).

For a data sequence $|x\rangle$ of length T, the most simple estimate of the spectrum is given by the magnitude squared Fourier transform as

$$S[f] = \frac{1}{T}|X[f]|^2 \tag{2.5}$$

We refer to this estimate as a raw spectral estimate and it is consistent with the Einstein-Weiner-Khintchine relation [*Therrien*, 1992]. This estimate is asymptotically unbiased, in

the sense that

$$S[f] \xrightarrow[T \to \infty]{} \hat{S}(f) \qquad (2.6)$$

where $\hat{S}(f)$ is the true spectrum (note that it is continuous) [*Jenkins and Watts*, 1968]. For T sufficiently large, we are certain that there is relatively small bias in our estimate.

Unfortunately, the variance in $S[f]$ is rather large

$$\sigma^2_{S[f]} \approx S^2[f] \qquad (2.7)$$

and does not decrease as $T \to \infty$ [*Therrien*, 1992]. Finite T, which is the case in all practical situations, gives rise to a phenomenon known as leakage [*Jenkins and Watts*, 1968; *Press et al.*, 1992], in which spectral information from frequency f will bleed into adjacent frequency components from dc to the Nyquist frequency. Such an effect arises because for finite T we are equivalently considering only a windowed portion of an infinite amount of data when we take the Fourier transform [*Press et al.*, 1992].

Confidence

We conclude then that the raw estimate (2.5) offers only a very crude approximation of the true spectrum $\hat{S}(f)$. Hence, we turn to various statistical means designed to improve our confidence in the spectral estimate. In this effort we have two principle aims: 1) reduce the bias induced via leakage and 2) reduce the variance in the estimate. Windowing is typically employed to reduce the bias and averaging or smoothing is used to reduce the variance in the spectral estimator [*Press et al.*, 1992; *Therrien*, 1992]; however, it should be noted that both processes involve some mutual interaction [*Chave et al.*, 1987].

It may seem confusing that windowing is used to reduce bias in the estimator when it is the window, owing to a finite amount of data, that causes leakage in the first place. Simply put, for finite T some sort of window is unavoidable. The windowing operation may be represented as

$$x_w[k] = w[k]x[k] \qquad (2.8)$$

In the simplest case, a rectangular window, $w[k] = 1 \, \forall \, k$. In practical situations, this window introduces the greatest amount of leakage, therefore we choose to construct a

window that minimizes this undesirable effect. In this thesis we make use of the following windows

$$w[k] = \frac{1}{2}\left[1 - \cos\left(\frac{2\pi k}{T}\right)\right] \qquad \text{Hanning window} \qquad (2.9)$$

$$w[k] = 1 - \left(\frac{2k - T}{T}\right)^2 \qquad \text{Welch window} \qquad (2.10)$$

either of which can be shown to substantially reduce the bias caused by leakage [*Press et al.*, 1992]. In our experience, and that of others [e.g., *Jenkins and Watts*, 1968; *Press et al.*, 1992], the exact choice of window — there are many — has little effect upon our results.

With regard to variance, it is helpful to consider that spectral estimates are distributed approximately as a chi-square with ν degrees of freedom [*Jenkins and Watts*, 1968]. In the case of the raw estimate (2.5), $\nu = 2$. Any step we take to increase the number of degrees of freedom will result in a decrease of the estimate's variance. As with windows, there are numerous schemes for variance reduction; from among them, we employ the method of *Welch* [1970].

The Welch method takes the original time series $|x\rangle$ and breaks it into K, possibly overlapping, subseries $|x_k\rangle$, each of length T/K. Fourier transforms of the subseries $|X_k\rangle$ are taken and averaged together, element by element, to form a spectral estimate $|\bar{x}\rangle$ with elements

$$\bar{x}[q'] = \sum_{k=0}^{K-1} x_k[q'] \qquad (2.11)$$

Note that there is a cost associated with this procedure. Whereas in the raw estimate we found $q \in [0, T/2]$ positive frequencies, the Welch method reduces the count of positive frequencies to $q' \in [0, T/2K]$.

We are more than compensated for the loss of spectral resolution. For non-overlapping subseries, we increase the degrees of freedom to $\nu = 2K$. Alternately, we reduce the variance in this manner by a factor of $1/K$ [*Therrien*, 1992]. We can further reduce the variance by overlapping the subseries, but only to a point. As we increase K by overlapping, the subseries become correlated, thus offsetting the reduction in variance [*Therrien*, 1992; *Krause et al.*, 1994]. For subwindows of length T/K an overlap of T/2K points can be shown to be optimal (D. Prichard, private communication, 1994). For this level of overlap, $\nu \approx 2K$.

Spectral matrices

Univariate signal processing is a luxury seldom afforded the space physicist. In our case, magnetometer records represent a sampling of the geomagnetic field, a vector quantity. As such, we derive at least a 2-dimensional time series from each station. If we consider an array of stations, the need to analyze N-variate (or N-dimensional) time series arises. In a series of papers, Samson and Olson showed that the spectral matrix offers a convenient representation of the spectrum of N-dimensional geophysical time series [*Olson and Samson*, 1979; *Samson and Olson*, 1980, 1981; *Samson*, 1983b].

Before we define the spectral matrix, we introduce the cross spectrum estimate of two time series

$$S_{ij}[f] = X_i[f]X_j^*[f] \tag{2.12}$$

Note that $S_{ii}[f]$ is simply the raw spectrum estimate (2.5); hence, all of our discussion concerning confidence applies [*Jenkins and Watts*, 1968]. Now, in terms of the cross spectrum estimate, the spectral matrix is defined as

$$\mathbb{S}[f] = \begin{pmatrix} S_{00}[f] & \dots & S_{0,N-1}[f] \\ \vdots & \ddots & \vdots \\ S_{N-1,0}[f] & \dots & S_{N-1,N-1}[f] \end{pmatrix} \tag{2.13}$$

This form is equivalent to that of *Samson and Olson* [1980] and is particularly useful, since the Welch method may be readily employed to calculate it. For N time series of length T, using length T/K subseries in the Welch method, we arrive at $T/2K + 1$ spectral matrices of dimension $[N, N]$. One can visualize the result as a stack of matrices, forming a rank three tensor of dimension $[N, N, T/2K + 1]$. Noting that $S_{ij}[f] = S_{ji}^*[f]$, we see that $\mathbb{S}[f]$ is Hermitian and thus contains only $N(N + 1)/2$ non-redundant elements.[4]

---

[4]It is computationally convenient then to perform some index gymnastics and map the spectral matrices into a reduced vector space as $S_{ij} \Rightarrow s[i + \sum_{\ell=0}^{j} \ell(N - i)]$ for each f, where $j \in [0, N - 1]$ and $i \in [j, N - 1]$. This allows us to effectively operate on the rank three tensor in machine memory by handling a simple matrix of dimension $[N(N + 1)/2, T/2K + 1]$.

2.1.3 Frequency-time localization

At any given magnetometer station, we record data from one of the field components for a length of time, resulting in a time series $|x\rangle$ of length T. Since T is finite, we can resolve a maximum of $T/2 + 1$ useful spectral estimates. This number will be reduced further via the Welch method in order to increase our confidence in the spectral estimates. We can increase our resolution by making our observing run appropriately long.[5] Long observation periods are not an inconvenience, as most magnetic observatories are automated; however, the processes that give rise to the magnetometer signals are not, in general, long-term.

Fourier spectral estimates are made with the underlying assumption that the data are stationary during the period of observation [*Therrien*, 1992]. Magnetometer data are only approximately stationary. Reliable spectra can be estimated if the first two moments of the data, the mean and variance, are roughly constant over long time periods, even if there are local excursions from these baseline values [*Chave et al.*, 1987]. An approximately stationary signal exhibiting this type of behavior — sporadic, short-term episodes of non-stationarity — is termed wide-sense stationary [*Akansu and Haddad*, 1992]. Figure 2.2 provides an example of the wide-sense stationary nature of our magnetometer data. Since the data depart locally from stationarity, we are interested in their spectrotemporal characteristics. That is, we wish to know two things: 1) the spectral information carried by the pulsations, and 2) the temporal evolution, or transient response, of that information. Ideally, for a time series $|x\rangle$ we would like to have complete knowledge of $|X\rangle$ for each sample $x[t]$.

An uncertainty principle prevents us from obtaining complete, instantaneous knowledge of the spectrotemporal characteristics of any sort of data, even in principle. One can show that the Fourier transform obeys the following form of the uncertainty principle [*Bracewell*, 1978]

$$\Delta f \Delta t \geq \frac{1}{4\pi} \tag{2.14}$$

---

[5]We can also gain resolution through a process known as zero-padding, in which we append an appropriate number of zeros to $|x\rangle$ [*Therrien*, 1992]. We must not think that by zero-padding we are gaining any information. The process does not add any spectral information to the system, nor does it change the shape of the spectrum; it merely interpolates the original spectral content among the newly opened frequencies. The process is useful however, when computational exigency requires sheer speed, as T can be made to be a power-of-two in this fashion.
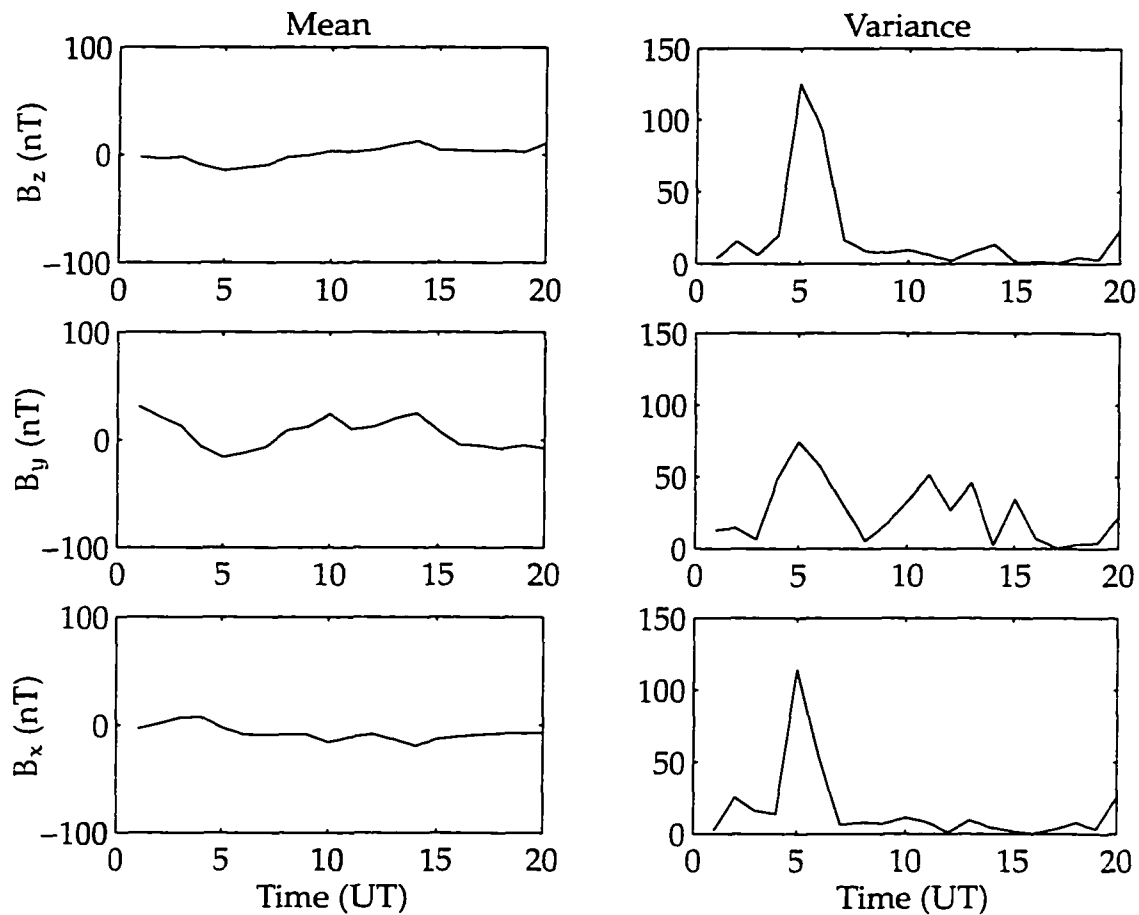
Figure 2.2. Magnetometer data mean and variance as functions of time. These data were derived from the fluxgate magnetometer at Longyearbyen on 9 January 1991 (a portion of which is shown in Figure 2.1). Each moment is calculated at one-hour intervals and shown for each component of the magnetic field. Since the mean and variance of the data are only approximately constant, we refer to them as wide-sense stationary. The marked excursion from baseline values near 0500 UT is of interest to us, as it presages the passing of magnetic local noon, and hence the cusp region.

where f and t are continuous. For the discrete time case, the uncertainty becomes a three-parameter relation [*Claerbout*, 1985]

$$\Delta f \Delta t \, \zeta_\nu^2 \geq 1 \tag{2.15}$$

where the parameter ζ_ν^2 is a function of the degrees of freedom ν in the spectral estimate, and f and t are discrete. The effects of windowing, ie. leakage, in effect cause us to be completely uncertain about our spectral estimates — spectral information for any frequency f is spread among all $T/2 + 1$ components. At best, we may only have a certain degree of statistical confidence in them. For practical purposes then, we are interested in what sort of frequency resolution f_r we may obtain from a time series. This information is governed by a simple relation

$$\frac{f_r}{f_s} = \frac{1}{T} \tag{2.16}$$

where f_s is the sampling rate.

Given the relations for uncertainty (2.15) and frequency-time resolution (2.16), the question becomes: How do we balance the gain/loss of time resolution against that of frequency resolution? Our answer lies in one of two signal processing techniques, frequency-time distributions or dynamic spectra. The former include applications of the family of Wigner-Ville distributions [*Najmi*, 1994] and the generalized Gabor transform [*Stockwell et al.*, 1996]. Much like the ME spectral method, these applications are best suited to problems in which the source and form of the time series is known *a priori* [*Gaunaurd and Strifors*, 1996]. It is the latter technique that proves the arbiter of our compromise in frequency-time resolution. A dynamic spectra is also referred to as a short-time Fourier transform [*Therrien*, 1992].

Consider a process which we wish to analyze, one that is assumed wide-sense stationary over a number of samples T_s. We take a time series $|x\rangle$ of length $T > T_s$ and subdivide it into a number of possibly overlapping subseries $|x_i\rangle$, of length T_i, where $T > T_i > T_s$. At this point we treat each subseries in isolation, estimating the spectrum via the Welch method, exactly as we did before. In doing so, we are looking for Welch subseries $|x_k\rangle$ of length $T/K \approx T_s$. In practice, T_s is not known, but can perhaps be deduced or estimated after some fashion.
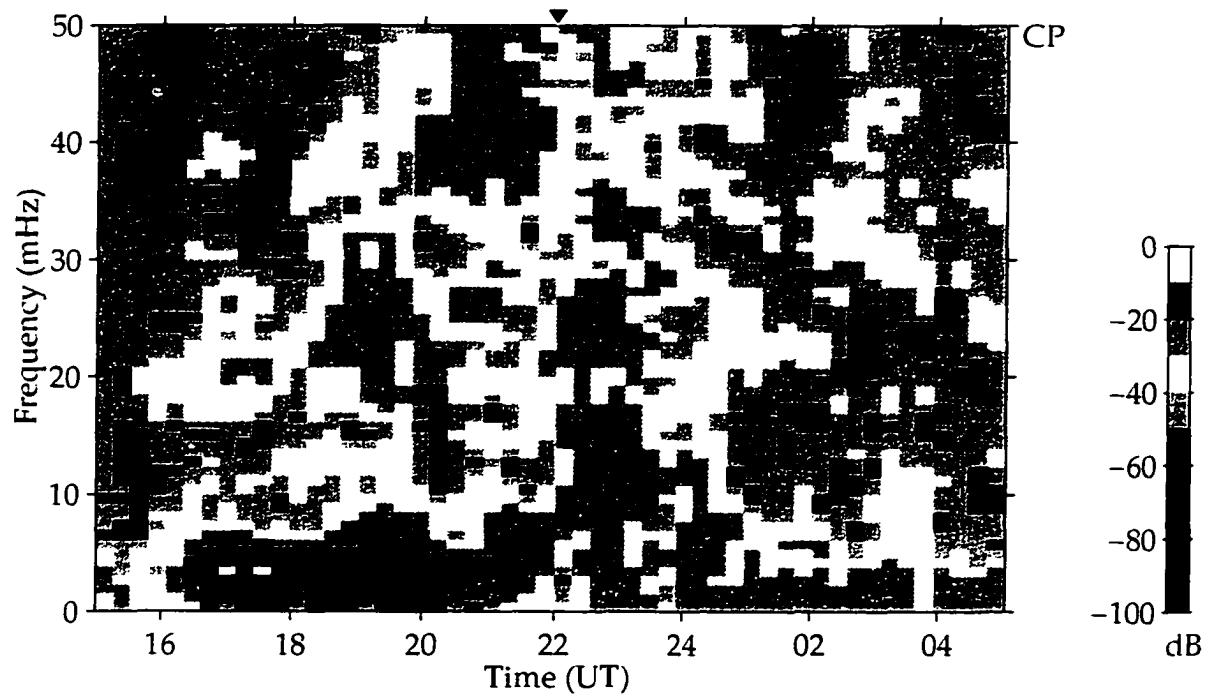
Figure 2.3. A typical magnetometer spectrogram. These data were taken from the induction coil magnetometer at Cape Parry on 20–21 May 1985. The small triangle approximately marks magnetic local noon at the station. Shown in the panel is the trace of the spectral matrix tr $\mathbb{S}$ in frequency and time as a dynamic spectrogram. Note that no one spectral feature is persistent over the entire time span of the data.

as an array, typically called a frequency-time spectrogram. See Figure 2.3 for a typical example of a spectrogram of magnetometer data.

2.1.4 Generalized coherence estimation: Coherence and polarization

When we examine N-dimensional time series, it is often necessary to characterize the signals in two or more of the data channels in terms of their likeness. In the time domain this operation is typically carried out as a cross-correlation [Therrien, 1992]. In the spectral domain, the chief measure of likeness is the coherence between signals. We employ two independent measures of coherence for N-dimensional magnetometer signals. The first is valid only for $N = 2$; however, this is often the case when we are considering interstation coherence. The second, a polarization estimator, is appropriate for $N \geq 2$ and can be shown

independent measures of coherence for N-dimensional magnetometer signals. The first is valid only for $N = 2$; however, this is often the case when we are considering interstation coherence. The second, a polarization estimator, is appropriate for $N \geq 2$ and can be shown to be an estimate of the generalized coherence [*Samson*, 1983a]. The N-dimensional polarization estimate may further be used to construct data-adaptive pure-state filters that are particularly useful in analyzing wave phenomenon, such as the signals we detect with our magnetometers [*Samson and Olson*, 1981].

The first coherence estimator is the traditional magnitude squared coherence function $C_{ij}[f]$, given by *Therrien* [1992]. It is defined at each frequency f as the ratio of the non-redundant elements of the 2-dimensional spectral matrix

$$C_{ij}[f] = \frac{|S_{ij}[f]|^2}{S_{ii}[f]S_{jj}[f]} \tag{2.17}$$

The second is the degree of polarization estimator derived by *Samson and Olson* [1980]. This estimator is based upon the invariants of the spectral matrix and is given by

$$P[f] = \frac{N\left[\text{tr } \mathbb{S}^2[f]\right] - \left[\text{tr } \mathbb{S}[f]\right]^2}{(N-1)\left[\text{tr } \mathbb{S}[f]\right]^2} \tag{2.18}$$

where N is the dimension of the system used to compute the estimate and $\text{tr } \mathbb{S}$ is the trace of the spectral matrix. It is important to note that for 2-dimensional data, the polarization estimator (2.18) can be shown to be identical to the classical form given by *Fowler et al.* [1967].

By definition $C_{ij}, P \in [0, 1]$, and both are biased estimators for finite amounts of data with a small number of degrees of freedom; indeed, for a naive estimate of the spectrum, both are identically 1. When the Welch method of spectrum estimation is used, the magnitude of each coherence estimator descends toward a limiting value, that of the true coherence. In this sense, both $C_{ij}[f]$ and $P[f]$ represent an upper bound to actual coherence present in the signals at each frequency. A central feature of each estimator is that they both tend toward a small value, or noise floor, for white noise processes when ν is sufficiently large, but finite. This property is a marked advantage in statistical coherence studies where quantization noise in magnetometers may dominate the signal and thus skew the results. *Jackson* [1996] has shown that such noise may be assumed to be approximately white.

We use both coherence estimators in concert, providing for a more accurate assessment of the true coherence; their advantages and limitations tend to complement one another. Since $P[f]$ is computed from the invariants of the spectral matrix it is independent of sensor orientation; however, a pronounced signal in any one of the N data streams will cause $P[f] \rightarrow 1$. In contrast, while $C_{ij}[f]$ does not benefit from the rotational invariance of $P[f]$, it is not biased toward unity for loud, single-channel signals. Thus, the use of both estimators as a check ensures that we are determining the true coherence present in a set of multi-dimensional signals.

2.2 New directions

The history of geomagnetic signal processing is steeped in Fourier theory. There are sound physical and mathematical reasons underpinning its widespread use in describing magnetometer data. While we are mindful of that success, our search for an improved understanding of the data must not be tradition-bound. There exist in the literature other methods of analysis which have proven themselves, if not for as long, in fields where sampled instrument data share many of the same properties as our magnetometer data.

The generalized coherence measure of *Samson and Olson* [1980] (2.18) serves as a transition between traditional approaches and new directions. In an age where multi-instrument arrays and collaborative data collection efforts have all but replaced single station measurements, the development of such estimators is important. The polarization estimator $P[f]$ extends classical theory to an N-dimensional instrument space that is rapidly characterizing data suites. Still, adoption of the estimator faced resistance after it was introduced to the magnetic pulsation community. Although rigorously developed nearly two decades ago, only recently has its use become widely accepted [e.g., *Olson and Fraser*, 1994; *Waters et al.*, 1995; *Ziesolleck et al.*, 1996].

In this section we turn from classical Fourier theory to examine the potential application of two transform techniques to the data. The Hilbert and Karhunen-Loéve transforms are well-known in electrical engineering and information theory circles, but within the geomagnetic community their use is somewhat novel. Rather than completely abandon the Fourier approach in their favor, we find application of these techniques in support of our

classical analysis. And although neither transform was developed from Fourier theory, each may be understood in terms of it.

2.2.1   The Hilbert transform

There are several probable sources of magnetic pulsations likely to produce monochromatic waves, particularly the high-latitude field line resonances [*Walker et al.*, 1992]. Under ideal conditions this assumption may hold, but in a realistic situation, where competing processes are likely to occur, we expect that these pulsations will be detected on the ground as quasi-monochromatic signals at best. The phase properties of such a quasi-monochromatic signal would be of interest to us, since a disruption in phase signature of the signal may indicate a change in the character of the source region [*Huang et al.*, 1992].

The uncertainty relation (2.15) prevents us from examining the spectral characteristics of our data for an arbitrarily short time period. Any information in the frequency domain represents an average over some number of samples in the time domain. For quasi-monochromatic signals however, a technique exists that allows us to examine the phase information of our signal at each point in the time series. This technique is known as the Hilbert transform and allows us to construct a phase-descriptive analytic signal from our original time series [*Bracewell*, 1978].

Although the Hilbert transform is valid, in general, for any time series [*Jackson*, 1996], we have found that our confidence in the phase-descriptive properties of the analytic signal is poor when the original time series differs greatly from a monochromatic signal. For this reason, we apply the technique only to processes which either are thought to be, appear to be, or are made to be band-limited.

The Hilbert transform stems from continuous transform theory via the Cauchy integral formula [*Morse and Feshbach*, 1953]

$$\psi_H(z) = \frac{1}{\pi} \mathcal{P} \int_{-\infty}^{\infty} \frac{\psi(z_0)}{z_0 - z} dz_0 \tag{2.19}$$

where $\mathcal{P}$ means take the Cauchy principal value of the integral and z is complex. In the discrete time case, Hilbert transformation of a time series

$$|x_H\rangle = \mathcal{H}\{|x\rangle\} \tag{2.20}$$

results in a new time series with all of the original frequency components shifted in phase by $\pm\pi/2$, often called the quadrature of $|x\rangle$. We use this phase shifting property to define the analytic signal [*Bracewell*, 1978]

$$|\tilde{x}\rangle = (1 + i\mathcal{H})|x\rangle \tag{2.21}$$

Note that $|\tilde{x}\rangle$ is in general a complex time series, even for $|x\rangle$ real.

From the analytic signal, we can determine several useful parameters. The instantaneous amplitude of the original signal is given by the magnitude of the analytic signal $|\tilde{x}[t]|$. More importantly, the instantaneous phase is given by

$$\varphi[t] = \tan^{-1}\left(\frac{x_H[t]}{x[t]}\right) = \tan^{-1}\left(\frac{\mathrm{Im}\,\tilde{x}[t]}{\mathrm{Re}\,\tilde{x}[t]}\right) \tag{2.22}$$

The instantaneous frequency may also be estimated via a numerical differencing scheme, $|\delta\varphi| \approx \frac{d\varphi}{dt}$, but it should only be considered as a local average over several adjacent samples [*Krause et al.*, 1994]. The instantaneous frequency estimate is useful for detecting phase skips in time series.

In practice, we need not calculate $|x_H\rangle$ as an intermediate step in constructing the analytic signal (2.21); rather, Fourier theory provides us with a direct route. Given our usual time series of length T, the analytic signal can be calculated as

$$|\tilde{x}\rangle = \mathcal{F}^{-1}\{|X\rangle \otimes |h\rangle\} \tag{2.23}$$

where $\mathcal{F}^{-1}$ represents the inverse Fourier transform (2.3b) and $\otimes$ is the array (element-by-element) multiplication operator. The vector $|h\rangle$ is akin to the the Heaviside step function with elements given by [*Krause et al.*, 1994]

$$h[q] = \begin{cases} 1 & q = 0, T/2 \\ 2 & 0 < q < T/2 \\ 0 & T/2 < q \leq T \end{cases} \tag{2.24}$$

The weights in $|h\rangle$ are unequal in order that $|x\rangle = \mathrm{Re}\,|\tilde{x}\rangle$. The analytical signal is then essentially the inverse Fourier transform of only the positive frequencies.

2.2.2 The Karhunen-Loéve transform

Much as with the Hilbert transform, the Karhunen-Loéve transform was initially developed for use with continuous variables [*Karhunen*, 1947]; however, its useful properties were eventually recognized for the discrete time case and several linear algebraic applications were found (see the review given by *Pike et al.* [1984]). We make use of the discrete Karhunen-Loéve transform (DKLT), which is known variously as singular value decomposition, principle orthogonal decomposition, or principle component analysis; it has also been shown to be equivalent to factor analytic methods [*Mees et al.*, 1987].

Use of the DKLT is most common in information theoretic and dynamical systems analyses [*Mees et al.*, 1987]. It has an optimal property in terms of data compression, so it also finds application in image analysis and pattern recognition [*Fu*, 1968; *Akansu and Haddad*, 1992]. Determination of the properties of the DKLT is based in matrix theory, so there are strong parallels to the quantum mechanical operator formalism [*Gasiorowicz*, 1974]. In the geomagnetic community, only *Samson* [1983a] has examined the concept, from a factor analytic standpoint. His efforts were aimed at optimizing the polarization estimator (2.18) in the presence of noise; eventually, he abandoned the idea in favor of other pursuits (J. C. Samson, private communication, 1995).

The DKLT is similar to the DFT (2.3b) in that we are seeking to expand the original time series $|x\rangle$ on an orthonormal basis set. The primary difference between the two lies in the fact that the Karhunen-Loéve basis cannot be known *a priori*, it must be determined directly from the data themselves. Additionally, the coefficients of the Karhunen-Loéve expansion form an orthogonal set. The expansion is given by

$$|x_m\rangle = \sum_{b=0}^{M-1} v_b[m] |a_b\rangle \tag{2.25}$$

where $|x_m\rangle$ is one of a set of M time series, each of length T, $|a_b\rangle$ is an orthonormal basis vector, and $v_b[m]$ is an expansion coefficient chosen from among a set of orthogonal vectors. As $T \to \infty$ the basis functions of the DFT for a general random process are qualitatively similar to those of the DKLT; for periodic random processes, the basis functions of the DFT are identical to those of the DKLT [*Therrien*, 1992]. However, for finite T, the DKLT provides the optimal description of the data in the mean square sense. For a formal

development of the DKLT, see Appendix A.

In terms of transform efficiency, the DKLT is unique in that it is the only transform which perfectly decorrelates the expansion coefficients and optimizes the storage of signal information (energy) among the basis functions [*Akansu and Haddad*, 1992]. This property has profound implications for pattern matching and feature selection problems in which the exact form of the input is unknown [*Fu*, 1968]. In the presence of contaminating noise, or unwanted signal, the DKLT can be used as for effective noise reduction [*Broomhead and King*, 1986]. Since the coefficients $v_b[m]$ scale as the information content of the signal, those that fall below some nominal value may be considered insignificant. We caution that this form of noise reduction carries with it the tacit assumption that signals comprise the bulk of the information content in a given data stream.

These properties of the DKLT are significant, considering the central problem we face in analyzing magnetometer data. The spectra we derive are largely the result of an un-specified process. While we may have a basic understanding of the cause of a portion of the spectrum, a large part of the information stems from processes unrelated to those we understand. As a result, we do not have a general mathematical description of the spectra, nor of the noise which appears with it.

In this work we have found two applications of Karhunen-Loéve theory in the field of geomagnetic pulsations. The first application takes advantage of its utility in pattern recognition processes, particularly the analysis of a large number of dynamic spectra. In the past, such examinations were conducted merely by eye [e.g., *McHarg and Olson*, 1992; *McHarg*, 1993; *Engebretson et al.*, 1995]; we attempt herein to place such analyses on more rigorous ground. The second involves using the noise reduction characteristics of the DKLT, in order to determine a possible characteristic ground-based magnetic signature of the magnetospheric cusp in the time domain. In both cases, we find that the technique provides new and useful physical insights.

2.3 Geophysical signal processing

The present work relies heavily on the techniques of discrete time series analysis to gain a physical insight into the processes which characterize the high-latitude coupling of the

magnetosphere and ionosphere. The use of such computationally intensive tools can lead us to equate deeper physical understanding with increased processing speed and algorithm efficiency. Nearly three decades ago we were cautioned that such is not the case; what we need is not more computational power, but better interpretive skills.

> In [our] experience, the fast computers which are now available are more than adequate for purposes of spectral analysis. Our present computing facilities are greatly in excess of our ability to make sense of practical data [*Jenkins and Watts*, 1968, p. 314].

Facility in the art of geophysical signal processing is tempered by two meta-principles. First, it is necessary to have an intimate knowledge of the characteristics of any technique brought to bear on the data. Each technique carries with it a set of advantages and limitations. The best way to develop a sense for these properties is to simply play with the techniques, gaining experience by applying them to both actual and contrived data sets. In this manner, one begins to gain an appreciation for what a particular method can extract from the data. Second, we must have the ability to separate physical results from non-physical ones.

2.3.1 Assumptions and results

When we consider our results, we are naturally mindful of the assumptions which we make when we model the physics of the situation. When we rely on signal processing to interpret the data, we must take a further step and become aware of how our signal processing assumptions constrain our results. In the application of a particular technique to data, we must be mindful that results peculiar to that technique can have a radical effect upon our interpretation.

Spectrum estimation provides an excellent example of how assumptions can influence an outcome. *Lacoss* [1971] showed that the shape of the spectrum varies greatly with the technique used to estimate it. He based his analysis on a known correlation function, so that he could determine the actual spectrum analytically. Employing various methods, he found that the ME-derived spectrum approximated the actual spectrum much more closely than the classical Fourier approach.

He cautions us however, that since the ME spectrum is model dependent, its application is most appropriate in situations where either the spectrum or the model order of the process responsible for the data are known *a priori*; in our case we have no such knowledge. We have found through numerical experimentation that ME spectra exhibit spurious spectral peaks. The number of ME spectral peaks varies roughly as half the model order. This causes us to find that the assumptions underlying the ME method are untenable, given what we know of the sources of our magnetometer pulsations.

At some point an assumption must be made concerning noise, or unwanted signal. We use the two terms interchangeably, as any signal not owing to the process we wish to study can be considered noise. In our case, where we have only incomplete knowledge of the input source, this assumption can lead us to discard information about the source as noise, or to include spurious information. Certainly this will have an effect on our results and interpretation. To mitigate this problem, we typically take a statistical approach to the data, so that we can average out the effects of noise and, hopefully, coax the signal to the fore.

Further, since we have incomplete knowledge of the noise in our magnetometer signals — whether it be unwanted signal from uninteresting magnetospheric or ionospheric processes, or instrument noise — we must make assumptions concerning its form. Typically, we assume white noise contamination in the signal, which can be shown to have a spectral matrix proportional to the identity matrix. We are cognizant that this assumption can break down at times, especially in the quantization noise from the instruments at extremely low signal levels, where the bit error level is of order the signal strength [*Jackson*, 1996]. This source of potentially correlated noise is a problem at high frequencies in fluxgate magnetometers, which have a pronounced rolloff in the Pc 3 frequency range [*Primdahl*, 1979].

2.3.2 Artifacts of processing

Fourier-based estimates taken with a small number of degrees of freedom can lead to unacceptable bias and variance. When we are processing signals with such methods, it is important that we determine whether a result is an artifact of our processing technique or a property of the data. A value of order unity for the polarization estimate (2.18) provides

an example. Is the estimate large due to a polarized signal, or is it because we have not made the estimate with enough degrees of freedom? If the latter is true, how do we know when we do have enough degrees of freedom in the estimate?

Such questions cannot be answered directly, but we can gain an intuition toward answering them. *Jenkins and Watts* [1968] describes a technique known as window closing, in which we are encouraged to explore the parameter space surrounding the construction of any estimate. This method allows us to gauge whether or not our processing technique will converge on a stable value or not. For the polarization estimate, we typically find that the value descends from order unity to a stable value as the degrees of freedom are increased to $\mathcal{O}(10)$ [*Olson and Szuberla*, 1997].

Finally, we caution against confusing feature-like properties in the results of processing techniques with physical reality. These are perhaps the most difficult artifacts to detect, because they appear to be real. *Wolfe et al.* [1994b] mistook the sidelobes of a particular window function to be peaks in the spectrum associated with a magnetospheric process. Sidelobes from leakage are a property of the window in question, not the physical process. The same window applied to any data would produce the same leakage characteristics in the sidelobes. Problems of this nature can be avoided through the use of surrogate or contrived data, allowing a determination of whether the feature is a function of the data or the technique [e.g., *Theiler et al.*, 1992a].

Chapter 3

Localized pulsations

In this chapter we begin our characterization of the cusp region through the analysis of magnetometer signals that are thought to have localized sources. A localized source of magnetic pulsations would presumably be a region of enhanced, modulated current at low altitude. This places the source region fairly close to the receiving station, nominally in the ionosphere. Given typical ionospheric currents, such sources should be situated no more than 150–200 km distant from a magnetometer station that can detect their signature [e.g., *Hughes*, 1974; *Hughes and Southwood*, 1976].

Engebretson et al. [1990] gave the first conclusive evidence of a localized source of magnetic pulsations at cusp latitudes. Their study made use of induction coil magnetometer, photometer and riometer data from two ground stations in Antarctica, one at cusp-latitude, the other poleward beneath the mantle. They found varying levels of correlation between the signals detected in each instrument. For a particular class of pulsations in the Pc 3 frequency band the photometer and magnetometer data streams were highly correlated, while the riometer data showed little correlation with either instrument.

Given the absence of an appreciable time delay between the photometer and magnetometer signals, they concluded that the Pc 3 fluctuations were generated in the overhead ionosphere and not in the distant magnetosphere. They infer that modulated precipitation of electrons is the proximate cause of the observed magneto-optical correlations. Beams of precipitating electrons will produce optical emissions during collisional interactions with ionospheric constituents; they will also modify local conductivities, allowing currents to

43

flow. When such beams are modulated at Pc 3 frequencies, the optical emissions and current magnitudes will also be modulated at like frequencies. The lack of a correlated riometer signal is taken to reflect an upper limit on the electron energies, since riometer observations reflect the density of electron populations with energies $\geq$ 5–10 keV [*Matthews et al.*, 1988]; this suggests cusp-like precipitation [*Newell and Meng*, 1988].

Localized source regions presumably give rise to pulsations that are detectable only over a finite spatial extent. *Olson and Szuberla* [1997] developed a quantitative technique to estimate an upper bound on the spatial scale size of this class of pulsations. They analyzed the characteristics of Pc 3 pulsations recorded over a period of thirteen days at Cape Parry and Sachs Harbor, specifically the distribution of interstation coherence in both time and frequency.

In this chapter we extend the work of *Olson and Szuberla* [1997] by examining magnetometer records drawn from a much larger database. We make use of several station pairs distributed throughout the statistical latitudinal extent of the cusp and boundary regions, in both hemispheres. We find that the original technique used to determine the coherence length is biased by the presence of uncorrelated noise and develop an unbiased method. From the measure of interstation coherence we arrive at a simple model that places an important physical constraint on the possible sources of this class of pulsations.

The analysis of localized pulsations that comprises this chapter serves a twofold purpose. Our first objective is to characterize the state of interstation coherence at cusp latitudes in the Pc 3 frequency band. Second, we want to estimate an upper bound for the horizontal coherence length of a precipitating electron beam as described by *Engebretson et al.* [1990]. Additionally, we would like to relate these two objectives to the future deployment of magnetic observatories at cusp latitudes.

3.1 Pulsations observed at multiple stations

The stations studied by *Engebretson et al.* [1990] were separated by more than 1300 km, a distance greater than the statistical latitudinal extent of the cusp as reported by *Newell and Meng* [1992]. Since the Pc 3 pulsations detected at cusp latitude were shown to be locally generated, it is not surprising that the magnetometer signals were poorly correlated

between the two distant stations.

Using a pair of more closely spaced stations (202 km) in the UA network we found that the spectra taken at each station were qualitatively similar. In Figure 3.1 we see representative spectra for five consecutive days at each station, both nominally at cusp latitude. Figure 3.1 depicts the regularity with which relatively large, band-limited amplitudes are observed near noon. Note that on each day we see peak power in each of two frequency bands: 1–15 mHz (nominally Pc 5) and 15–50 mHz (nominally Pc 3). Pulsations of the type reported by *Engebretson et al.* [1990] are present in the spectra at each station, centered roughly on magnetic local noon.

In the database of Cape Parry and Sachs Harbor magnetometer spectral records, we find several events in the Pc 3 frequency band that bear a striking similarity to one another. One such event is shown in Figure 3.2, which is created from data taken 29 May 1985. At roughly magnetic local noon (2200 UT at each station) we observe a broadband signal, from 25–45 mHz, at each station. The signal is of significant power and persists for one-half hour. Here the data have been four-channel pure-state filtered to reduce the signal contamination by uncorrelated noise present in the station spectra [*Samson and Olson*, 1981]. Several such events, with characteristic spectral and temporal structure, were simultaneously observed at both stations.

Olson and Szuberla [1997] noted the character of the Pc 5 power [*McHarg and Olson*, 1992] associated with the Pc 3 events and concluded that the latter were associated with the overhead passage of the ionospheric footprint of the cusp-boundary region. They stressed the need for a quantitative comparison of the data taken at each station. Despite the marked similarity in the Pc 3 portion of the spectra, a visual comparison of spectral provides only a qualitative understanding.

For each Pc 3 event noted between the two stations, they performed a correlation analysis and found that the correlation between stations in the Pc 3 frequency band generally increased with the passage of local noon and the cusp-boundary region; following the passage, correlation levels subsided to their pre-noon levels. The results of such an analysis for the event shown in Figure 3.2 are given in Figure 3.3. An important finding of the cross-correlation study of the Pc 3 events was that the maximum magnitude of each half-hour cross-correlation estimate shown in Figure 3.3 occurred at zero lag. Uncertain-
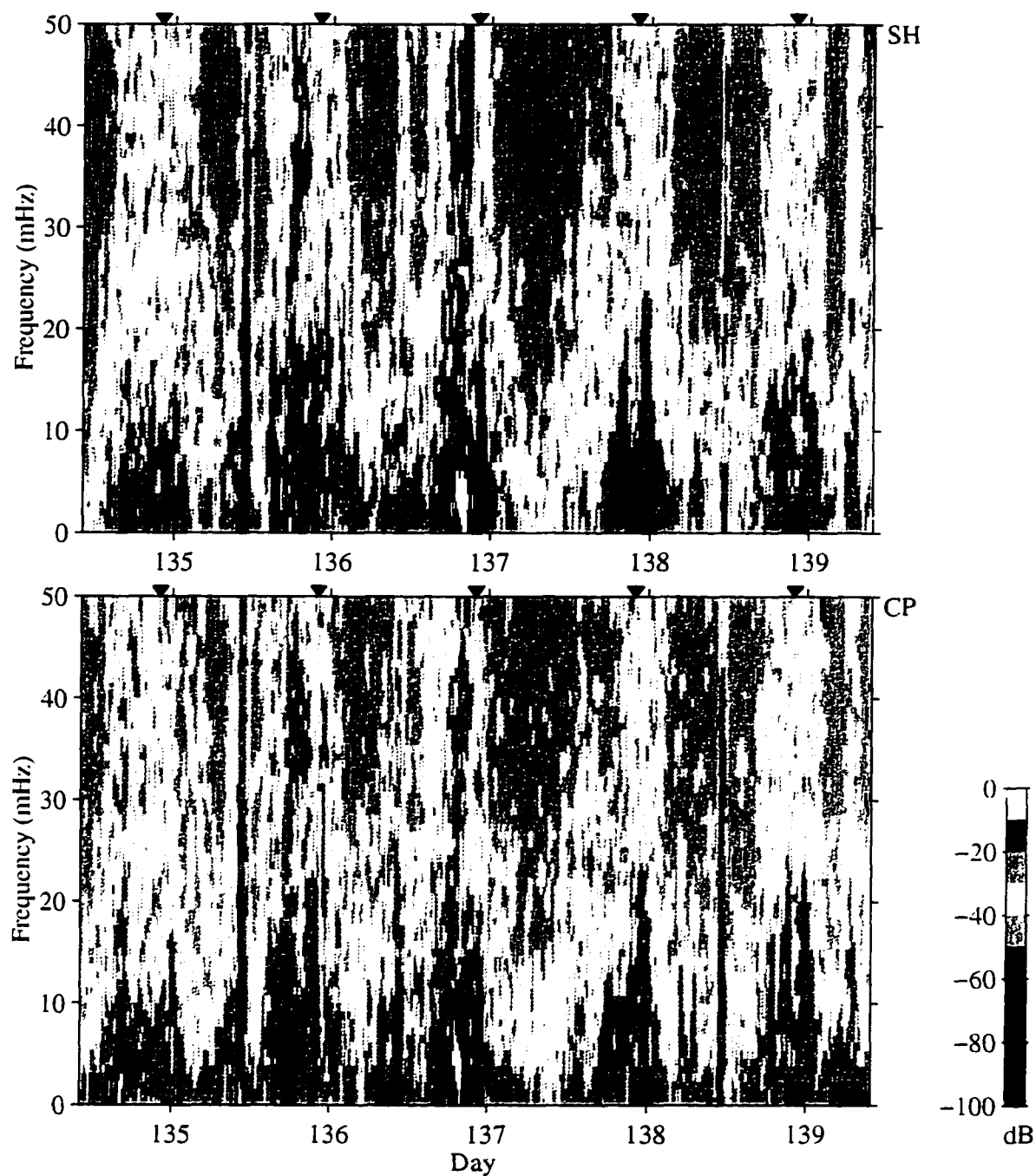
Figure 3.1. Representative spectra of five consecutive cusp passages. The data were taken at Cape Parry and Sachs Harbor 14–19 May 1985. The panels depict trace power in the horizontal components of the induction coil magnetometer data taken at each station separately. Magnetic local noon is approximately 2200 UT and is marked by small triangles in each panel. At each station there is a general increase in Pc 3 power centered roughly on local noon.
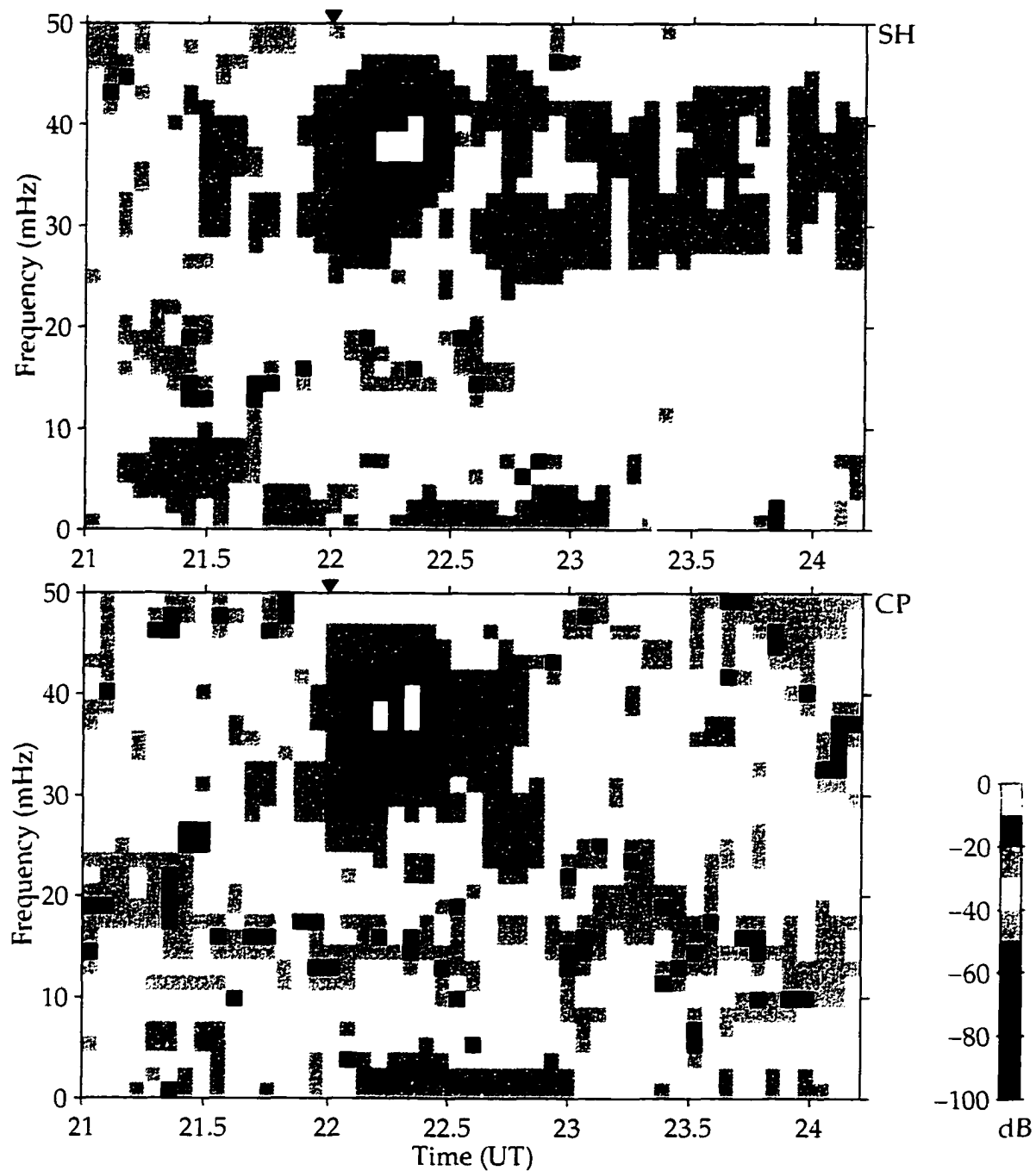
Figure 3.2. Pc 3 event recorded at two stations. The data were taken at Cape Parry and Sachs Harbor on 29 May 1985. Shown in the panels are four-channel pure state filtered trace spectrograms from each station. Note the similarity in enhanced Pc 3 power for one-half hour at both sites, beginning at approximately local noon (2200 UT).
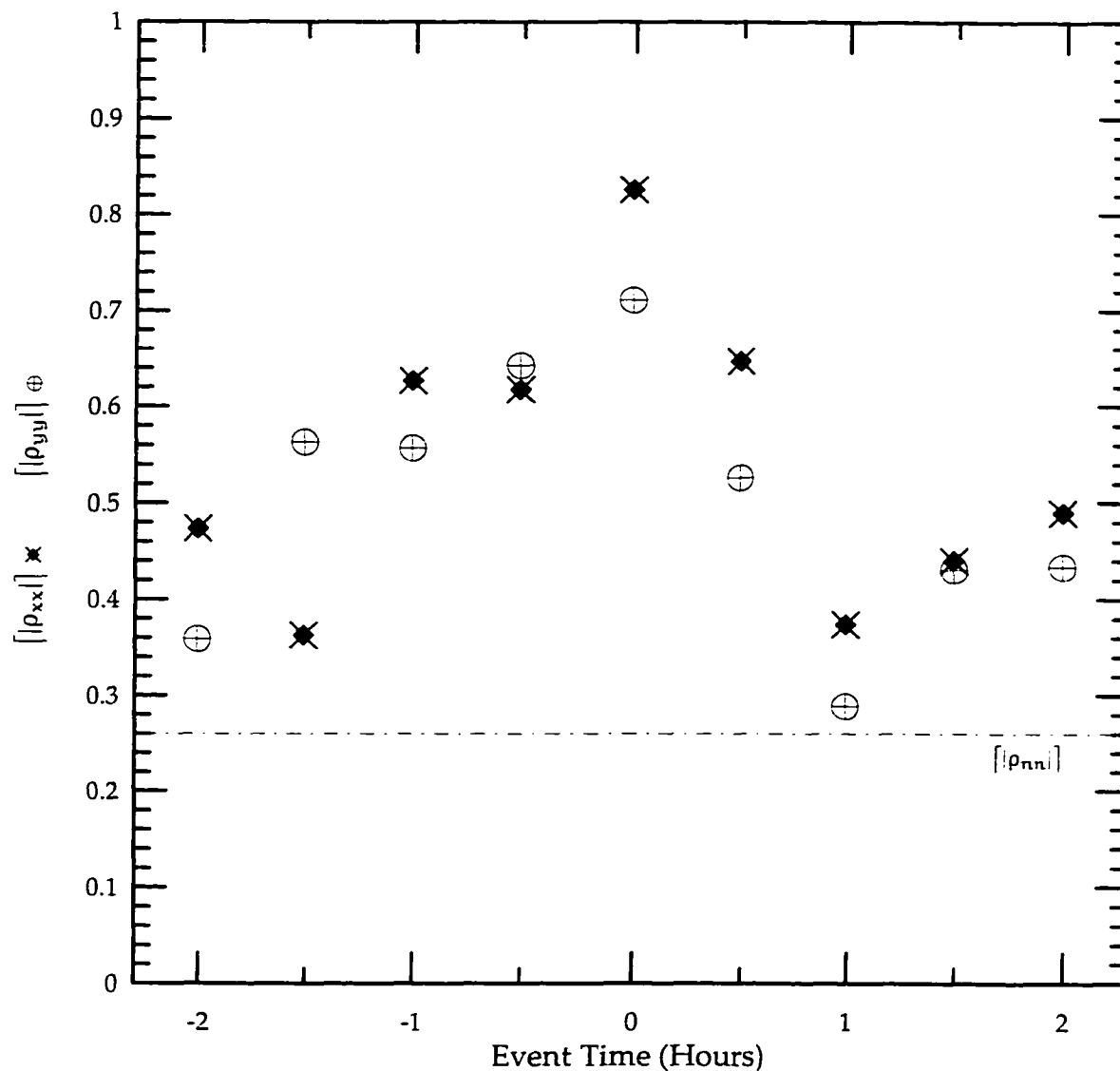
Figure 3.3. Maximum amplitudes of interstation cross-correlations for a Pc 3 event. The data were taken at Cape Parry and Sachs Harbor on 29 May 1985. Zero-hour for the event is taken to be 2200 UT, roughly magnetic local noon. Each point plotted is the maximum magnitude of the cross-correlation function between interstation x- and y-components. The cross-correlation functions were estimated from bandpass filtered (25–45 mHz) time series of one-half hour in length. Each series was centered on the time indicated for each point in the plot. The dashed line represents the expected value plus one standard deviation for two signals of white noise. In each case, the maximum magnitude of the interstation components is the value at zero lag.

ties in the time base at each station, derived from the time code signal transmitted by the GOES satellites, are limited to ± 1 s. Unlike an earlier study by *Olson* [1989] in the Pc 5 frequency band using the same database, which showed a 1–5 km/s poleward motion for those pulsations, the broadband Pc 3 appeared stationary within the view of each station.

The simultaneity of the broadband Pc 3 pulsations at each station gave the first concrete evidence that their localized source must have some finite spatial size. These results were consistent with those of *Engebretson et al.* [1990] in that the broadband Pc 3 were associated with the cusp. The high levels of correlation between the two sites were indicative of a common source. Comparing the results of their own correlative study to those of *Engebretson et al.* [1990] (noting a lack of correlation over a 1300 km station separation in the latter) led Szuberla and Olson to postulate that a spatial extent on the order of the Cape Parry and Sachs Harbor station separation (202 km) was not unreasonable for the localized source of the broadband Pc 3 pulsations. The correlative analysis alone however, was insufficient to accurately estimate that spatial scale size.

3.2 Statistical coherence length

Once the correlations of broadband Pc 3 pulsations at Cape Parry and Sachs Harbor had been established, *Olson and Fraser* [1994] extended the work, using interstation coherence as an indicator of the presence of these signals. Estimates of the coherence function between stations have an advantage over estimates of the cross-correlation function in that the data need not be filtered to isolate certain frequency bands; the coherence estimator is by definition a function of frequency. Further, the coherence-based analysis allowed for a simultaneous comparison of pulsations in different frequency ranges. This is important because *McHarg and Olson* [1992] identified the passage of the cusp and boundary layers via correlations between optical measurements and Pc 5 magnetic pulsations. *Olson and Fraser* [1994] again concluded that the scale size of the localized source of broadband Pc 3 pulsations ought to be of order the station separation. Their analysis, like the previous correlative study, was strictly event-based, and as such afforded no way to estimate the scale size.

While event-based studies are an important facet of research in space physics, *Chapman*

[1968] cautions us that there is a need for statistical studies as well. With regard to magnetometer studies, we cannot emphasize this remark strongly enough. Magnetic pulsation event studies are conducted on the assumption that signals present in the data will conform to some preconceived notion of how a known physical process will manifest itself. Unfortunately, not all the processes in the Earth's magnetosphere and ionosphere are well understood. A statistical study can help us set aside our "cartoon" understanding and let us see what the data themselves will tell us.

In that light, *Olson and Szuberla* [1997] turned to an ensemble of thirteen days of data, taken from Cape Parry and Sachs Harbor, in an effort to determine the scale size of these pulsations statistically. Herein we extend that work with an examination of several more pairs of cusp latitude stations and more than 900 days of interstation magnetometer data. Using the larger data set we determine that the interpretation of the coherence length by *Olson and Szuberla* [1997] was biased by noise; the present study eliminates that bias. The expanded analysis results in a reliable estimate of an upper bound for the coherence length of localized Pc 3 pulsations at cusp latitudes. This leads us to develop a simple model for this class of pulsations. Table 3.1 provides details of the station pairings used in this study.

3.2.1 Broadband pulsations

A wide variety of magnetic variations is ordinarily observed as a ground station rotates beneath the ionospheric footprint of the cusp and boundary regions. The nature of these pulsations, as they are detected on the ground, and their associated spectra were well documented roughly a decade ago [*Kato et al.*, 1985; *Troitskaya*, 1985; *Tonegawa et al.*, 1985; *Olson*, 1986; *Engebretson et al.*, 1986, 1987]. In particular, the Pc 3 portion of the spectrum is comprised of at least three distinct types of wave energy: quasi-monochromatic wave packets [*Engebretson et al.*, 1994; *Olson and Fraser*, 1994], band-limited pulsations [*Engebretson et al.*, 1990; *Olson and Szuberla*, 1997], and colored noise with power proportional to frequency: $P(f) = kf^{-\alpha}$ [*Wolfe et al.*, 1994a]. The localized Pc 3 pulsations described by *Engebretson et al.* [1990] differ from noise in that they have band-limited spectral characteristics (see Figure 3.2); they typically have a bandwidth of $\gtrsim$ 10 mHz and are what we term broadband. These pulsations are distinct from the quasi-monochromatic wave packets observed both on the ground and in the outer dayside magnetosphere [*Takahashi and McPherron*,

Station Pair	Separation (km)	Mean MLN (UT)	No. of Days
Pelly Bay – Gjoa Haven	252	1841	217
Repulse Bay – Pelly Bay	267	1808	104
Coral Harbor – Repulse Bay	301	1745	81
Cape Dorset – Coral Harbor	320	1715	62
Davis – Zhong Shan	110	0920	31
Cape Parry – Sachs Harbor	202	2200	13
Gjoa Haven – Repulse Bay	473	1828	93
Repulse Bay – Cape Dorset	513	1725	48
Pelly Bay – Coral Harbor	569	1758	86
Pelly Bay – Cape Dorset	753	1738	57
Gjoa Haven – Coral Harbor	754	1818	71
Gjoa Haven – Cape Dorset	983	1758	46

Table 3.1. Station pair parameters for the coherence length study. The upper block contains the MACCS which are adjacent to one another. The next blocks contain the ANARE array and the UA network. The final block, separated by double lines, contains the MACCS stations which are not adjacent to one another. Data from the MACCS stations were kindly provided by Mark Engebretson of Augsburg College, and the ANARE station data were supplied courtesy Brian Fraser of the University of Newcastle.

1982; *Engebretson et al.*, 1986; *Olson and Fraser*, 1994].

At this point we note an important difference in convention between this thesis and the work of *Engebretson et al.* [1990]; the pulsations they refer to as narrowband we term broadband. Largely, the matter is one of interpretation. Given their effective 500 mHz Nyquist frequency, what they see as narrowband fairly fills our spectra. Our term broadband is used to explicitly differentiate between the background of wave energy and the short-lived, quasi-monochromatic wave packets that comprise the spectrum. These wave packets typically have a bandwidth $\lesssim 1$ mHz; e.g., less than Δf in the spectra shown in Figure 3.4. We stress that both studies are consistent in their findings, if not their terminology, as each refers to the same general class of Pc 3 pulsations.

It is also important to note that our study does not rely on differentiating between the two classes of Pc 3 pulsation. Rather than attempt to isolate and extract the packet-like information from the data, we rely on spectral and statistical methods that treat the entire Pc 3 band as a whole. Resolving any packet-like structure (which comprises only a fraction of time series at any given station) within the broadband Pc 3 requires a detailed inspection of the time series used to compute the spectra shown in Figure 3.2. [e.g., *Engebretson et al.*, 1986; *Olson*, 1989].

Based on previous studies of cusp latitude pulsations, we extend the operational definition of Pc 3 pulsations of *Jacobs et al.* [1964] (22–100 mHz) to include all pulsations between 15 mHz and 100 mHz. This spectral division into bands at roughly 15 mHz is a feature common to cusp-latitude stations [*Olson and Fraser*, 1994; *McHarg et al.*, 1995]. Twelve station pairs were used to estimate the interstation coherence of localized Pc 3 pulsations. In Figures 3.4 and 3.5 we present typical examples of spectra taken from station pairs in the MACCS and ANARE arrays (examples of Cape Parry and Sachs Harbor are shown in Figures 3.1 and 3.2). Note the similarities and differences among each pair.

There is a striking difference in the characteristic power rolloff with frequency between Figures 3.4 and 3.5. This is a characteristic of the instrumentation at each station, not the pulsations recorded there. The MACCS array (Figure 3.4) is equipped with fluxgate magnetometers, which record the magnetic field at the station, while the ANARE array (Figure 3.5) is equipped with induction coil magnetometers, which record the time rate of change of the field. Thus the latter instrument effectively multiplies the trace power

j
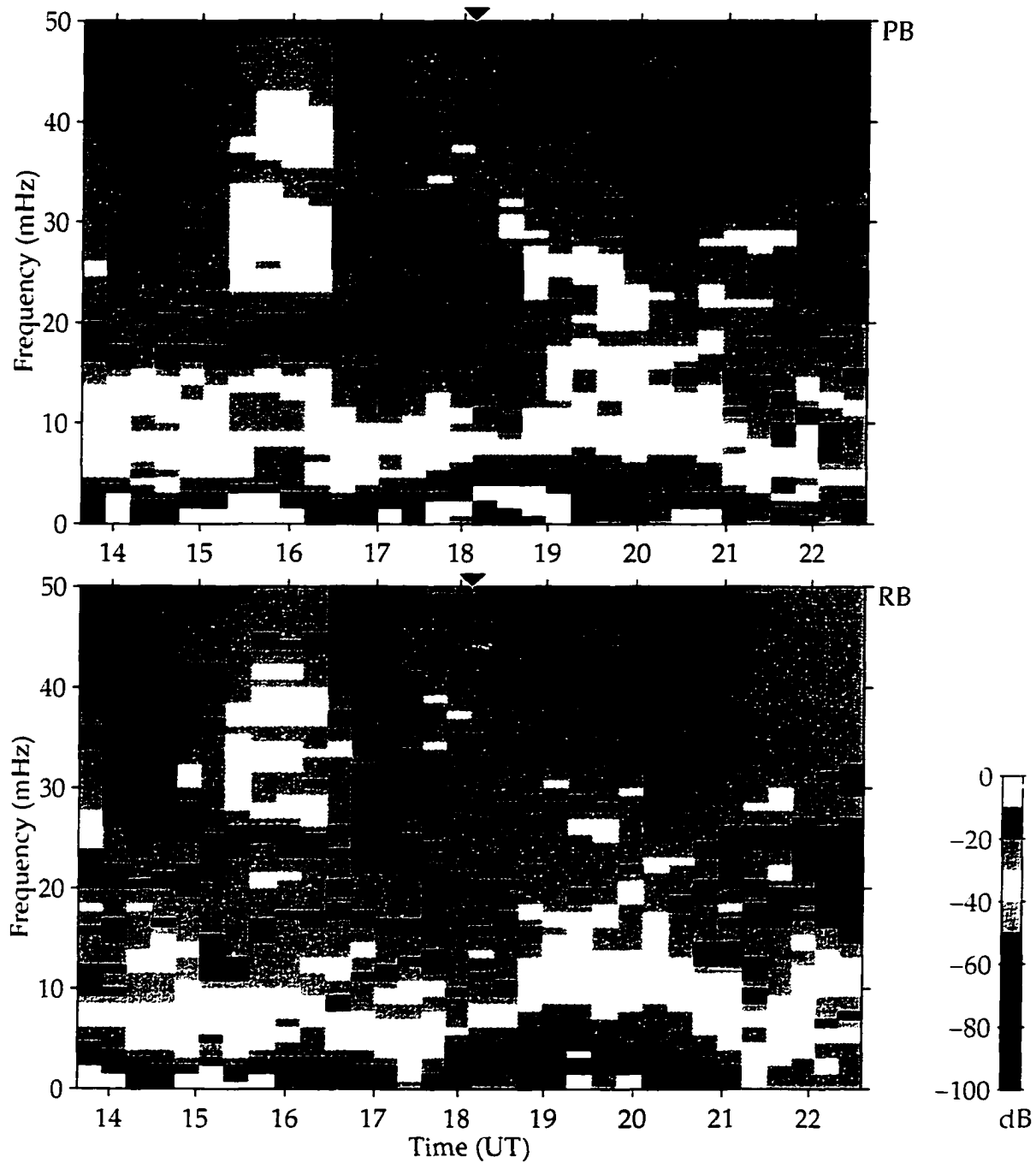
Figure 3.4. Dynamic spectra for 17 October 1994 taken from the MACCS stations at Repulse Bay and Pelly Bay. Shown in each panel is the trace power in each of the horizontal components at each station. The stations are separated by a distance of roughly 267 km. Note the near simultaneous Pc 3 power enhancement near 1500 UT at both stations. Another Pc 3 enhancement appears near 2200 UT, but only at one station.
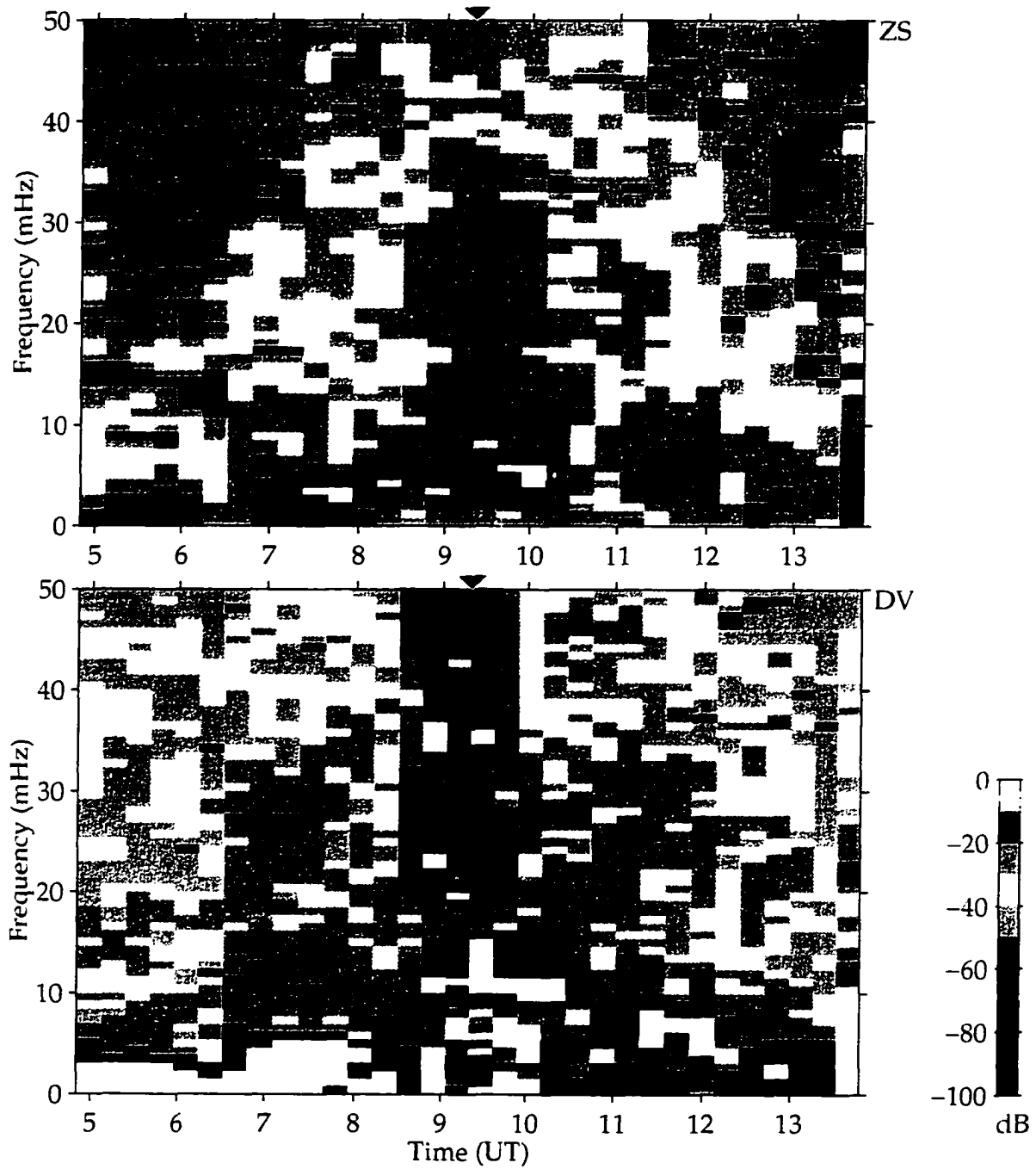
Figure 3.5. Dynamic spectra for 29 June 1996 taken from the ANARE stations at Davis and Zhong Shan. The format is as for Figure 3.4. The stations are separated by a distance of roughly 110 km. This is a prime example of a Pc 3 power enhancement near local noon. Note the marked difference in power rolloff with frequency in this figure and Figure 3.4.

at each frequency estimate by a factor proportional to the frequency squared. Thus, the induction coil is a more sensitive instrument at higher frequencies. As we shall see, this has some bearing on our statistical analysis.

3.2.2 Statistical analysis

Coherence measures are based on spectral analysis; the frequency resolution of such an estimator varies as the amount of data used to compute it. Thus a coherence estimate with high frequency resolution necessarily has low time resolution. In satisfying our first objective, characterizing the state of interstation coherence at cusp latitudes, it is important not only to arrive at a characteristic coherence level (either in the mean or limiting sense) but also to determine how that coherence varies in time (if at all). We must therefore find an optimal length for the data streams that feed our analysis.

For a small number of degrees of freedom, coherence estimates are biased toward unity; in a similar, but unrelated, effect, the estimator values tend to be biased artificially high for short data streams. Recognizing this, we begin by taking short data streams and increasing their length until the coherence values descend toward a stable value. Selecting data streams spanning from one-third to two hours, we find that for times one hour or longer a stable coherence value is generally attained. We take this as evidence that the coherence estimates have descended to near the true values. From this behavior, we also conclude that we cannot confidently resolve interstation coherence estimates to better than one hour in time. Hence we use one-hour data streams from each station as the basis for all coherence estimates in the study.

A one-hour length of data is optimal for estimating interstation coherence in terms of reliably maximizing both frequency and time resolution. We select individual one-hour periods from our data via a rectangular window and thus obtain a coherence estimate across a band of frequencies for that particular hour. In order to later build a statistical description of independent coherence estimates, we select hours of data sequentially, such that they do not overlap in time. By "stepping" these hour-long rectangular windows through the data, we begin to build a picture of the time evolution of interstation coherence.

For each day in our study, Pc 3 pulsation activity is clearly peaked at both stations near local noon (e.g., Figure 3.1). This increased activity gives us a natural starting point for

our analysis. We select an interval which spans a number of hours centered on local noon and compile coherence estimates for those hours. For spans in the range 6–14 hours, we find no noticeable change in the coherence statistics outlined below. On the basis of this we have taken our standard interval to be eight hours in length, centered on the median value of magnetic local noon at each station pair (see Table 3.1). This choice of analysis parameters is consistent with previous studies of the cusp at the same stations used in our study [*Olson*, 1986; *Engebretson et al.*, 1995; *Ables et al.*, 1996].

From each station we select eight hours of induction coil magnetometer data centered on local noon. We pair off their x- and y-components together in order to calculate two interstation measures of coherence, $C_{xx}(f)$ and $C_{yy}(f)$. Taking a component pair, x-x for example, we step a one-hour rectangular window sequentially through the eight hours of data to make coherence estimates. Within each hour the *Welch* [1970] method employs a series of overlapping subwindows to estimate power spectral densities with approximately ten degrees of freedom. In this manner we reduce the bias toward unity in the coherence estimates.

The work of *Olson and Szuberla* [1997] was carried out across a single array. In this study we contend with three different sampling rates: 0.1 Hz at the UA stations; 0.2 Hz at the MACCS array; and 0.5 Hz at the ANARE array. To make this study consistent with that of *Olson and Szuberla* [1997] we choose the length of each Welch subwindow such that the number of frequency estimates is identical in the frequency range available to the original Cape Parry and Sachs Harbor study. The net result is two (one for each component) 33 by 8 matrices of coherence estimates in frequency and time for each day, for each station pair. The matrix elements have dimension 1.52 mHz by 1 hour, for a total of 264 estimates of interstation coherence in each channel. The span of these estimates is from dc–50 mHz in frequency and MLN±4 hours in time.

A graphical representation of this matrix takes the form of a coherence spectrogram. Such spectra are common to pulsation studies at or near the cusp [e.g., *Bering et al.*, 1995; *Waters et al.*, 1995]. In Figure 3.6 we show a set of such spectrograms taken from Repulse Bay and Pelly Bay in the MACCS array (the same data were represented in Figure 3.4 as a traditional spectrogram). The top and bottom panels depict the interstation coherence estimates for the x- and y-components, respectively. Comparing Figures 3.4 and 3.6 we
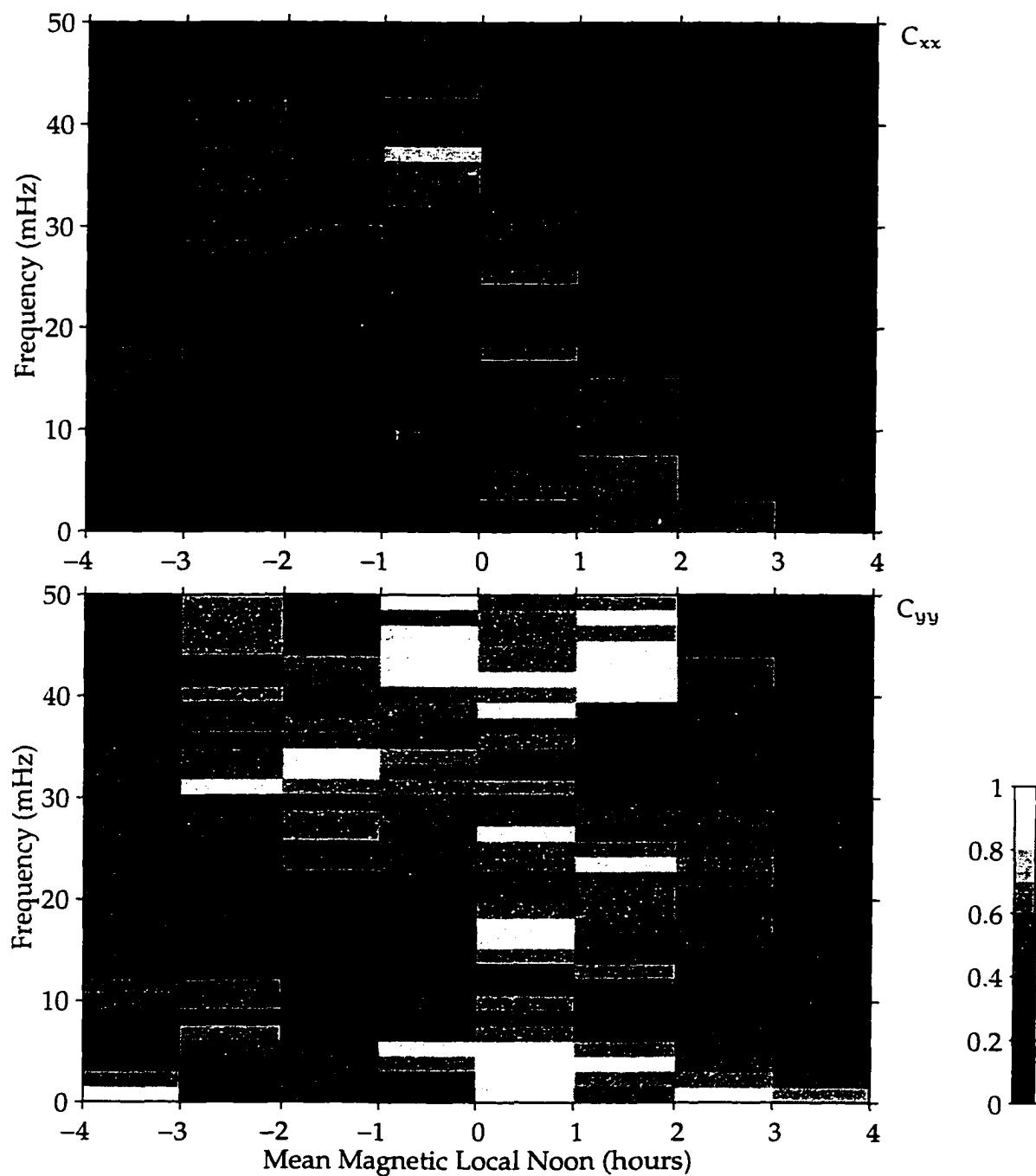
Figure 3.6. Coherence spectra for 17 October 1994 taken from the MACCS stations at Repulse Bay and Pelly Bay. Shown in each panel is the interstation coherence for the x-components C_{xx} (top) and y-components C_{yy} (bottom). Note that the interstation coherence bears little resemblance to the trace power shown in Figure 3.4.

58

caution that a visual inspection of power spectra is not a reliable indicator of interstation coherence. The ensemble of such spectra we derive from our magnetometer data exhibit no obvious ordering in amplitude, frequency or time. On this basis we turn to a statistical description of the coherence data.

Since the interstation coherence estimates at each (f, t) pixel in the coherence spectra are computed independently of one another we can collect them together and analyze their distribution. From among the coherence estimates we select only those that correspond to our operational definition of the Pc 3 frequency band (15–50 mHz). This gives us 184 estimates in each component for each day at each station pair (e.g., those displayed in the upper portions of Figure 3.6).

We are interested in two statistical properties of the coherence data: the probability density function and the cumulative distribution function [*Jenkins and Watts*, 1968]. We can estimate them, in a manner consistent with *Prichard et al.* [1996], via the probability and distribution functions, respectively. The probability function assesses the probability that a particular coherence level will be observed. The distribution function determines the probability that a coherence estimate will fall below a certain value; equivalently, it gives the coherence level at which a particular fraction of the data is accounted for. Rather than simply bin the coherence data, we use the technique of kernel density estimation to compute the probability function [*Rosenblatt*, 1956]. Following the method of *Silverman* [1978] we find that a kernel width $\delta C = 0.048$ gives us a stable statistical description of the coherence data. Figure 3.7 shows the result when the data used to produce Figure 3.6 are selected. The upper panels (a) depict the probability functions, $f(C_{xx})$ and $f(C_{yy})$, for the coherence estimates. The lower panels (b) show the distribution functions, $F(C_{xx})$ and $F(C_{yy})$, corresponding to the probability function in (a). Also indicated in the lower panels is the approximate value of $1 - F(0.5)$, which indicates the percentage of the coherence that is not due to noise.

Olson and Szuberla [1997] considered the probability and distribution functions of the interstation coherence estimates only for Cape Parry and Sachs Harbor. The probability functions (like those shown in Figure 3.7) were relatively uniform among the thirteen days of data available for study. Based on this information they determined that the coherence level which accounted for a particular fraction of the data (they selected the 90 percent
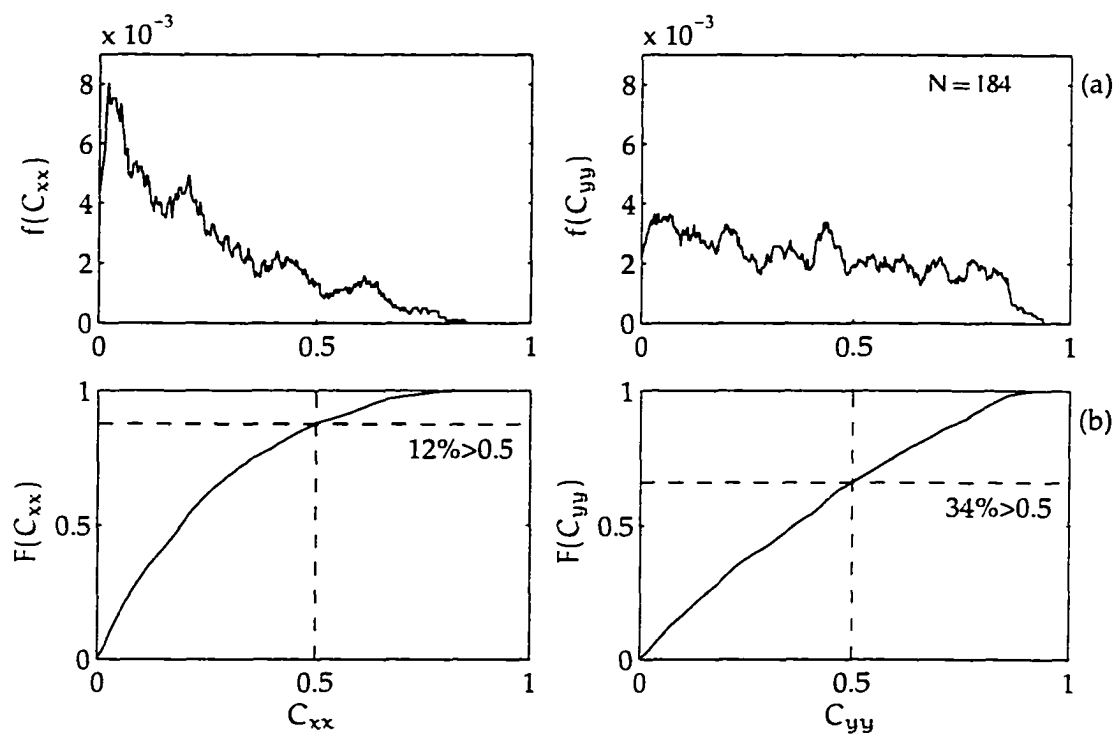
Figure 3.7. Pc 3 coherence statistics for 17 October 1994 taken from the MACCS stations at Repulse Bay and Pelly Bay. Statistics are derived from coherence spectra of Figure 3.6. (a) Probability functions, $f(C_{xx})$ and $f(C_{yy})$, for the 184 Pc 3 frequency band interstation coherence estimates in the x- and y-components. Arbitrary units are used on the vertical scale, and a kernel width $\delta C = 0.048$ is used to compute the probability function. N indicates the number of coherence estimates used to compute the probability function. (b) Distribution functions, $F(C_{xx})$ and $F(C_{yy})$, calculated from the probability functions, which indicate percentage of the coherence values that fall above a fiducial noise value, $C \geq 0.5$ in this case (see text for details).

level) was a reliable indicator of the general level of interstation coherence. Given the opportunity to examine a much larger database, we find that the probability functions exhibit a wide variety of shapes (note the disparity between the form of $f(Cxx)$ and $f(Cyy)$ in Figure 3.7). What we have found is that a noise-dominated probability function can yield the same results as one that is dominated by a coherent signal; ie., the coherence length measure of *Olson and Szuberla* [1997] was biased by the presence of noise at each station.

In order to arrive at an unbiased measure of the coherence length we first consider the

probability and distribution functions of the coherence estimator for a white noise process. We simulate 1300 days of white noise interstation data and display the results in Figure 3.8. We find that virtually all (99.74 percent) of the noise-derived coherence estimates fall below a value of $C = 0.5$. It can be shown that this level roughly corresponds to the mean coherence level plus one standard deviation for a white noise process [*Olson and Fraser*, 1994]. With a relatively high degree of confidence we select $C = 0.5$ as our fiducial noise value; coherence estimates above this value may be considered reliable, those below owing to noise. By discriminating among coherence estimates with regard to this fiducial noise level, we have eliminated the bias in our determination of the coherence length. After this fashion we determine that the percentage of coherence estimates that satisfy $C \geq 0.5$ is a reliable characterization of the state of interstation coherence. [1]

We next gather all available coherence estimates together for each of the station pairs listed in Table 3.1 and analyze their distributions in the same way we looked at a single day in Figure 3.7. In Figures 3.9 through 3.12 we show a sampling from this catalog. Note the variety in the form of the probability functions (a, in each figure). Comparing the distribution functions (b, in each figure), we find that the percentage of coherence estimates that satisfy $C \geq 0.5$ falls off roughly as the station separation increases (Figures 3.9 through 3.12 are presented in order of increasing station separation).

To test whether these distributions differ significantly from that of noise (ie., $f(Cnn)$ in Figure 3.8) we employ the Kolmogorov-Smirnov (K-S) test. The K-S test assesses the probability of the null hypothesis that two sets of data are drawn from the same distribution [*Press et al.*, 1992]. For all twelve station pairs, we find the probability of their distributions being noise-derived vanishingly small. We do note however that the probability of a noise-derived distribution rises remarkably quickly with increasing station separation (from $\mathcal{O}(10^{-100})$ to $\mathcal{O}(10^{-4})$) in the range available to our study).

Among the cumulative distributions we compile, we find that the percentage of coherence estimates that satisfy $C \geq 0.5$ is not dominated solely by either the x- or y-component. Since we rotated the MACCS data into geomagnetic coordinates, we are concerned that any measure of interstation coherence we develop is roughly rotationally invariant. What

---

[1] An identical analysis of interstation polarization yields similar results; however, for the sake of clarity we present only the coherence results here. Recall that we use the two estimators in concert as a check that our estimate of the coherence level is reliable.
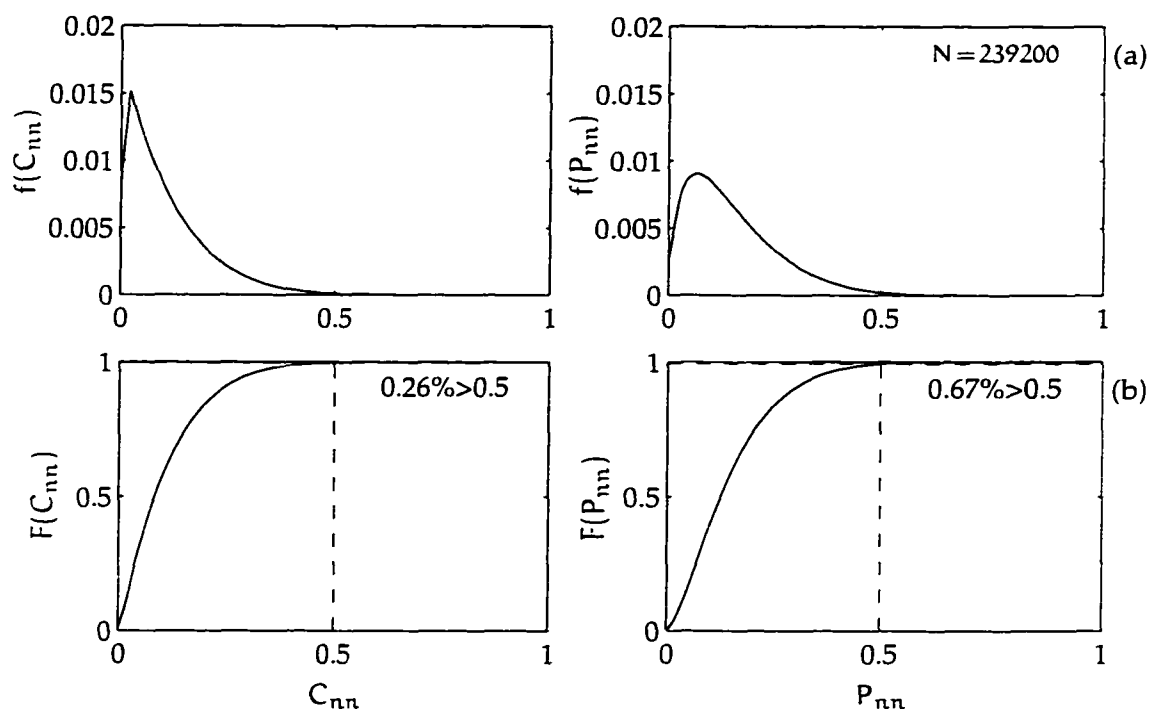
Figure 3.8. Pc 3 coherence and polarization statistics for 1300 days of simulated noise. The format is as for Figure 3.7, except that the noise characteristics of the polarization estimator are shown for comparison. For the coherence estimator (a and b, left), only 0.26 percent of the coherence estimates fall above the fiducial noise value.

we have found is that the mean of the component-wise percentage levels satisfying $C \geq 0.5$ is roughly rotationally invariant, to within a few percent.[2] This gives us a quantitative measure of the interstation coherence, or "coherence level" C_L, which we define to be

$$C_L \equiv 1 - \frac{F(C_{xx}) + F(C_{yy})}{2} \tag{3.1}$$

in Table 3.2 we list the values of C_L computed across all the station pairs available to this study. We notice a general trend: C_L falls off as the station separation increases. The results from the induction coil magnetometers are given separately, as they seem to yield smaller values for C_L than similarly spaced fluxgate magnetometers (the same trend is

---

[2]Concerning our parallel polarization analysis, we note that the distributions produced are not rotationally invariant in the same strict sense as the polarization estimator itself. The polarization estimator is defined trace invariant. The percentage of polarization estimates that satisfy $P \geq 0.5$ is only roughly rotationally invariant. This effect is caused by our method of breaking the eight-hour time series into hour-long segments and is further complicated by the subwindowing inherent in the Welch method.
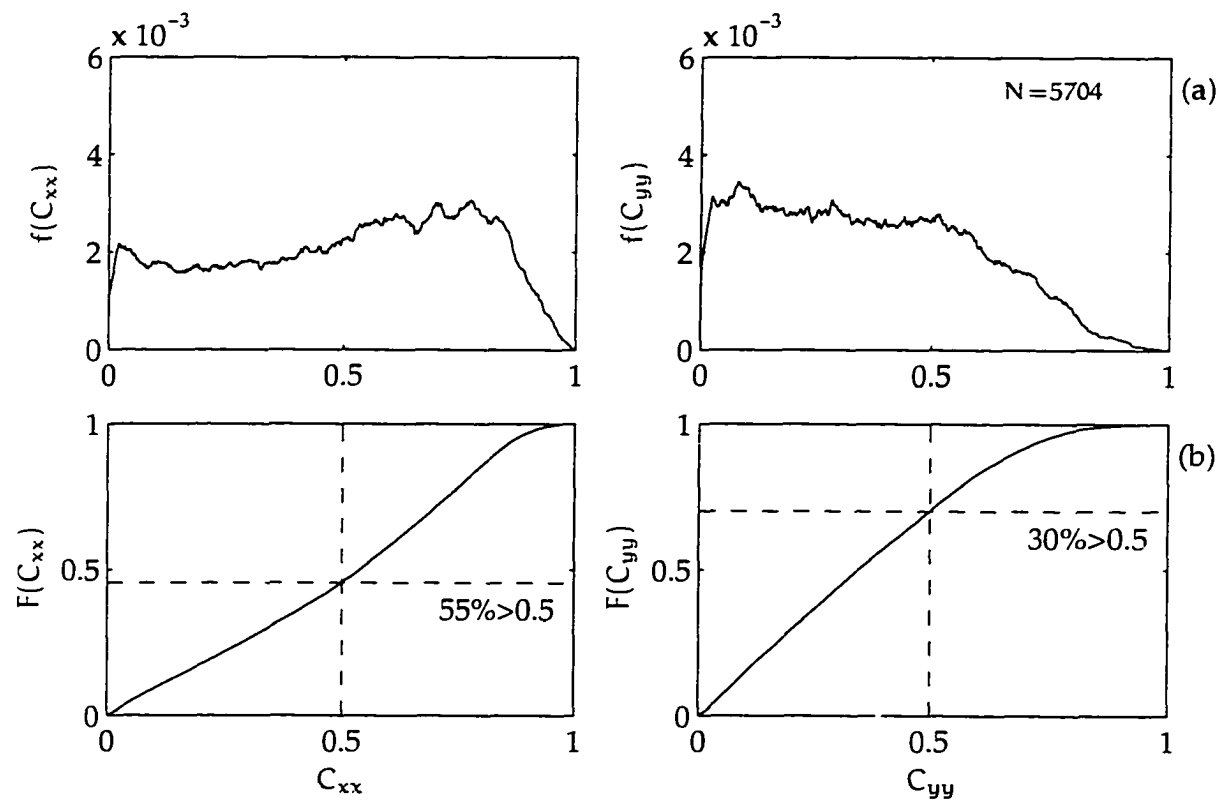
Figure 3.9. Cumulative Pc 3 coherence statistics for Davis and Zhong Shan. The station separation is 110 km. Figure format is as for Figure 3.7 (see text for details).
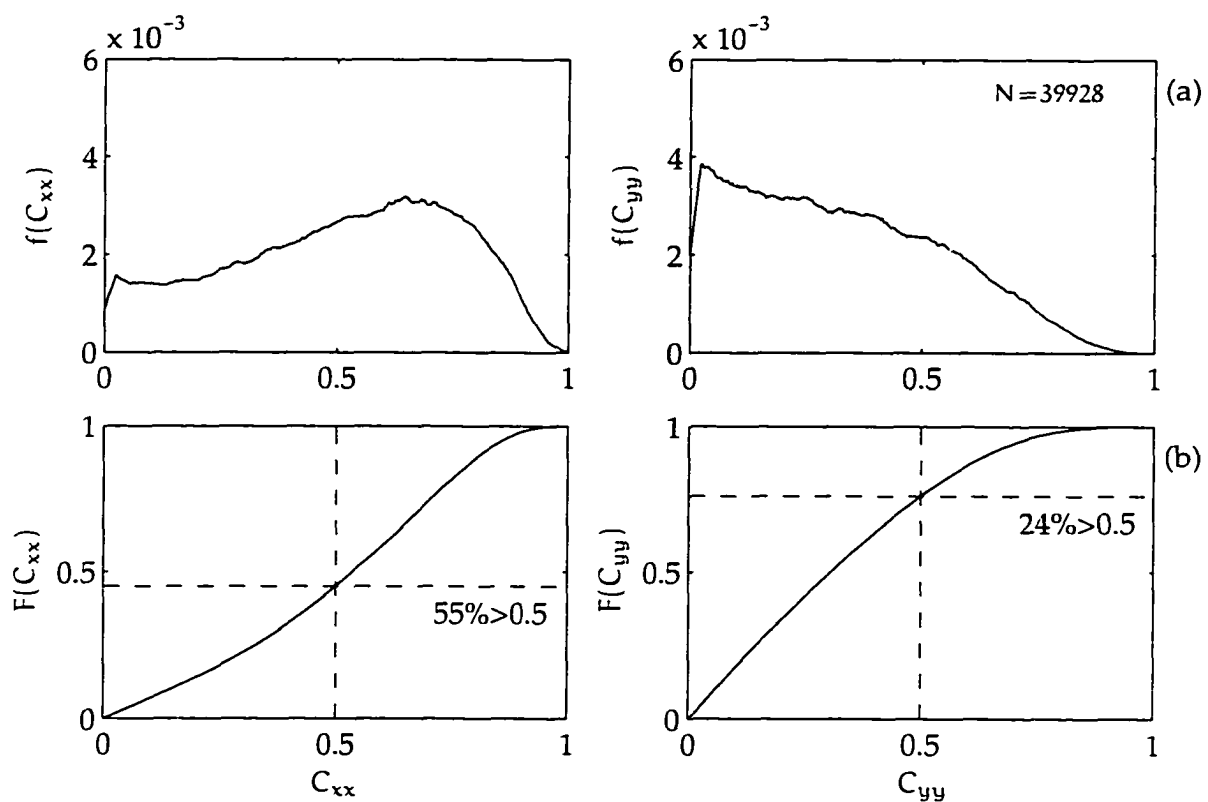
Figure 3.10. Cumulative Pc 3 coherence statistics for Pelly Bay and Gjoa Haven. The station separation is 252 km. Figure format is as for Figure 3.7 (see text for details).
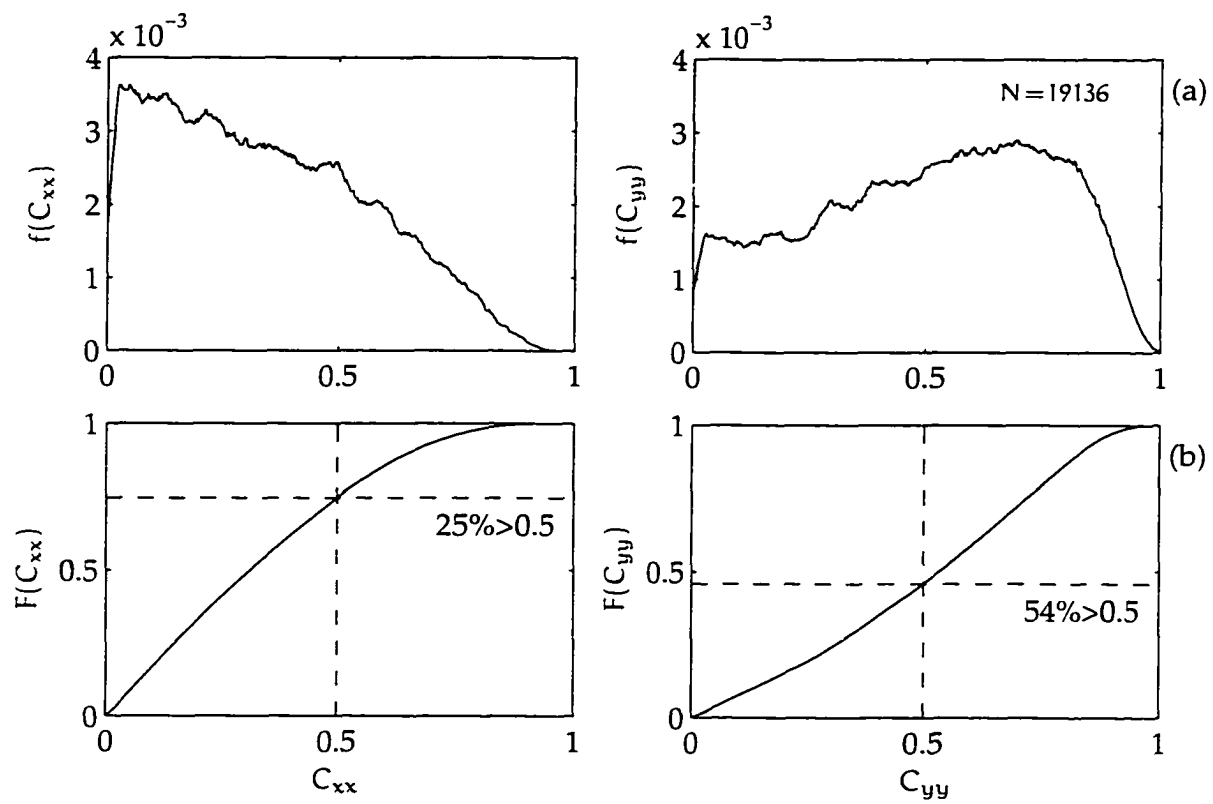
Figure 3.11. Cumulative Pc 3 coherence statistics for Repulse Bay and Pelly Bay. The station separation is 267 km. Figure format is as for Figure 3.7 (see text for details).
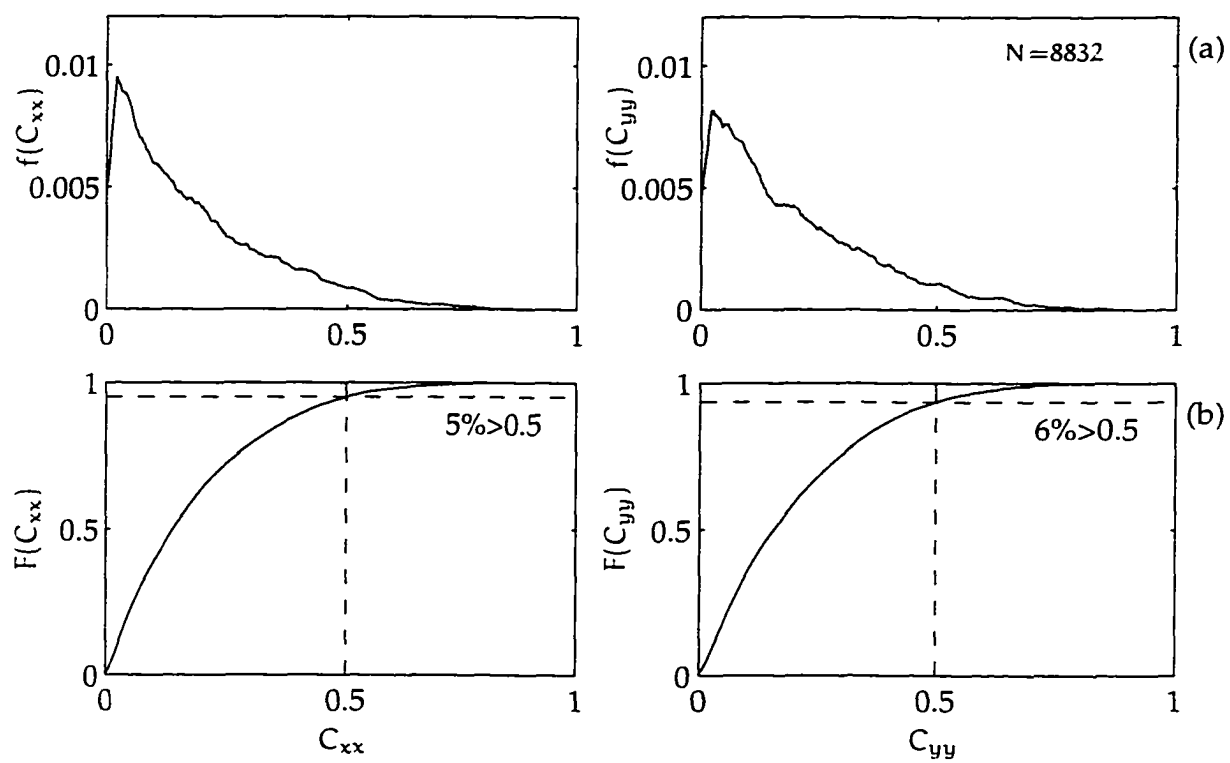
Figure 3.12. Cumulative Pc 3 coherence statistics for Repulse Bay and Cape Dorset. The station separation is 513 km. Figure format is as for Figure 3.7 (see text for details).

Station Pair	No. of Days	Separation (km)	C_L
Pelly Bay – Gjoa Haven	217	252	0.39
Repulse Bay – Pelly Bay	104	267	0.40
Coral Harbor – Repulse Bay	81	301	0.23
Cape Dorset – Coral Harbor	62	320	0.13
Gjoa Haven – Repulse Bay	93	473	0.11
Repulse Bay – Cape Dorset	48	513	0.06
Pelly Bay – Coral Harbor	86	569	0.08
Pelly Bay – Cape Dorset	57	753	0.04
Gjoa Haven – Coral Harbor	71	754	0.03
Gjoa Haven – Cape Dorset	46	983	0.02
Davis – Zhong Shan	31	110	0.42
Cape Parry – Sachs Harbor	13	202	0.19

Table 3.2. Coherence level C_L as a function of station separation. The fluxgate magnetometer (MACCS) results are given in the upper block; induction coil magnetometer results are given in the lower block. The observed trend is that C_L falls off as the station separation increases; however, the induction coil results seem to be less than those of similarly spaced fluxgates.

noted in the polarization analysis). We posit that this difference is caused by the response of each type of instrument and is not a function of the coherence estimator.

We noted that fluxgate and induction coil magnetometers display different characteristic spectra (see Figures 3.4 and 3.5). This is due to the frequency response of each instrument. The Narod fluxgate magnetometer has a "flat" frequency response, well beyond the dc–50 mHz passband of interest here, such that the magnitude of the detected field is precise to within ± 0.025 nT [*Narod*, 1990].[3] An induction coil magnetometer detects the time rate-of-change of the magnetic field, thus it has a frequency response that is proportional to frequency. This proportionality holds for frequencies $\lesssim$ 1Hz, below the resonant frequency (2 Hz) of the coils. Since both of our generalized coherence estimates ($C_{ij}[f]$ and $P[f]$) are functions of a single frequency, their response to an input signal is unaffected by

---

[3]This is in contrast to an uncorrected fluxgate design, which has a frequency response that is roughly inversely proportional to frequency [*Primdahl*, 1979].

any amplitude scaling of the Fourier components of that signal. The response of $C_{ij}[f]$ to a signal with the Fourier components $A_i[f]$ and $A_j[f]$ will be identical to a signal with Fourier components $\alpha[f]A_i[f]$ and $\alpha[f]A_j[f]$, where $\alpha[f]$ is an arbitrary function of frequency. Thus, ideal induction coil and fluxgate magnetometers would yield identical results for C_L.

For physically realizable magnetometers, the fluxgate is relatively insensitive to high frequency signals when compared to the induction coil. This causes the fluxgate to reject a higher proportion of those signals which cannot be detected across a station pair. Such signals represent noise in terms of interstation coherence; thus, a pair of fluxgates will have a higher effective interstation coherence signal-to-noise ratio than a pair of induction coils. Consider two stations, each equipped with fluxgate and induction coil magnetometers. A modulated ionospheric current will produce a magnetic perturbation at each station according to the Biot-Savart law. Whether the instruments at each station will respond to the perturbation is a function of the noise floor and frequency response of each type of instrument. The observability of such a signal across each instrument pair will determine the effect of that perturbation upon C_L for each instrument type. Table 3.3 summarizes these effects. Category I and III signals, observable for both instrument types in equal measure, will not contribute to the difference between fluxgate and induction coil coherence levels. Category II signals represent an interstation detection threshold (greater/less than for induction coils/fluxgates); category IV signals represent the noise floor of the fluxgate magnetometers. The relative probabilities of these two pulsation categories determines the difference in C_L between instrument types. If the probability of category II pulsations is greater than twice that of category IV, we would expect the induction coil coherence levels to be greater than for the fluxgates.

Since we find C_L greater for the fluxgates, we can conclude that category IV pulsations, those below the noise floor of the fluxgates, are at least twice as likely to occur in the Pc 3 band near the cusp. This indicates that highly localized small amplitude pulsations characterize a significant portion of the cusp and boundary regions. For interstation coherence studies then, fluxgate magnetometers effectively form an incoherent noise filtration system, where noise in this sense is taken to mean incoherent signals between stations. The disparate C_L levels should be a function of frequency, owing to the disparate responses of each type of magnetometer. It is also likely that the difference diminishes with interstation

	Observability		C_L Effect	
Category	IC	FG	IC	FG
I	both	both	↑	↑
II	both	one	↑	↓
III	one	one	↓	↓
IV	one	none	↓	—

Table 3.3. Interstation observability effect on C_L for two stations, each equipped with induction coil (IC) and fluxgate (FG) magnetometers. A signal observed across both instruments of a given type will cause an increase in C_L for that type (↑); a signal observed at only one of a given pair will cause a decrease in C_L (↓) for that type. If the probability of category II pulsations is greater than twice that of category IV, we would expect the induction coil coherence levels to be greater than that of the fluxgates. Our observations indicate that category IV pulsations are at least twice as likely to occur near the cusp.

separation (e.g., Figure 3.14). Clearly, this effect warrants further study.

Our statistics to this point were compiled without regard to frequency or time. In order to confirm our characterization of coherence near the cusp, we recompile our coherence level results by day, hour and frequency. In Figure 3.13 we present a representative sample of such a compilation taken from Pelly Bay and Gjoa Haven. In all of our station pairs we find considerable variance in C_L on a daily basis, yet no seasonal trend. For the eight hours surrounding mean magnetic local noon we find that C_L is relatively stable across all station pairs. We note that C_L increases away from noon in the example shown in Figure 3.13. Given the variance in the hourly values (plotted in Figure 3.13(b) as $C_L \pm \sigma_{C_L}$) we find this minimum to be significant for this station pair; however, the trend is not consistently observed among the pairs. We will discuss the behavior of Pc 3 pulsations near local noon further in the following chapter. For C_L in the Pc 3 frequency band (15–50 mHz) we note a rolloff with increasing frequency. Despite the variance in the by-frequency compilation (plotted in Figure 3.13(c) as $C_L \pm \sigma_{C_L}$), a similar rolloff is observed across all station pairs.

The trend indicated by the data in Table 3.2 is that C_L falls off as the station separation increases. A model for this trend would be useful in predicting a coherence level for a given station separation. Since the fluxgate and induction coil magnetometers appear to
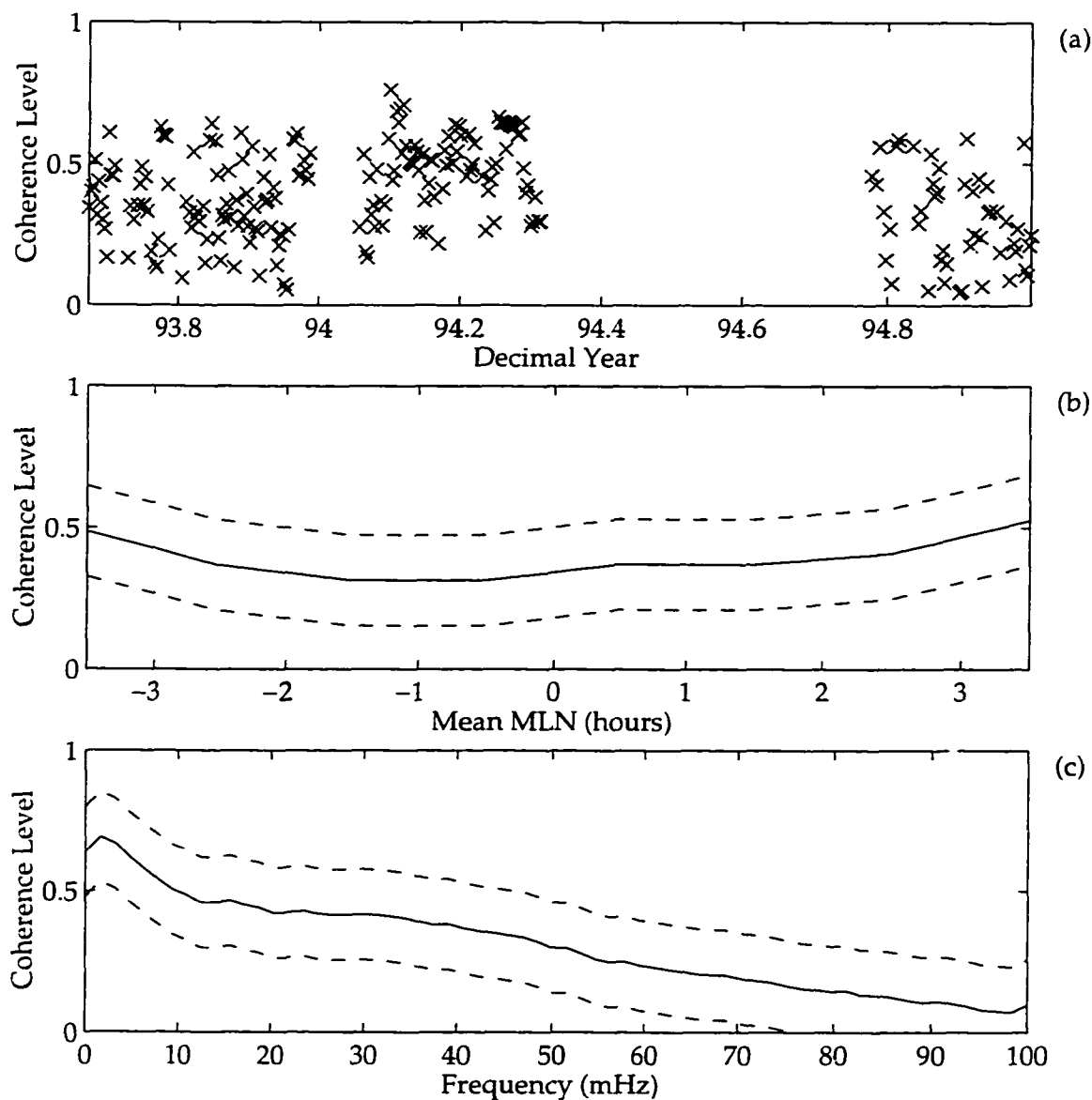
Figure 3.13. Coherence level C_L as a function of day, hour and frequency for Pelly Bay and Gjoa Haven. The data presented here represent 217 days, the largest set available to this study. (a) C_L as a function of each day available for the study. (b) $C_L \pm \sigma_{C_L}$ as a function of hour relative to mean magnetic local noon at the station pair (1841 UT). (c) For reference, $C_L \pm \sigma_{C_L}$ is shown as a function of frequency for the entire passband at the MACCS stations. The coherence levels indicated throughout the rest of the study are restricted to those derived in our operational Pc 3 frequency band, 15–50 mHz. For uncorrelated noise, $C_L \approx 0.0026$ throughout the passband.

respond differently in terms of C_L, we will fit only those data points for the MACCS array.[4] Comparing $\log C_L$ with the station separation we find a significant linear trend; therefore, we model the data via the design matrix approach of *Press et al.* [1992].

For our linear model, $\log C_L = ms + b$, where s is the station separation in km, we find $m = (-4.0 \pm 0.5) \times 10^{-3}$ and $b = -0.3 \pm 0.3$. Despite the uncertainty in the intercept, the linear correlation coefficient is significant.[5] Most of the uncertainty is in the intercept, which is likely a function of the lack of data points for less than 250 km station separation. This linear fit of $\log C_L$ gives us a device for predicting the interstation coherence level at the cusp: $C_L \approx 1.4e^{-s/250}$. In Figure 3.14 we show such a curve, along with uncertainty curves obtained in the standard fashion [*Taylor*, 1982].

The development of the coherence level C_L and a means to predict its value for various station separations concludes our characterization of interstation coherence at the cusp. We now turn our effort toward linking this measure to a simple physical model that can be used to estimate an upper bound for the coherence length of the precipitating electron beams presumed responsible for the localized Pc 3 pulsations at the cusp.

3.2.3 Precipitation model

The apparent exponential decay of the coherence level C_L with station separation (see Figure 3.14) leads us to suspect that the localized pulsations near the cusp have a finite physical scale size. In terms of our coherence-based measure, this scale size is termed a coherence length. Although they did not enjoy the advantage of a multi-pair study, *Olson and Szuberla* [1997] developed a simple model for the coherence length that we adopt for the present study. Their model was based on the roughly north-south pair at Cape Parry and Sachs Harbor; we modify that model to take into account different station alignments with respect to the magnetic field and also allow for the mean latitudinal difference between station pairs.

Our model for estimating the coherence length is based on the first order assumption

[4]Inclusion of the ANARE and UA stations does not greatly alter the fitted curve, since the stations lie within the uncertainty of the model function using only the MACCS data (see Figure 3.14).

[5]We find $R = -0.95$ for the standard linear correlation coefficient. Since the statistical significance of R is relatively uncertain, we also calculate a non-parametric, or rank, correlation coefficient for our fitted curve. Kendall's τ is the measure selected. It gives us $\tau = -0.96$ and probability $Pr = 1.2 \times 10^{-4}$ that the station separation in km and $\log C_L$ are not linearly correlated [*Press et al.*, 1992].
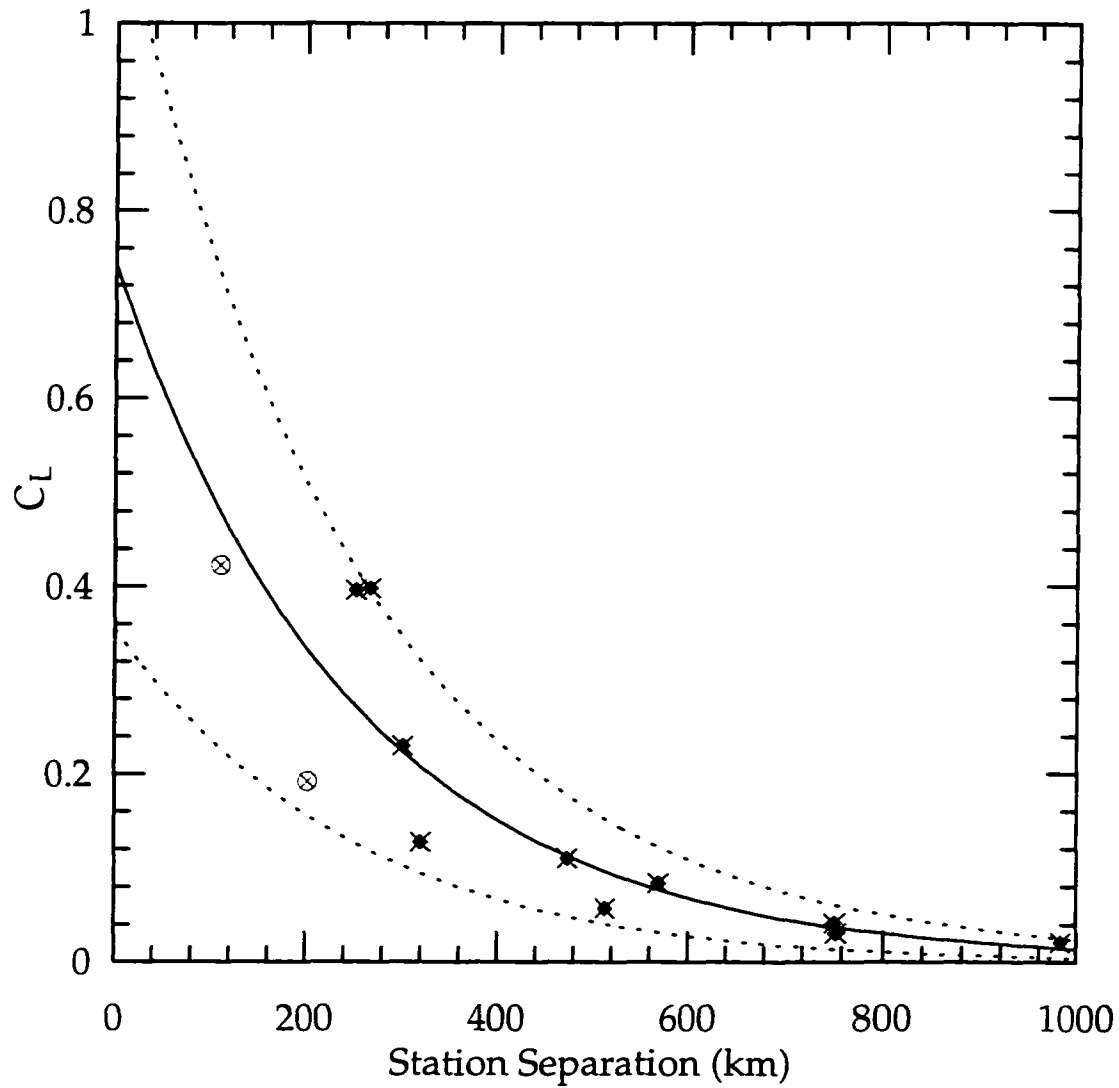
Figure 3.14. Coherence level C_L as a function of station separation. The fluxgate magnetometers of the MACCS array are plotted as cross-hatched diamonds; for comparison, the induction coil magnetometers of the ANARE and UA arrays are plotted as cross-hatched circles. The solid curve represents a generalized linear least-squares model of the function $C_L = e^{ms+b}$ to the fluxgate data, where s is the station separation in km; the dotted curves represent the uncertainty in the fitted curve (see text for details). The solid curve might be used to predict the coherence level for a pair of stations separated by a distance s as $C_L \approx 1.4e^{-s/250}$.

.l

that the modified conductivities in the overhead ionosphere, as described by *Engebretson et al.* [1990], are circular in horizontal cross-section. This would correspond to the iono-spheric footprint of a roughly cylindrical beam of precipitating electrons. With this picture in mind, we expect that stations directly beneath that footprint will observe roughly the same Pc 3 variations, and so show high coherence; those which do not will exhibit low co-herence. The coherence level has a straightforward interpretation in our model. Since C_L represents the percentage of coherence estimates that exceed our fiducial noise value for a station pair, it is equivalent to the probability of dual station coverage. This interpretation is a significant change from that of *Olson and Szuberla* [1997].

We stress that our model is strictly *first order* in its treatment of the magnetometer's re-sponse to ionospheric currents. Actual magnetometers sense changes in the magnetic field as a function of both their response pattern (which is roughly dipolar along a given com-ponent axis) and how the field itself will respond to a current as given by the Biot-Savart law. This simplification has the following implication for our model: our coherence length estimate will represent an upper bound. A more realistic modeling of the magnetometer response pattern and precipitation footprint would reduce the magnitude of our finding.

In the model we consider a rectilinear region with a longitudinal and latitudinal extent of 15° by 5°. The former dimension is consistent with the 1-hour windows used to estimate interstation coherence and is based on the mean latitudinal location of the stations; the latter is taken to represent the angular separation between the equatorward edge of the low-latitude boundary layer and the poleward edge of the mantle. This choice is consistent with both our assumptions about the cusp region and the statistical work of *Newell and Meng* [1992]. In the center of this region we place our two stations, according to their separation and orientation within the magnetic field. An example of the model geometry is given in Figure 3.15.

We model the beam footprints as circles drawn on the planar region containing both stations. The problem then is to determine the probability that a circle of radius r will cover both stations. Circle radii and center locations are drawn from uniformly random distributions; however, we place a restriction on the location of circle centers, as a function of radii, so that no part of a circle falls outside the 5° latitudinal extent of the model box. This is done in order that the beam areas are consistent with an ionospheric mapping
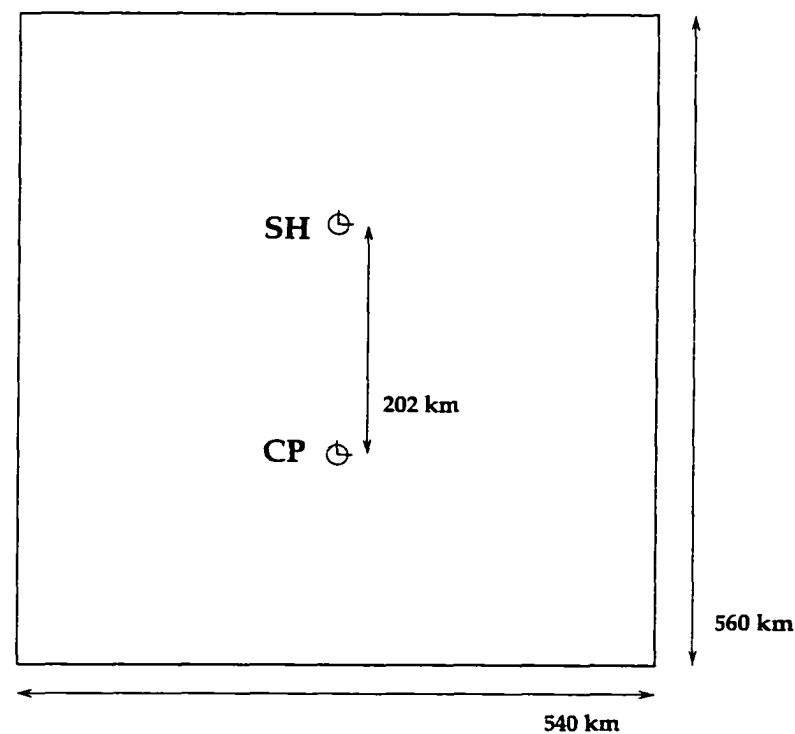
Figure 3.15. precipitation model geometry for Cape Parry and Sachs Harbor stations. The longitudinal extent of the box (540 km) represents roughly one hour of local time at this latitude. The latitudinal extent of the box (560 km) represents the roughly 5° statistical extent of the cusp and boundary regions. Model geometries for the other station pairs are similar but take into account the particular orientation of the particular pairs.

of satellite observations of near-cusp particle populations [see, e.g., *Aparicio et al.*, 1991; *Newell and Meng*, 1988, 1992]. The probabilities for dual station coverage are derived via a Monte Carlo approach, using 500 million circles randomly drawn according to the above constraints. Examples of results from two of the station pairs are given in Figure 3.16. Note that the probability rises monotonically, though not linearly, with circle radius.

We note that not all station pairs were modeled. It is difficult to reconcile our first order model with station separations greater than about 350 km. We note that for the MACCS coherence level results, the four adjacent station pairs appear to follow a somewhat different trend than the six non-adjacent station pairs (see Figure 3.14). Working within this constraint we are able to model all six of the adjacent station pairs available to our study. The results of this modeling effort are given in Table 3.4.
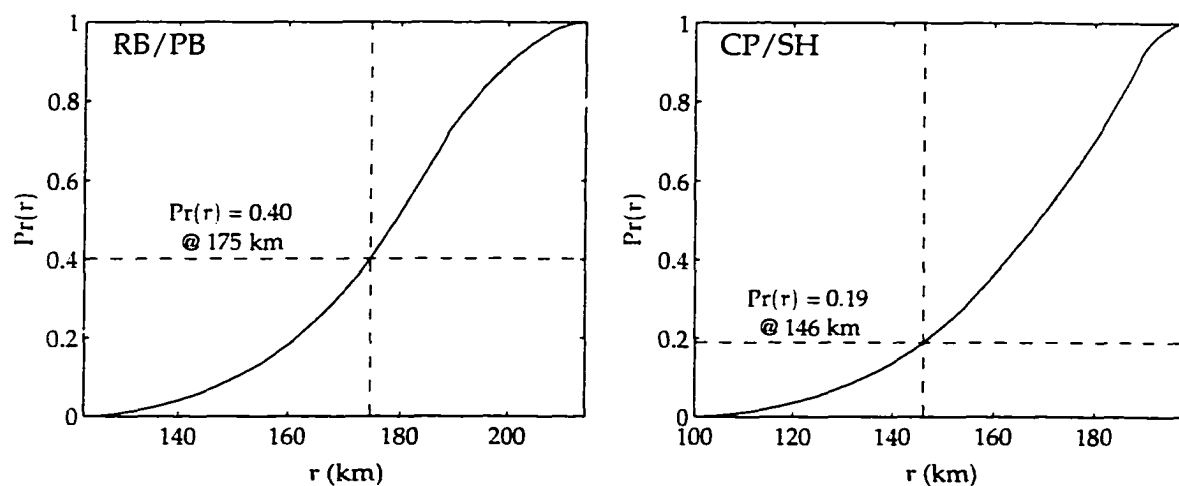
Figure 3.16. Probabilities of electron beam coverage for two station pairs. Shown is the probability of dual station coverage as a function of beam radius for (right) Repulse Bay and Pelly Bay; (left) Cape Parry and Sachs Harbor. Indicated in each panel is the beam radius that satisfies the condition $Pr(r) = C_L$ (see text for details).

From Table 3.4 it is evident that the fluxgate magnetometers of the MACCS station pairs give different results than the induction coils of the ANARE and UA pairs. This result is consistent with our analysis of the discrepancy in coherence levels noted between fluxgate and induction coil magnetometers. A decrease in C_L will require a smaller diameter circle to reproduce the result.

Via our simple precipitation model we have found a link between our measure of inter-station coherence C_L and the coherence length of localized Pc 3 pulsations at cusp latitudes. We found that the estimate of the coherence length is instrument dependent, and arrive at a value of 180 km for fluxgate magnetometers; 140 km for induction coil magnetometers. This result is smaller than that of *Olson and Szuberla* [1997] by nearly a factor of two. We conclude that the earlier result was biased to a larger value by the presence of noise at each station.

3.3 Discussion

In this study we moved from our earlier event-based studies of cusp latitude Pc 3 pulsations to develop a statistical description. We expanded and improved upon the work of

Station Pair	C_L	Model Result (km)
Pelly Bay – Gjoa Haven	0.39	177
Repulse Bay – Pelly Bay	0.40	175
Coral Harbor – Repulse Bay	0.23	182
Cape Dorset – Coral Harbor	0.13	182
Davis – Zhong Shan	0.42	141
Cape Parry – Sachs Harbor	0.19	147

Table 3.4. Precipitation model results for selected station pairs. Note that the MACCS pairs (upper block) tend to give results that are greater than those of the ANARE and UA pairs (lower block). We believe this to be related to the difference in sensitivities between the fluxgate and induction coil magnetometers.

Olson and Szuberla [1997] in characterizing the localized Pc 3 pulsations at cusp latitudes. In so doing we have satisfied our two objectives for this chapter. First we characterized the state of interstation coherence by developing a quantitative measure of its magnitude in the coherence level C_L. We determined that this measure, the percentage of coherence estimates that exceed a fiducial noise value, is a function of station separation. Second, we estimated an upper bound for the horizontal coherence length of a precipitating electron beam as described by *Engebretson et al.* [1990]. Using a simple physical model, we translated the results of our coherence level into a coherence length, which is a function of the type of magnetometer used. Both of these results are significant in that they represent the first and only quantitative measures of these physically meaningful coherence-based parameters.

3.3.1 Observational evidence

Our measure of the upper bound for the coherence length corresponds to the physical scale size over which magnetometer stations are likely to receive coherent Pc 3 pulsations. Since fluxgate and induction coil magnetometers are differently sensitive to coherence levels, this scale size will vary with the instrument used to study pulsations. Given that our estimate is an upper bound, we would expect to find that the ionospheric source regions of these pulsations would be $\mathcal{O}(100$ km) in size.

The most recent evidence of such a scale size comes from a study conducted using the same instruments as the original *Engebretson et al.* [1990] study and additional radar data (K. Baker and M. Engebretson, private communications, 1997). The radar data were taken from the Halley PACE HF radar, located at the British Antarctic Survey base on the Brunt ice shelf [*Baker et al.*, 1995]. This radar was chosen because its field-of-view (geomagnetic latitudes $\lambda \in [65°, 85°]$) covers the magnetometer stations used by *Engebretson et al.* [1990]. The radar data were correlated specifically with the occurrence of Pc 3 modulations in both the magnetometer and photometers at the cusp. Preliminary results indicate that when correlations between magnetometer and photometer were found with no appreciable delay, the radar data indicate the presence of electron precipitation patterns that are roughly 100 km in diameter.

Another study currently being conducted provides evidence that our coherence level prediction is correct at large station separations (B. Fraser, private communication, 1997). An event-based study is being used to study the propagation characteristics of Pc 3 waves across a portion of the ANARE array. Two stations used in the study (Davis and Mawson) are separated by 640 km and the investigators find few events coherent between the two sites. Preliminary figures are in general agreement with our estimate of C_L for such a pair of stations.

In other work at cusp latitudes, *Mitchell et al.* [1995] used tomographic imagery and the EISCAT incoherent scatter radar to determine that large-scale structures were present in electron densities in the E- and F-regions of the ionosphere; such density variations lead to conductivity variations, and hence currents. They found that the horizontal scale sizes of these structures could be as small as 50 km, but were often at least 200 km. *Pinnock et al.* [1995] used the Halley PACE HF radar to find similar scale sizes for precipitating electrons near the cusp.

Several investigators have found similarly-sized patterns in optical data taken at cusp latitudes, as the coherence length is of order the size of patches in dayside diffuse aurora [*Vallance Jones*, 1974]. Although the dominant emission in the diffuse cusp aurora is at 630.0 nm, its utility in determining the scale size of processes related to localized Pc 3 pulsations may be limited because the lifetime of the emission (110 s) is of order the maximum period of such pulsations [*Carlson and Egeland*, 1995]. Despite the lifetime of the emission, *Eather*

[1969] observed pulsating auroral forms with a periodicity of ~20 s at this wavelength. More recent studies have relied on the less intense dayside emissions at 427.8 nm and 557.7 nm, owing to their short lifetimes, 0.8 s and ~10^{-6} s, respectively [*Chamberlain*, 1961]. Optical evidence for the precipitation patterns was originally obtained by *Engebretson et al.* [1990] using 427.8 nm emissions and their correlation with the magnetometers. *Sandholt et al.* [1992] give evidence for cusp and boundary region precipitation of order 200 km and smaller in patches of 630.0 nm emissions with enhancements in the 557.7-nm emission. Although no magnetometer correlations were made in the latter observations, the optical evidence does indicate that precipitation patterns with appropriate horizontal scale sizes do exist in the cusp ionosphere.

In light of another multipoint study by *Engebretson et al.* [1995] in the Pc 3 frequency band, we emphasize that our inferred physical scale size is based strictly on the estimated state of interstation coherence between the two stations. They analyzed data recorded across the MACCS array and found that roughly a third of their observations showed broadband Pc 3 to be nearly simultaneous across the entire (> 4-hours magnetic local time) longitudinal extent of the network. We do not find their results to be in conflict with our own, as the two studies are not directly comparable. A visual reckoning of spectrograms will provide evidence to distinguish between spatial and temporal features across the network; however, such an examination provides no information as to the interstation coherence of such features. What it does offer is a qualitative understanding of near simultaneous power enhancements across an array.

Given the observational evidence, we feel confident in suggesting that the broadband Pc 3 observed on the ground at cusp-latitudes are generated in the local ionosphere. The work of *Engebretson et al.* [1990] prompted our study, and represents the only reasonable physical alternative that justifies our (albeit simple) model. For coherent pulsations, we find that our constraint on the coherence length is reasonable and should serve as a guide for a theoretical understanding of the nature of these pulsations.

3.3.2 Physical implications

Our findings regarding the coherence level and coherence length relate directly to the future deployment of magnetic observatories at cusp latitudes. We first note that the model

result for the coherence length is roughly the same across the entire MACCS array, which spans the entire statistical latitudinal extent of the cusp and boundary regions. This indicates is that there is perhaps no preferred latitude for a cusp magnetic observatory in the range of geomagnetic latitudes $\lambda \in [75°, 80°]$.

Since the statistical width of the cusp and boundary regions are a function of latitude [*Newell and Meng*, 1992], one might expect that the precipitating electron coherence lengths would be also be a function of latitude. Such a scenario is depicted in the left column of Figure 3.17. What we find is that the coherence length is uniform for all four station pairs spanning the MACCS array (the case presented in the right column of Figure 3.17). We note however that if the footprint of such precipitation were indeed circular the component-wise coherence levels would be uniform; we find that the dominant level changes from x to y at various station pairs, indicating an elliptical footprint. This view is consistent with the findings of *Aparicio et al.* [1991] and *Lockwood et al.* [1994], who have found evidence for such elliptically shaped precipitation patterns at the cusp.[6]

Our determination of the coherence level as a function of station separation enables us to specify an optimal station separation for pulsation studies in the Pc 3 frequency band which require coherent signals to be observed at two remote sites. Such studies might include the horizontal propagation of Pc 3 waves or the determination of other physically relevant scale sizes. In order to simultaneously optimize the probability of observing coherent pulsation activity between two stations and the area covered by an array we suggest that fluxgate magnetometers be deployed about 250 km apart; the figure is about 100 km for induction coil magnetometers. Our work in developing C_L has recently been cited in a proposal for augmenting the ANARE array with a series of short-baseline induction coil magnetometer stations in Antarctica, each with an interstation separation of roughly 100 km (B. Fraser, private communication, 1997).

3.3.3 Source mechanisms

The work of *Engebretson et al.* [1990] and our own coherence study leads us to suggest that the broadband Pc 3 pulsations near the cusp are indeed locally generated. Our results

---

[6]There is weak evidence that this may also be related to the coastal nature of all the stations used in the study and the conductivity differential between seawater and earth.

Coherence lengths:

Non-uniform   Uniform
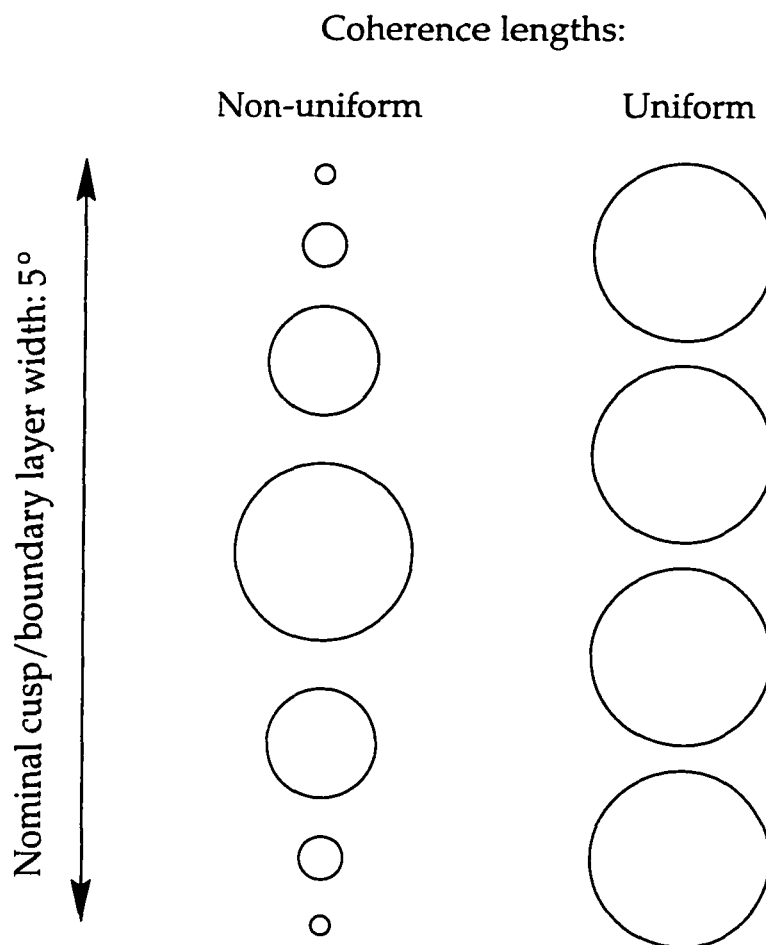
Figure 3.17. Cartoon representation of coherence lengths at cusp latitudes. We expected to find a pattern with diminishing size away from a central latitude (left). We found that the coherence length was uniform across the statistical latitudinal width of the cusp (right).

indicate that they are not cusp-specific, but rather related to the low-latitude boundary layer, cusp and mantle. As evidence of this we find elevated coherence levels for several hours to either side of local noon across a wide latitudinal extent, consistent with the statistical study of *Newell and Meng* [1992]. *Engebretson et al.* [1990] found similar results with correlations between magnetic pulsations and 427.8-nm emission. The lack of a correlated riometer signature in the latter study indicates that the electrons responsible for the optical signature were magnetosheath-like, with energies < 1 keV. Their finding is consistent with the satellite measurements of *Lundin* [1988] and *Newell and Meng* [1988].

An upstream source of Pc 3 wave packets in the cusp is typically invoked due to well-established correlations with solar wind parameters [*Troitskaya*, 1985; *Engebretson et al.*, 1986; *Olson*, 1986]. Such a source mechanism is not likely responsible for the broadband Pc 3 we have studied here. *Engebretson et al.* [1989] have shown that the packet-like structure is observed over distances as large as 1300 km, and *Olson and Fraser* [1994] have shown them to be coherent between conjugate sites. Further, such narrowband features only comprise a small portion of the spectrum.

On the basis of our coherence-based study of magnetometer data alone we cannot reliably determine the exact cause of broadband Pc 3 pulsation activity; however, there are several studies which may offer clues as to the nature of this type of pulsation activity. Using soft electron (< 200 eV) observations from the early low-altitude DMSP satellites, *Meng and Candidi* [1985] found filamentary structures present throughout the cusp region. In their original paper, *Engebretson et al.* [1990] noted this as a possible cause for the observed magneto-optical correlations near the cusp. *Maggs and Morales* [1996, 1997] have found evidence in theoretical and laboratory work that such filamentary structures (in the form of density depletions) can lead to significant coherent wave activity. This wave activity can further lead to localized ion and electron heating in the auroral ionosphere. From their laboratory work, they find a significant peak in wave energy at a fraction of the ion cyclotron frequency, about $0.09\omega_{ci}$. In the Pc 3 frequency range, this would correspond roughly to density depletions originating on field lines of $L \sim 15$. Wave activity at these frequencies and L-shell positions could account for both our observations and those of *Engebretson et al.* [1990].

Johnson and Cheng [1997] have done a theoretical study of plasma transport across the magnetopause due to kinetic Alfvén waves and find indications that the broadband pulsations in the range 10–500 mHz detected in the magnetosheath may be related to this process. This process offers two methods of Pc 3 modulation delivery to low altitudes: either direct magnetosheath entry through the cusp, or time-dependent reconnection. Magnetosheath-like electron precipitation modulated at these frequencies would be consistent with the lack of correlation between optical and riometer signatures found by *Engebretson et al.* [1990]. The periodic reconnection scenario has also been suggested to us in a different light as a Pc 3 generation mechanism at the magnetopause (T. Onsager,

private communication, 1996). Such patchy reconnection occurring at the appropriate frequencies might account for a portion of the broadband Pc 3 signature at the ground. The FTE-driven pulsating cusp model of *Smith and Lockwood* [1990] is consistent with this suggestion. Given the fairly large latitudinal and local time extent of this class of pulsations, we expect that there will be more than one source mechanism which drives the Pc 3 frequency band modulations of cusp latitude electron precipitation. Our determination of the coherence levels and coherence lengths provide important physical constraints in identifying any such source.

For the small, but non-zero, coherence levels found at station separations greater than 350 km, we suggest three possible sources. First, we noted that between stations we often observed coincident power enhancements in the Pc 3 frequency band. These events, while not reliable indicators of local interstation coherence, can provide a coherent signal at large station separations if they are intense enough. *Engebretson et al.* [1995] has found such events across the entire MACCS array and at Longyearbyen we have noted Pc 3 events with trace power on the order of Pc 5 pulsations known to be observed at large station separations. Second, the coherence length of the quasi-monochromatic wave packets present in the Pc 3 spectrum has not yet been fully assessed. Although such coherent signals make up only a fraction of the spectrum, they have been observed simultaneously over large distances [*Engebretson et al.*, 1989] and may be able to account for C_L across large distances. Finally, large-scale patterns in the cusp-latitude ionosphere known as traveling convection vortices (TCV) exist on the scale of our greatest station separation [*Friis-Christensen et al.*, 1988; *Glassmeier et al.*, 1989]. Very recent results (Bering et al., poster given at the 1997 GEM Workshops) have shown that there may be a significant correlation between Pc 3 activity and TCV passage. The latter two source mechanisms may be considered non-local contamination of our coherence levels. It is plausible that a combination of all three of these sources contribute to the observed values of C_L at large station separations.

Further insight into the exact sources of localized Pc 3 magnetic pulsations will require simultaneous, multipoint *in situ* information, perhaps as provided by the successor to the Cluster mission. Low- and mid-altitude satellite coverage of the cusp and boundary regions, currently being provided by DMSP and POLAR, should provide more information about the modulation mechanism acting on the precipitating electrons. Ground-based

measurements will also need to be taken in concert with these satellite passes; our determination of the coherence length suggests a magnetometer array spacing for such studies. We have shown in this chapter that it is possible to extract meaningful physical information regarding this important class of pulsations from the analysis of magnetometer records. Such analyses further our present understanding of cusp-latitude physics (see the recent review given by *Smith and Lockwood* [1996]).

Chapter 4

Long-period pulsations

In this chapter we continue our characterization of the cusp region by considering long-period pulsations, nominally those in the Pc 5 frequency band. These Pc 5 pulsations are a persistent and dominant feature of the high-latitude power spectrum near local noon (see Figure 4.1). Current observational and theoretical evidence places the source of these dayside pulsations variously in the magnetosheath and among the boundary regions associated with the magnetopause (see the reviews given by *Sibeck* [1994] and *Schwartz et al.* [1996]). Signals generated in these regions presumably carry information concerning their source, although the information content may be degraded in transit through the ionosphere [*Hughes*, 1974; *Glassmeier*, 1983, 1984].

Using data taken at Longyearbyen, *McHarg and Olson* [1992] established a strong correlation between long-period magnetic pulsations and optical signatures of the cusp and boundary regions. In particular, they found a magnetic Pc 5 spectral feature that correlated well with an increase in the ratio of 630.0-nm to 557.7-nm optical emissions, indicating the presence of low-energy particle precipitation. This led them to speculate that the presence of this magnetic feature could be used as a discriminant of the passage of the cusp nearby a ground magnetometer station. Figure 4.1 depicts an example of this feature, which *McHarg* [1993] dubbed the "arch." The magneto-optical correlations of *McHarg and Olson* [1992] imply that it is possible to identify the passage of the cusp via the analysis of magnetometer spectra. An expanded study of Longyearbyen data by *McHarg et al.* [1995] confirmed this view by making further ground-based magnetic correlations with interplanetary magnetic

83
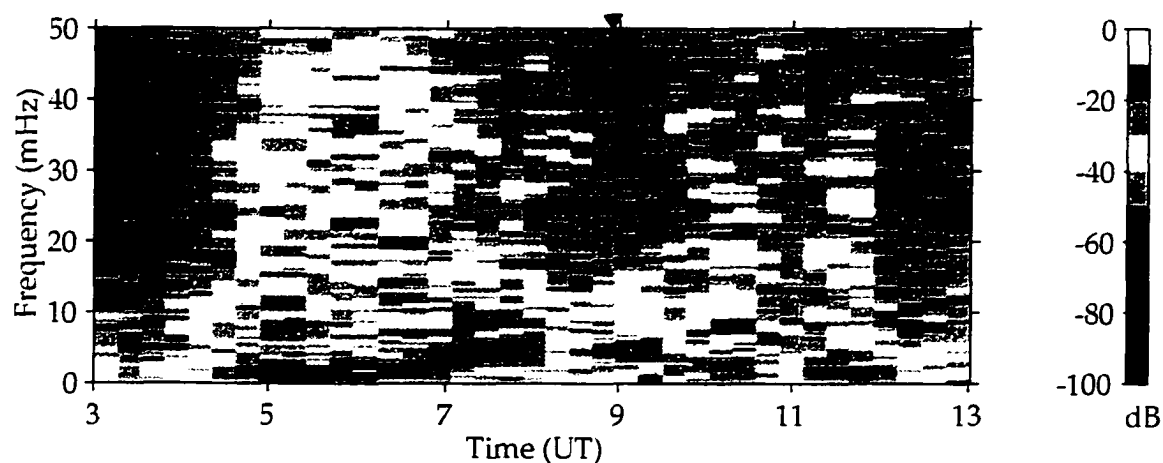
Figure 4.1. Representative induction coil spectra at high latitude. The data were taken at Longyearbyen on 9 January 1991, with magnetic local noon approximately 0857 UT (marked by the small triangle). Shown in the panel is the trace power, tr S. Note that the dominant signal near noon is in the Pc 5 frequency band. The arch-like feature near 5 mHz, lasting roughly from 0730–0930 UT, was identified by *McHarg* [1993] as a characteristic of the cusp spectrum (see text for details).

field data from the IMP 8 satellite and particle characteristics from the DMSP satellites.

Engebretson et al. [1995] studied data taken across the MACCS array, in part, to test the low-frequency cusp identification scheme of *McHarg and Olson* [1992]. They found that a large number of spectral features appeared and disappeared simultaneously across the entire longitudinal extent of the array. Spatial features, such as those pertaining to the cusp and boundary regions, should manifest themselves in local time, owing to the rotation of the station beneath them. What they observed were temporal features, appearing in universal time. Based on these temporal observations, they concluded that single-station spatial identifications were unreliable.

The primary goal of this chapter is to reconcile the disparate findings of *Engebretson et al.* [1995] and *McHarg et al.* [1995]. Both groups concede that there is spatiotemporal information contained in the cusp latitude spectrum; the former/latter argues that the information is primarily temporal/spatial. We examine the databases used by each group and find that spatial identifications may be made from single-station spectra. In particular, we find that polarization spectra are more reliable for such identifications. To begin our spatiotemporal characterization of the cusp spectrum, we provide a justification for characterization in the

acterization in the spectral domain. We then lead the reader through a novel approach to the data, an information theoretic spectral analysis. Finally, we conduct a statistical analysis of Pc 5 interstation coherence (similar to that of Chapter 3), the results of which are consistent with our spectral findings. This analysis allows us to comment on the reliability of a ground-based magnetic separatrix identification.

4.1 The cusp discriminant

In his thesis work, *McHarg* [1993] identified the arch as a cusp discriminant in the spectral domain. A time-domain event study of the arch on 9 January 1991 (see Figure 4.1) revealed that it was characterized by relatively small amplitude, phase coherent wave trains lasting approximately 5–10 periods. The arch was bounded by larger amplitude pulsations, presumably stemming from the boundary regions, which were phase incoherent pulses (1–2 periods). These phase skips between pulsations can be indicative of multiple, decoupled source mechanisms, distinguishable spatial structures, or an impulsive excitation of a boundary [*Sibeck*, 1990; *Menk and Yumoto*, 1994; *Stellmacher et al.*, 1997]. Since a number of workers [e.g., *Olson*, 1986; *Sakurai et al.*, 1993] had reported similar amplitude and phase relationships at cusp latitudes, *McHarg* [1993] concluded that the phase characteristics of Pc 5 pulsations might make a time-domain identification of the cusp and boundary regions possible.

In an effort to ascertain a time-domain cusp discriminant, *Szuberla et al.* [1994] examined the phase characteristics of Longyearbyen magnetometer records for which there was a coincident overflight[1] of the DMSP F10 satellite. Such passes accounted for roughly 30 percent of the 103 days they selected for study. With the satellite particle data they were able to confirm the presence of the cusp and/or boundary regions nearby the station; the arch correlated well with the satellite data. In the 8 January 1992 data they found an arch centered at 0800 UT, while the F10 satellite flew through cusp-like particles (as defined by *Newell and Meng* [1988, 1992]) for approximately eight minutes centered on 0802 UT. This particular pass was examined in detail.

---

[1]Since the DMSP satellites are in an eccentric polar orbit, *Szuberla et al.* [1994] defined an "overflight" to be any pass where the satellite was >15° above the horizon at Longyearbyen. On 8 January 1992, F10 flew 43° above the northern horizon, well within the wide effective "field-of-view" of the magnetometer.

In Figure 4.2 we show the results of the analysis technique used to infer phase information from the time series. The upper panel of Figure 4.2 shows the y-component of the time series, which was Fourier lowpass filtered[2] at 7 mHz. The lowpass filtered data is Hilbert transformed in order to construct the complex analytic signal from the real time series. Instantaneous phase information may be estimated from the analytic signal by taking the ratio of imaginary to real parts. Lowpass filtration is necessary to make the signal quasi-monochromatic, so that the phase information will not be corrupted by spurious high-frequency phase shifts. Justification for discarding the high-frequency content of the time series stems from the work of *McHarg* [1993], which established the frequency of the cusp discriminant at 4 mHz ± 2 mHz. The lower panel of Figure 4.2 depicts the estimate of the instantaneous frequency of the time series. This estimate is obtained by taking the magnitude of the numerically differenced phase information, $|\delta\varphi|$. We stress that this method of frequency estimation in the time domain is reliable only for quasi-monochromatic signals [*Bracewell*, 1978], such as our lowpass filtered data; we employ it because phase skips may be easily identified by discontinuities in the instantaneous frequency data. The dash-dotted line in the panel represents the mean frequency present in the data; the dotted lines represent the 85 percent confidence limits. The "spikes" in the instantaneous frequency which exceed the confidence limits may be interpreted as phase skips. We note that the mean frequency is 4 mHz ± 2 mHz for the data depicted.

Szuberla et al. [1994] noted that the cusp signature is evident in the time series (upper panel) in the relatively small amplitude pulsations lasting from approximately 0730–0815 UT. They found that the larger amplitude pulsations bounding the cusp signature were representative of the boundary regions. Note that the amplitude is larger on the morning side of the cusp. These amplitude characteristics were similar among all the days identified by an arch and a cusp-like satellite overflight. As can be seen in the phase information (lower panel), they found significant phase skips appear to be more frequent in the cusp than in the relatively stable morning-side boundary regions, in contradiction to the findings of *McHarg* [1993]. As an event-based study, this result is not surprising — exceptions

---

[2]Fourier bandpass filtration is carried out by: 1) taking the FT of a times series and putting to zero all positive and negative frequencies outside the passband, and 2) taking the inverse FT of the resulting frequency series. The technique introduces no phase distortion in the passband. Such a bandpass filter is acausal, hence it is not physically realizable. The lowpass filter we construct is simply a limiting case of the bandpass filter.
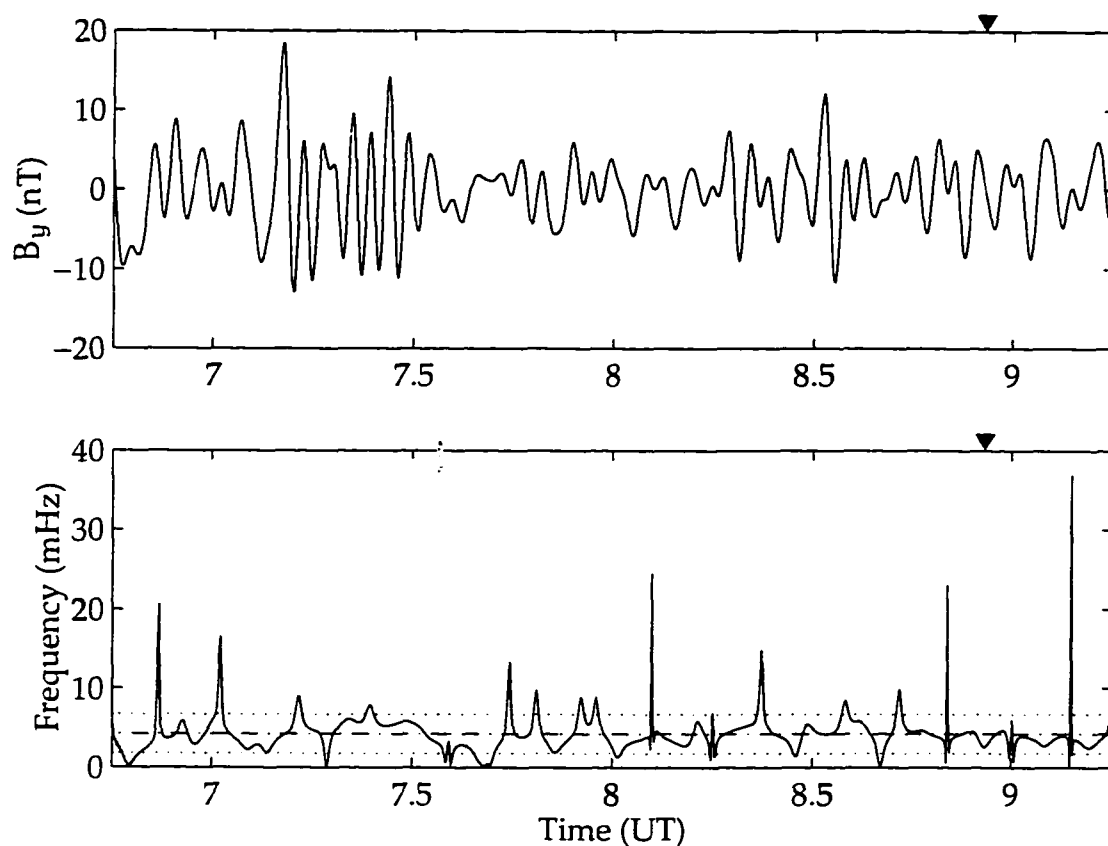
Figure 4.2. Phase skips associated with cusp and boundary region pulsations. The data were taken on 8 January 1992 at Longyearbyen, with magnetic local noon approximately 0853 UT (marked by the small triangles in each panel). The panels depict (top) the y-component of the magnetic field at the station (lowpass filtered at 7 mHz), and (bottom) the instantaneous frequency of the filtered y-component. The mean frequency and 85 percent confidence limits are plotted as the dot-dashed and dotted lines, respectively (see text for details).

can always be found; however, *Szuberla et al.* [1994] examined the entire database and found that the phase information contained in the central cusp portion of the time series was, for all practical purposes, indistinguishable from that of the boundary regions.

The results of *Szuberla et al.* [1994] lead us to conclude that a phase-based characterization of the cusp is difficult to achieve. For our ground-based magnetic characterization of the cusp and boundary regions we expand upon the approach of *McHarg and Olson* [1992] in analyzing dynamic spectra. We use the technique of frequency-time localization to examine the trace power and polarization of cusp latitude magnetometer records. Estimation of these two properties destroys the phase information present in the data, as each is based on the trace of the spectral matrix, tr$S$. Our technique approximately preserves the time-domain amplitude characteristics we noted for the cusp discriminant, plus it allows us to examine the frequency content as it evolves in time. We are confident that phase skips (such as those shown in Figure 4.2) do not affect our analysis, as *Theiler et al.* [1992b] have shown that spurious phase information does not affect the linear properties of a time series; namely, the Fourier amplitudes we are interested in. It is in the spectral domain that we find unambiguous spatial information regarding the cusp and boundary regions.

4.2 Spatiotemporal characteristics of cusp spectra

Apart from the fact that *McHarg et al.* [1995] used only a single-station database, there are significant differences between their approach and that of *Engebretson et al.* [1995]. Before we begin our own analysis of cusp spectra we note these differences. The former group concentrated on the power spectrum determined from the trace of the spectral matrix, tr$S$, while the latter examined only the single-channel spectrum for each component. *McHarg et al.* [1995] examined the data from induction coil magnetometers at Longyearbyen and *Engebretson et al.* [1995] used a combination of induction coil and fluxgate data across the MACCS array. The fluxgate data in their study were numerically differenced ("whitened") in order to make the spectrograms visually compatible with those of induction coils. Finally, *McHarg et al.* [1995] weighted each pixel in their spectrograms by the degree of polarization squared, effectively pure state filtering their data according to the prescription of *Samson and Olson* [1981].

An element common to both studies was the "by-eye" categorization of spectra. Each group attempted to move beyond this level of data analysis by making a statistical comparison between their spectral classification scheme and interplanetary magnetic field (IMF) parameters. In this section we develop a quantitative measure that reproduces the qualitative spectral classifications of *McHarg et al.* [1995]. We feel that this measure satisfactorily resolves the disparate spatiotemporal interpretations of the two groups.

4.2.1 Trace power spectra

The basis for the classification scheme of *McHarg et al.* [1995] was the diurnal repeatability of certain qualitative spectral features at a single station; they interpreted them as signatures of various spatial regions. As a simple test for the daily presence of a spatial feature one can examine the "mean" spectrogram from a single station. We construct such a mean by calculating the pixel-by-pixel mean of an ensemble of trace power spectrograms from each station (see Figure 4.3). Since spatial characteristics should manifest themselves in local time, these features should be present in the mean spectra. Temporal characteristics, which manifest themselves in universal time, will be spread across a range of local time.

From Figure 4.3, the information contained in the mean trace spectra at each station appears to be both spatial and temporal. At each station there is a dawn-dusk asymmetry in Pc 5 power, a feature noted by *McHarg* [1993] in his development of spectral classifications at Longyearbyen. This asymmetry extends into the Pc 3 at Repulse Bay and Cape Dorset. Gjoa Haven exhibits spatial structure to either side of local noon in the Pc 3 frequency band. Looking across frequency bands, the change in power with local time is typically less than 10 dB across the eight hours shown here, indicating the spreading effect of temporal information.

We note that the features evident in Figure 4.3 are stable with respect to the parameters used in spectral estimation. For the image displayed we selected 8 hours of data, centered on magnetic local noon, and used a Welch window roughly 1 hour in width to estimate the trace of the spectral matrix. The Welch window was advanced through the data in roughly 15 minute increments. Employing this method gives us approximately 10 degrees of freedom. The degrees of freedom give us confidence in our spectral estimation, but the relative stability in the mean spectra give us confidence in our frequency-time localization.
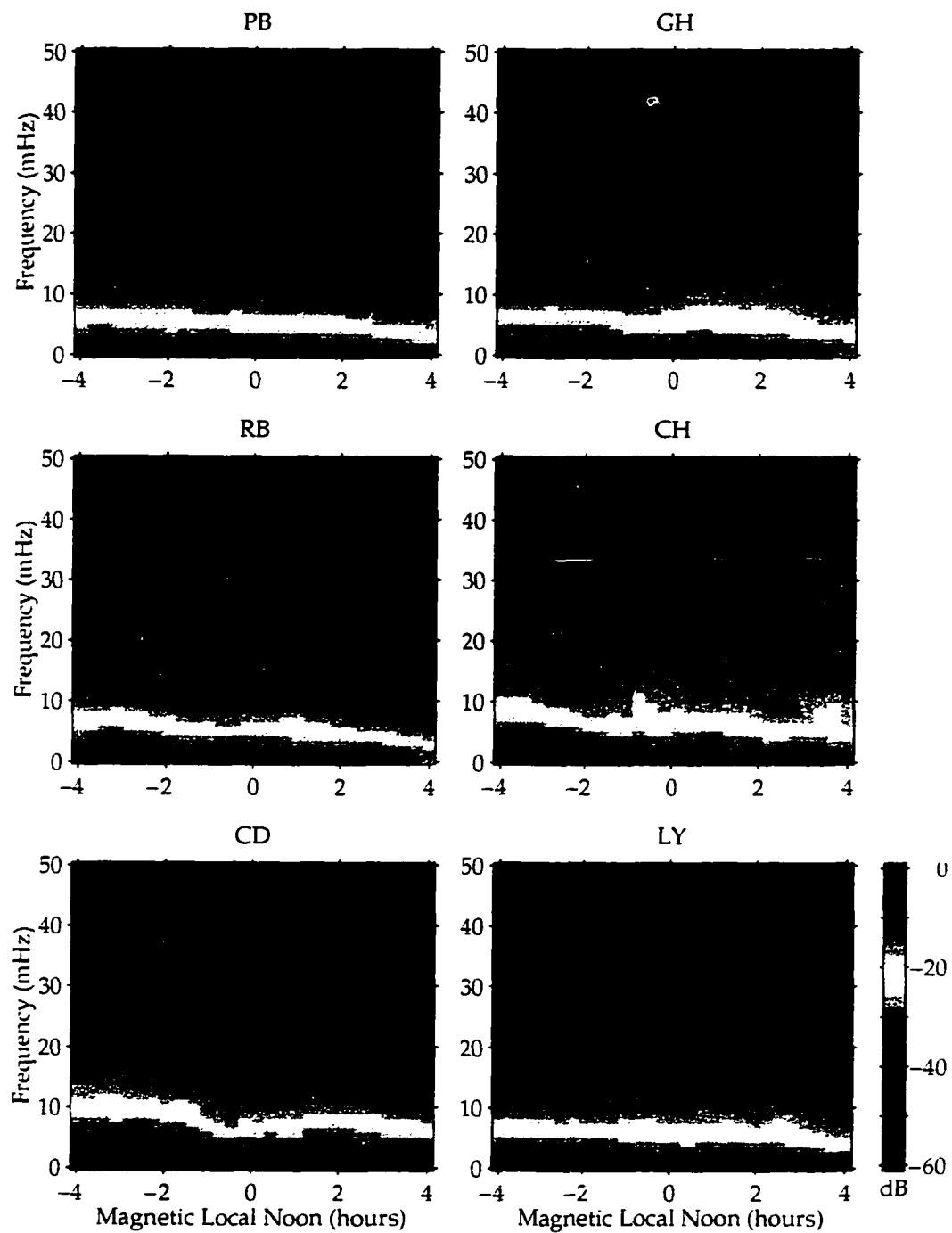
Figure 4.3. Mean trace power spectra centered on magnetic local noon. Shown in each panel are the pixel-by-pixel means of the trace power at each station (see text for details). The logarithm of the peak power at each station is normalized to unity for display purposes. The stations are displayed in order of descending L-shell: Pelly Bay (PB), Gjoa Haven (GH), Repulse Bay (RB), Coral Harbor (CH), Cape Dorset (CD) and Longyearbyen (LY).
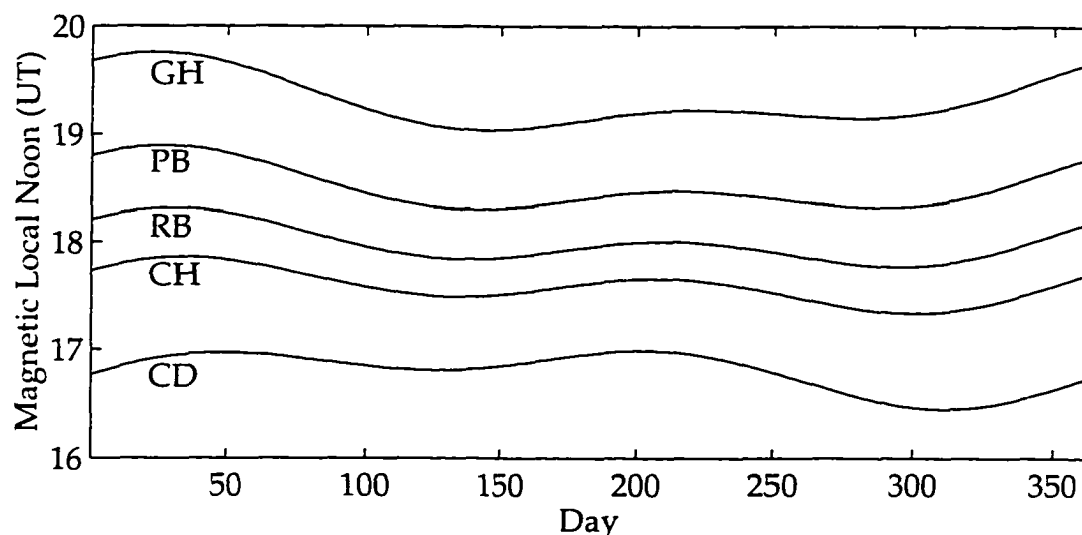
Figure 4.4. Magnetic local noon as a function of Julian date. The annual fluctuation, calculated via the dipole tilt angle, spans roughly ±15 minutes at each station. Longyearbyen (LY, not shown) undergoes a similar variation about a mean value of 0902 UT.

We find that tracking local noon causes certain features to become more distinct. This characteristic argues for a spatial interpretation, as the cusp is a feature that passes by the station in magnetic local time. In Figure 4.4 we show the annual variation in local noon for the MACCS array.

In analyzing the mean trace spectra, we found that it was difficult to assess the significance of the spatial features. Since no feature stood out by more than ~10 dB from any other in a given frequency band, we found these results difficult to reconcile with the spatial interpretation of *McHarg et al.* [1995]. Qualitatively, the trace spectra indicate that temporal information may dominate the cusp spectrum, causing a blurring of any spatial information. Moreover, different stations appear to be representative of different categories under the classification of *McHarg et al.* [1995] (see Table 4.1). Gjoa Haven, with its apparent spatial structure in the Pc 3 frequency band, appears to be category 1. Pelly Bay, Repulse Bay, Cape Dorset and Longyearbyen all appear to be category 2; Coral Harbor falls under either category 2 or 3.

Engebretson et al. [1995] noted that these spectral classifications were based primarily on the character of Pc 3 power in the spectra. They found that roughly thirty percent of the spectra taken across the MACCS array exhibited Pc 3 events that were temporal features,

Category	Description
1	Distinct pre- and post-noon Pc 3 power with at least 10-dB decrease in power between. Pre-noon Pc 5 power dominant signal.
2	One or none 10-dB pre- or post-noon Pc 3 power enhancement. Pre-noon Pc 5 power dominant signal.
3	Distinct pre- and post-noon Pc 3 power with no decrease in power between. Active days, Pc 3 power of order Pc 5.
4	Quiet days with no significant increase in power above background levels.
5	Other days, not fitting categories 1–4.

Table 4.1. Cusp spectral categories. These categories were established by *McHarg et al.* [1995] upon examination of 253 days of Longyearbyen magnetometer trace power spectra. Correlations between the categories and IMF parameters were also made.

appearing across >4 hours of local time. Our own analysis of the Pc 3 power spectrum is inconclusive. There appears to be some spatial information in the mean spectrum at some stations; however, that information is not consistently present at cusp latitude stations.

4.2.2 Polarization spectra

Recall that *McHarg et al.* [1995] weighted their trace spectra by the degree of polarization. Effectively, each pixel in their power spectra was given by the product $(P_{xy}^2[f, t] \ \text{tr} \, S[f, t])$. We estimate the degree of polarization spectra separately, where each pixel is given simply by $P_{xy}[f, t]$, and found the spatial information reported by *McHarg et al.* [1995]. Since the polarization estimator gives no indication of the sense of polarization, right- or left-handed, we also estimate the mean ellipticity [e.g., *Fowler et al.*, 1967] spectrum for each station. We feel that consideration of this polarization information explains the disparate results of each group. The pure state filtration technique used by *McHarg et al.* [1995] tends to suppress broadband noise; it was broadband Pc 3 that *Engebretson et al.* [1995] cited as evidence for a temporal interpretation. The lack of significant structure in the Pc 3 band in local time favors a temporal interpretation. In essence, both groups were considering separate aspects of the cusp spectrum.

In Figures 4.5 and 4.6 we display the results of a mean polarization and ellipticity spectral analysis, using spectrum estimation techniques identical to those used to produce Figure 4.3. At each station there is evidence for a minimum in Pc 5 polarization levels near local noon. The sense of this polarization changes sense from left- to right-handed roughly across local noon. Given the >10-hour universal time separation of the stations, we take these features as unambiguous evidence of a spatial signature in the cusp spectrum.

We have a quantitative measure for the significance of features in the mean polarization spectra. *Samson and Olson* [1981] have shown that the expectation value of the estimator falls off as a function of degrees of freedom in the spectral estimate; for approximately ten degrees of freedom, $\langle P_{xy}[f] \rangle = 0.25$. Signals resulting in polarization values below this value may be considered noise. Thus, the Pc 5 minimum near local noon is significant in that the polarization tends away from noise-like values in the morning and afternoon sectors. It is interesting to note that the degree of polarization falls off near local noon, at roughly the same time the sense of polarization is switching from left- to right-handed.

4.2.3 State-space discriminant

The information displayed in Figures 4.5 and 4.6 gives strong evidence for the presence of a repeatable, diurnal signature associated with the cusp spectrum. Since the signature tracks in magnetic local time, its interpretation must be spatial. Qualitatively, the result shown in Figure 4.6 has been noted in a number of event-based studies [e.g., *Samson et al.*, 1971; *Olson and Rostoker*, 1978]. In a new result, we find that the mean polarization spectrum may be used in an information theoretic sense to develop a cusp spectrum discriminant. This discriminant replaces the "by-eye" classification scheme of *McHarg et al.* [1995] with a quantitative measure. *Szuberla et al.* [1994] developed the basic procedure for the state-space measure we use here. They applied it to cusp time series and found that stochastic phase skips in the data confounded the measure. Since the degree of polarization contains no phase information, we find it useful in constructing a state-space discriminant of the cusp spectrum.

The principle behind our state-space measure is simple. The greater/smaller the "distance" between the mean polarization spectrum and the spectrum for a particular day, the less/more cusp-like that spectrum is. To establish an easily interpretable metric for the

Figure 4.5. Mean polarization spectra centered on magnetic local noon. Shown in each panel are the pixel-by-pixel means of the degree of polarization at each station (see text for details). The stations are arrayed as for Figure 4.3.
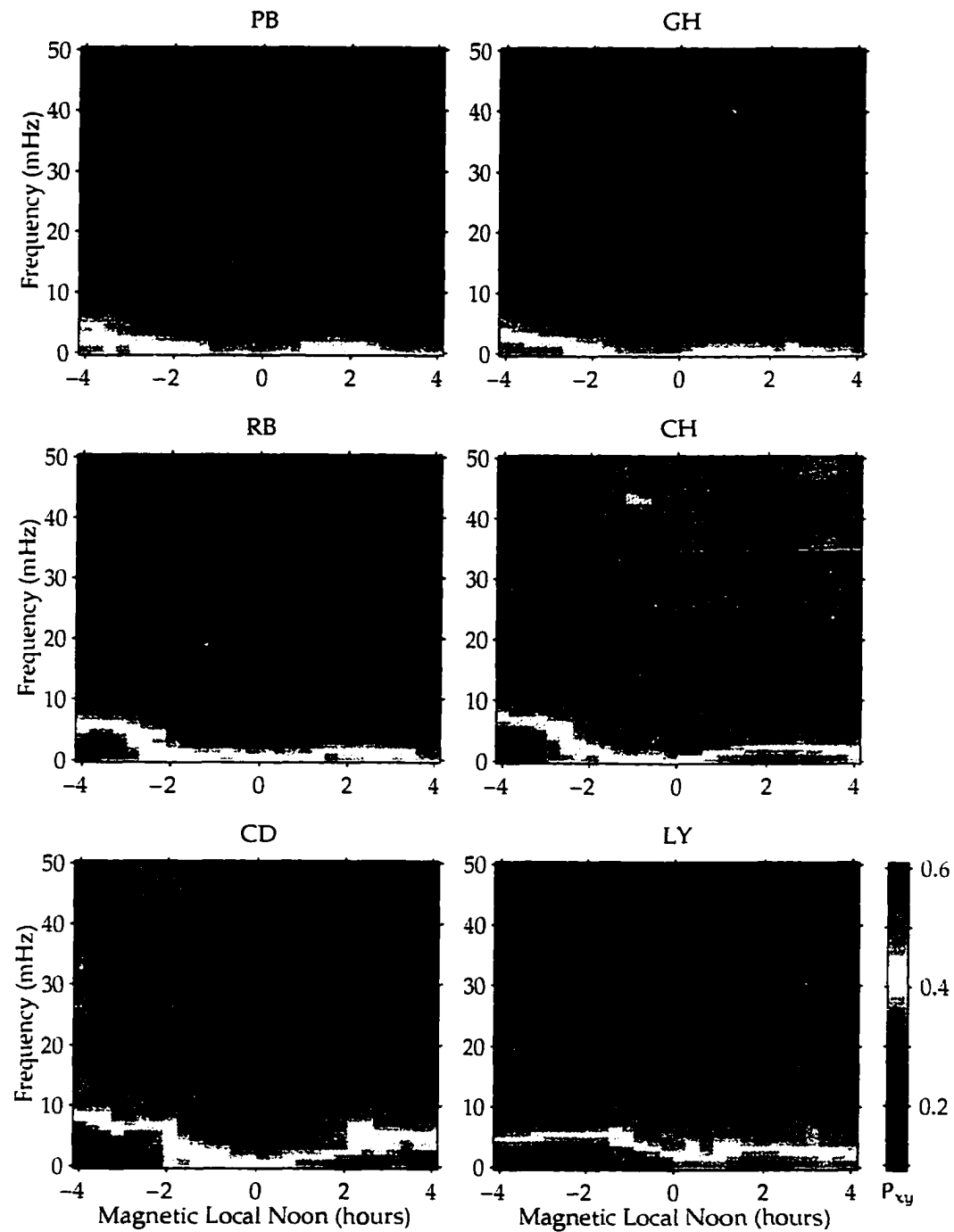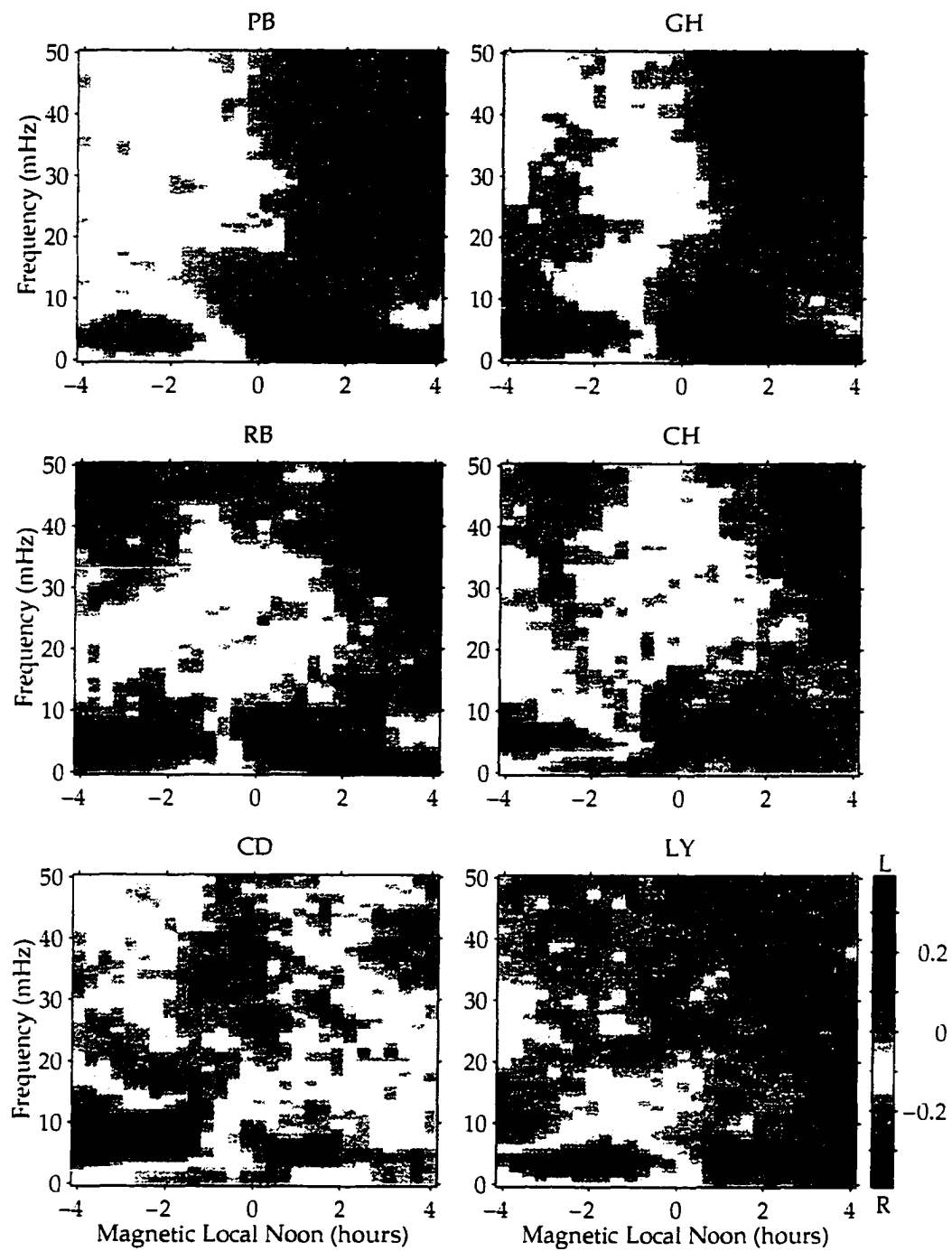
Figure 4.6. Mean ellipticity spectra centered on magnetic local noon. Shown in each panel are the pixel-by-pixel means of the ellipticity (in the x-y plane) at each station (see text for details). The stations are arrayed as for Figure 4.3.

"distance" between two matrix entities we map the polarization matrix elements into a vector space according to the mapping given by

$$P_{ij} \Rightarrow p\,[i + jM] \tag{4.1}$$

In this vector space we denote mean polarization vector as $|\bar{p}\rangle$ and the polarization vector for the n-th day as $|p_n\rangle$. We define the "distance" between the vectors $|p_n\rangle$ and $|\bar{p}\rangle$ in standard fashion as the Euclidean norm L_2 of their vector difference

$$Q_n = \big\||p_n\rangle - |\bar{p}\rangle\big\| \tag{4.2}$$

We compile the set $\{Q_n\}$ for a given station and examine its probability function. In Figure 4.7 we display the results for Longyearbyen and Gjoa Haven. Both distributions are similar in that they exhibit a sharply peaked maximum, a small shoulder and outliers toward higher values of Q. We note that across all six stations $Q < 5$ was not observed. The mean polarization vector then represents the centroid of a region in state space about which the daily realizations of the polarization vector fall, always with radius greater than 5.

We first consider only the Longyearbyen data, especially those days for which *McHarg et al.* [1995] had IMP 8 IMF data available. When we determine where in the distribution the corresponding values of Q_n fall, we find that we can reproduce the spectral classifications of *McHarg et al.* [1995]. Taking the peak in the Longyearbyen distribution separately, we find that Q is approximately normally distributed, with $\bar{Q} = 6.75$ and $\sigma_Q = 0.272$. Category 1 and 2 days all fall within one standard deviation of this mean; ie., $Q_{1,2} = 6.7 \pm 0.3$. We find that category 3 days fall on the shoulder of the distribution, $Q_3 \in [7.4, 8.6]$. Quiet days, category 4, fall anywhere in the range $Q > 7$.

The distributions across the MACCS array are qualitatively similar to the distribution at Longyearbyen. The few category 1 and 2 days[3] indicated in the published study of *Engebretson et al.* [1995] also fall into the range $\bar{Q} \pm \sigma_Q$ at each MACCS station. Category 1 and 2 days were those used by *McHarg et al.* [1995] to make strong optical, DMSP and IMP 8 correlations with the passage of the cusp nearby the station; therefore, our state-space measure provides the first and only quantitative means of discriminating the spatial passage of the cusp by strictly ground-based magnetic means.

---

[3]Category 1 and 2 of *McHarg et al.* [1995] roughly translate to group 2C and 3A of *Engebretson et al.* [1995].
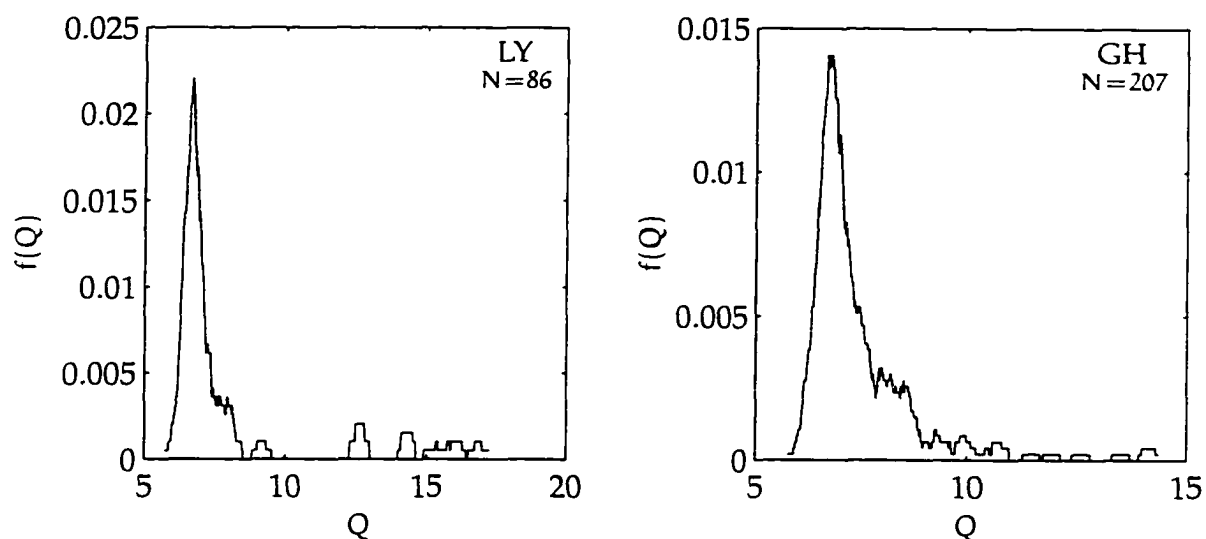
Figure 4.7. Probability functions of the state-space measure Q for Longyearbyen and Gjoa Haven. N indicates the number of days available for study at each station. Note that each probability function exhibits a sharply peaked maximum, a shoulder and outliers toward higher values of Q (see text for details).

4.2.4 Eigenspectra analysis

Since our state-space measure is based on a mean polarization spectrum which is never physically realized ($Q > 5$), we use another information theoretic tool to determine its significance. We construct the set $\{|p_n\rangle - |\bar{p}\rangle\}$ and then decompose it via the Karhunen-Loéve transform.[4] This procedure is equivalent to decomposing the set of mean-detrended polarization vectors into a statistically orthogonal basis set that spans our original vector space [*Aubry et al.*, 1991; *Therrien*, 1992]; in other words, we are decomposing the polarization spectrum into its eigenspectra. Having removed the mean polarization vector, the eigenvectors of the decomposition represent a standardized set of deviations from that mean. The eigenvalues of the Karhunen-Loéve decomposition determine the information theoretic significance of each corresponding eigenvector or deviation.

The significance of the mean spectrum can be assessed by examining the cumulative normalized eigenvalues of the Karhunen-Loéve decomposition. They are a measure of how efficiently the basis set accounts for deviations from the mean. In Figure 4.8 we show

---

[4]The mathematically motivated reader may wish to read Appendix A prior to this section; therein we develop the Karhunen-Loéve transform formally.
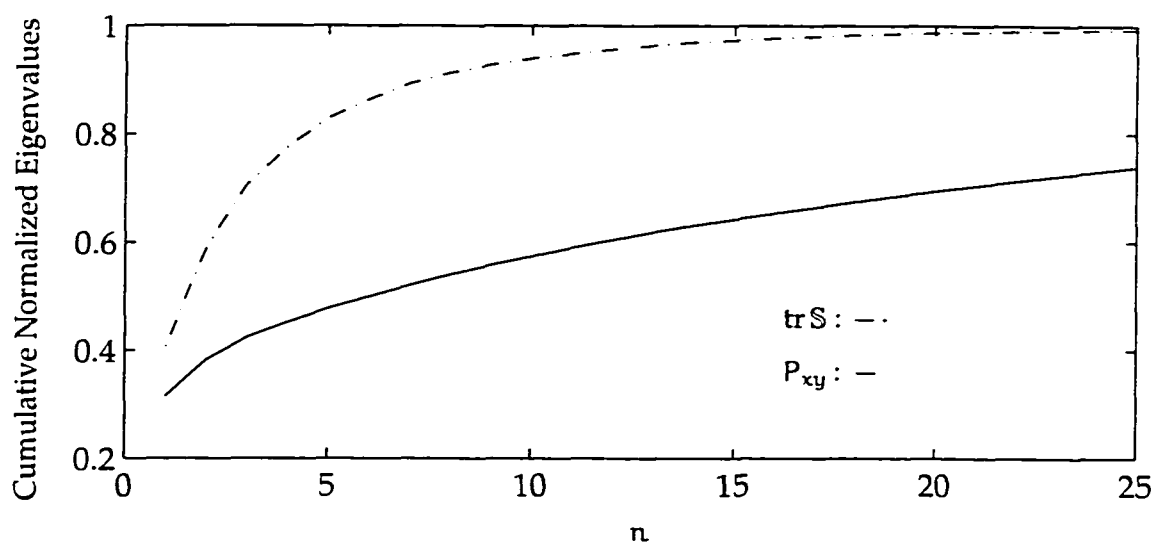
Figure 4.8. Polarization and trace power spectra eigenvalues. Shown are the cumulative normalized eigenvalues of the trace power (tr S) and degree of polarization (P_{xy}) as a function of eigenvalue (n). This format allows us to examine how efficiently the deviations from the mean spectra are encoded in the basis of the Karhunen-Loéve decomposition (see text for details).

the results of such an analysis for both the polarization and trace power spectra. We note that the trace power deviations (dot-dashed curve) are much more efficiently encoded by the Karhunen-Loéve transform; more than 80 percent of the deviations from the mean can be accounted for by the first 5 eigenvectors. The encoding is much less efficient for the polarization spectrum (solid curve). The relatively small, constant slope of the polarization eigenvalues is a feature commonly ascribed to the decomposition of an uncorrelated noise process [e.g., *Broomhead and King*, 1986; *Mees et al.*, 1987; *Aubry et al.*, 1991].

The daily deviations from the mean polarization spectrum are essentially noise. We can compare the information content of the mean with the cumulative information content of the daily polarization deviations to establish an effective signal-to-noise ratio; we find this value to be 2.1. The corresponding S/N ratio for the trace power spectrum is 0.21. The mean polarization is then an effective first-order description of the daily values; the mean trace power is not. We interpret this result to signify that the mean polarization spectrum accounts for the bulk of the information content in the daily realizations of the polarization spectrum. As such, we have confidence in it as the fiducial spectrum for our state-space
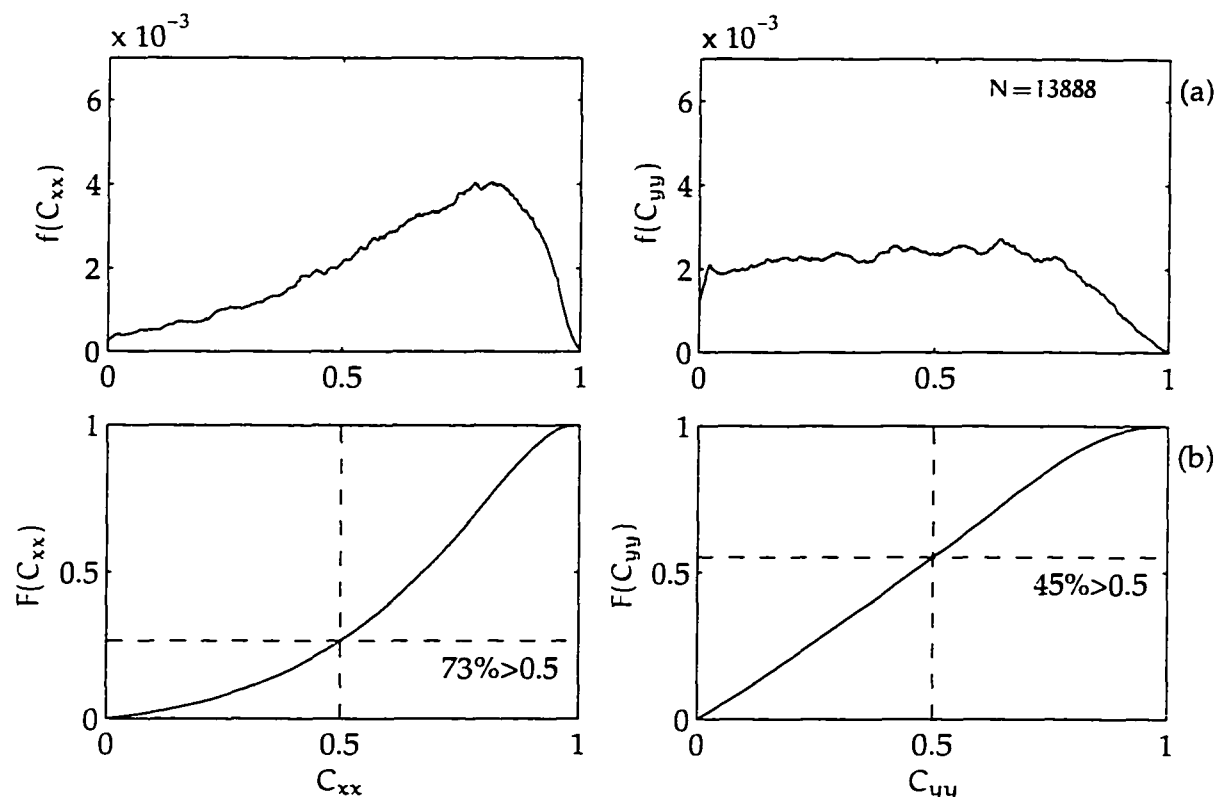
Figure 4.9. Cumulative Pc 5 coherence statistics for Pelly Bay and Gjoa Haven. The station separation is 252 km. Figure format is as for Figure 3.7 (see text for details).

discriminant.

4.2.5   Statistical coherence

The procedure for determining the interstation coherence level of localized Pc 3 pulsations (see Chapter 3) may be trivially modified to examine long-period pulsations. From Figure 4.5 we see that most of the mean polarization information is concentrated below 10 mHz. On this basis we select dc–10 mhz as our operational Pc 5 frequency band and examine the distribution of interstation coherence estimates in that band. The Pc 5 and Pc 3 coherence estimates display markedly different probability and distribution functions (compare Figure 4.9 with Figures 3.9 through 3.12); the low frequency probability functions are clearly not noise dominated.

A feature common to all the MACCS station pairs available for study is a minimum in the Pc 5 interstation coherence centered roughly one hour prior to local noon. This feature is similar to the one seen in Figure 4.5, where the intrastation polarization below 10 mHz exhibits a minima near noon. The interstation coherence levels for the Pc 5 frequency band also decrease with increasing station separation. A linear model[5], similar to the one constructed for the Pc 3 coherence level data, allows us to estimate the Pc 5 coherence level as a function of station separation: $C_L \approx e^{-s/300}$, where "s" is the station separation in km.

The fact that generalized coherence characteristics are common to both inter- and intrastation observations is not surprising. Since the trace power is consistently dominated by signals in the Pc 5 frequency band (e.g., Figure 4.3), coherence levels should increase among station pairs; a relatively loud signal will have a greater probability of being observed between two distant stations. By the same token, a pronounced signal at a single station in either (or both) the x- or y-component will result in increased polarization levels. Since the polarization estimator is independent of sensor orientation, we need not be concerned that the signal may be present in greater part in one or the other of the channels.

4.3 Discussion

McHarg et al. [1995] suggested that the different spatiotemporal interpretations of the cusp spectrum might might stem from the fact that the MACCS array is perpetually sunlit at magnetic local noon. Longyearbyen lies beneath the terminator at noon for several months.[6] Greater conductivity in the sunlit ionosphere above the MACCS array would account for the observations of *Engebretson et al.* [1995]; namely, large-amplitude, broadband Pc 3 pulsations in the local time-frame proposed as central cusp by *McHarg et al.* [1995]. Since both groups concentrated on the presence/absence of broadband noise above 20 mHz, we find their interpretations were guided by their analysis techniques. In this chapter we have shown that a polarization analysis is the key to making a spatial interpretation of the cusp spectrum, especially in the Pc 5 frequency band. We stress that neither group

---

[5]We again calculate Kendall's τ for the Pc 5 data, giving $\tau = -0.91$ and probability $Pr = 2.5 \times 10^{-4}$ that the station separation in km and log C_L are not linearly correlated.

[6]The days we studied at Longyearbyen were all taken when the terminator was at least 64 km above the station at local noon (H.–C. Stenbaek-Nielsen, private communication, 1994).

arrived at an incorrect interpretation, they were merely considering separate aspects of the cusp spectrum. We find that broadband Pc 3 noise gives a good temporal description of the cusp spectrum, while polarized Pc 5 pulsations provide the spatial information.

The significant result of this chapter is we have developed the first and only quantitative means of discriminating the spatial passage of the cusp by ground-based magnetic means. We accomplish this discrimination with our state-space polarization measure, which gives us a quantitative equivalent of the spectral categories of *McHarg et al.* [1995] (see Table 4.1). We note that our state-space measure cannot distinguish between category 1 and 2 spectra un⁴er that scheme. Since the distinction between these categories lies in broadband noise above 20 mHz, our polarization-based measure will suppress the distinction. We find that the spatial information regarding the cusp spectrum lies in the Pc 5 frequency band, thus we consider category 1 and 2 to be the same. This finding is consistent with the temporal interpretation of broadband Pc 3 by *Engebretson et al.* [1995].

When we consider the sense of polarization in the Pc 5 frequency band, given by the ellipticity spectrum, we find a convincing physical interpretation of our results. In Figure 4.6 we see that the polarization at each station is dominantly left-handed in the morning sector. Near local noon the sense changes to right-handed, although to a lesser magnitude than in the morning sector. *Lee et al.* [1981] showed that conditions along the LLBL are particularly favorable for the Kelvin-Helmholtz instability at the magnetopause. In agreement with the work of *Southwood* [1968], he gave a theoretical explanation for the switch in polarization observed at high latitude. *Lee et al.* [1981] further showed that the morning sector should exhibit enhanced wave power. Observationally, our determination of the mean ellipticity spectrum is consistent with the event-based findings of of *Samson et al.* [1971] and *Olson and Rostoker* [1978].

The adiaroic line (separatrix between open and closed field lines) is commonly placed at or near the cusp [*Smith and Lockwood*, 1996]. Since the fundamental FLR continuum mode is in the Pc 5 frequency range at cusp latitude [*Singer et al.*, 1981], it should be possible to infer the location of the last closed field lines with an appropriately spaced array of magnetometers. In principle, the cross-phase technique of *Waters et al.* [1995] could be used in this determination; however, our results bear on the reliability of such a determination. The scale length of coherent Pc 5 pulsations, $\mathcal{O}(300 \text{ km})$, indicates that the location of the

last field lines cannot be resolved to better than this distance by ground-based magnetic means. This conclusion is supported by the magnetic observations of *Ables et al.* [1996], where they noted FLR characteristics well into the polar cap.

Waters et al. [1995] and *Ables et al.* [1996] have each given evidence that the polarization and ellipticity characteristics of Pc 5 pulsations at high latitude are indicative of the continuum mode FLR. While the coupling of Kelvin-Helmholtz excitations to resonant shear Alfvén waves along the magnetopause is certainly plausible, there is not yet enough *in situ* evidence to support the conclusion that the FLR is the dominant carrier of information near the cusp. *McHarg* [1993] gives evidence of magneto-optical correlations in the Pc 5 frequency band when the cusp is clearly equatorward of the Longyearbyen, placing the station under open field lines. *Friis-Christensen et al.* [1988] and *Glassmeier et al.* [1989] each give evidence that a TCV can generate the same Pc 5 polarization signature we see in Figures 4.5 and 4.6. Both observational and theoretical evidence has been given that some of the Pc 5 pulsations at the cusp may be generated by localized ionospheric effects [*Chisham et al.*, 1995; *Leonovich and Mazur*, 1996; *Streltsov and Lotko*, 1997]. It is reasonable to assume that the FLR accounts for a portion of the information present in the cusp spectrum; however, there are other source mechanisms which may contribute in equal or greater measure in the Pc 5 frequency band.

In the not-too-distant future, we should have greater *in situ* data coverage of the cusp and boundary regions from the POLAR and upcoming Cluster satellites. Recently deployed radars should provide valuable observations regarding the difficult problem of wave interactions in the high latitude ionosphere, especially the multiple-site configurations with overlapping fields-of-view. Eventually, the physics of wave generation and propagation near the cusp will be understood in terms of theoretical treatments backed by correlations made between data taken on the ground, at the source region and at points in between. For the present, we are working to merge the individual spectral classification schemes of *Engebretson et al.* [1995] and *McHarg et al.* [1995] in order to apply our state-space cusp discriminant uniformly across both databases. A collaborative effort between the two groups is required and long overdue; such a collaborative study is presently being organized by the author.

Chapter 5

Conclusion

The main purpose of this thesis is to ascertain how well the cusp region can be characterized through the analysis of ground-based magnetometer records. We couch this characterization in terms of three specific, open problems of the physics of magnetic perturbations in the cusp and boundary regions: 1) the coherence of localized pulsations, 2) the spatiotemporal nature of the cusp magnetic spectrum, and 3) the ground-based magnetic determination of the separatrix. In this final chapter we summarize our findings regarding these problems and offer recommendations for further research.

5.1   Summary

Our characterization of the cusp region begins with the first problem in an analysis of magnetometer signals in the Pc 3 frequency band. The work of *Engebretson et al.* [1990] suggests that these pulsations are generated in the overhead ionosphere and not in the distant magnetosphere. We assume that these pulsations are detectable only over a finite spatial extent and develop a statistical measure of interstation coherence to quantify that length scale. We find that our measure of interstation coherence, C_L, falls off with increasing station separation and may be approximated by an exponential function: $C_L \approx 1.4e^{-s/250}$, where "s" is the station separation in km. We link our coherence measure to a simple physical model for the precipitating electron beams presumed responsible for the localized Pc 3 pulsations. With this model we estimate an upper bound of $\mathcal{O}(200 \text{ km})$ for the coherence length. A

103

number of obsevations confirm this result. Our estimate for the coherence length serves as an important constraint in identifying the source of Pc 3 frequency band modulations of cusp latitude electron precipitation.

We address the second problem by examining the disparate spatiotemporal interpretations of the cusp spectrum made by *Engebretson et al.* [1995] and *McHarg et al.* [1995]. We examine the databases of each group and find evidence that supports the temporal/spatial interpretation of the former/latter. We find that broadband Pc 3 noise gives a good temporal description of the cusp spectrum, while polarized Pc 5 pulsations provide unambiguous spatial information. We use the polarization spectrum to establish a quantitative means of discriminating the spatial passage of the cusp by ground-based magnetic means. We use the discriminant to quantify the spectral classifications of *McHarg et al.* [1995]. This is a significant result because these spectral classifications have been linked to ground-based optical observations, low-altitude satellite particle observations in the cusp and boundary regions, and interplanetary magnetic field parameters.

Finally, we consider the third problem by employing our statistical measure of inter-station coherence in the Pc 5 frequency band. We find that the scale length of coherent Pc 5 pulsations precludes ground-based magnetic resolution of the location of the last field lines to better than $\mathcal{O}(300 \text{ km})$. Higher resolution measurements will likely have to be carried out by other means (e.g., optical or radar).

In this thesis we have demonstrated that judicious application of various signal processing techniques can yield new, physically meaningful results from ground-based magnetometer records; it can also aid in understanding disparate reports from groups using different analysis techniques on like data. In that sense, we have attained our goal with an improved characterization of the cusp region.

5.2 Recommendations for further work

Despite our achievements, there is much work to be done in the field of ground-based magnetic pulsations. While we have convincing observational evidence that modulated electron precipitation gives rise to localized Pc 3 pulsations at the cusp, we lack a theoretical understanding. In particular, we lack an explanation of a localized mechanism which

would account for the precipitation of the observed magnetosheath-like electrons. We think the work of *Maggs and Morales* [1996, 1997] holds promise in this regard. They have shown in theory and in laboratory experiment that localized, field-aligned plasma striations can lead to significant wave generation. A preliminary calculation shows that their results are applicable to our own in terms of both geomagnetic latitude and Pc 3 frequency band. We are presently exploring their work to see if it agrees with our determination of the upper bound on the coherence length of localized Pc 3 pulsations.

Our work in establishing generalized coherence-based measures points to potential new applications of the degree of polarization estimator of *Samson and Olson* [1980]. An increasing trend in space physics research is the deployment of arrayed instrument suites with overlapping "fields-of-view." An example of such a deployment in the northern hemisphere is the twin CUTLASS HF radars which overlook the magneto-optical observatories at Longyearbyen and Ny Alesunde. Each of these stations currently has *in situ* coverage provided variously by POLAR and the DMSP satellites, with further coverage to be provided the upcoming Cluster mission. The polarization estimator is specifically designed to treat the N-dimensional instrument space that characterizes the data generated by these instrument suites. We feel that the development of generalized coherence-based measures from multiple-instrument data sets is a field of research ripe with possibility.

Appendix A

The discrete Karhunen-Loéve transform

Developments of the discrete Karhunen-Loéve transform are typically performed under the assumption of square matrices [e.g., *Fu*, 1968; *Preisendorfer*, 1988; *Therrien*, 1992]. While this simplifies the analysis greatly, real-world data seldom afford us that luxury. What follows is a general development of the DKLT, one that may be applied to typical data sets that do not lend themselves to square analysis. Note that although we have assumed real data throughout this thesis, the following development of the DKLT is quite general and valid for complex data.

We develop a two-pronged eigensystem approach to the DKLT, similar to the singular value decomposition of *Akansu and Haddad* [1992]. This method is used to avoid the numerical difficulties found by *Mees et al.* [1987]. For practical computation, such as the analysis of magnetometer time series and spectral data, we find the procedure quite sound.

A.1 Development

Given a set of N-dimensional random vectors, $\{|x_m\rangle\}$, with $m \in [0, M-1]$, we can expand each of the vectors in terms of a finite set of orthonormal basis functions

$$|x_m\rangle = \sum_{b=0}^{M-1} v_b[m] |a_b\rangle \qquad (A.1)$$

106

In our "bra-ket" notation we define the complex conjugate transpose of a vector (A.2a) and the inner product (A.2b) as

$$|x_m\rangle = \langle x_m|^\dagger \tag{A.2a}$$

$$\langle x_m|x_m\rangle = \sum_{n=0}^{N-1} x_m[n]\, x_m^*[n] \tag{A.2b}$$

such that the inner product of a "bra"-vector and its corresponding "ket"-vector is positive, semi-definite. The orthonormality requirement

$$\langle a_i|a_j\rangle = \delta_{ij} \tag{A.3}$$

placed on the basis functions makes the bases form a complete set; they span the R^N space of the original set of vectors [*Aubry et al.*, 1991].

Orthonormal bases are characteristic of functional decomposition, as we have seen in the case of the DFT (2.3) and complex exponentials. In the DKLT formalism however, we further require an orthogonal set of vectors formed from the expansion coefficients: $\{|v_b\rangle\}$, where $|v_b\rangle = \left(v_b[0]\, v_b[1] \dots v_b[M-1] \right)^\dagger$. This orthogonality requirement is given by

$$\langle v_i|v_j\rangle = c_i\delta_{ij} \tag{A.4}$$

If the random vectors $\{|x_m\rangle\}$ are all zero-mean, then (A.4) specifies that the coefficients are uncorrelated [*Therrien*, 1992]. The restriction (A.4) carries with it several advantages in the information theoretic sense.

The expansion coefficients of the DKLT in (A.1) can be solved for directly, using both (A.3) and (A.4)

$$\langle a_i|x_m\rangle = \sum_{b=0}^{M-1} v_i[m]\, \langle a_i|a_b\rangle = v_i[m] \tag{A.5}$$

This relation (A.5) between the coefficients, bases and original random vector is the forward DKLT, and the decomposition in orthogonal basis functions (A.1) is the Karhunen-Loève expansion — also known as the inverse transform.

In the case of the DFT, the orthonormal basis functions were known — complex exponentials or sinusoids. Solving for the expansion coefficients completes the problem of the

DFT. In the case of the DKLT however, we have solved for the expansion coefficients in principle only. Since we seek an orthonormal set $\{|a_b\rangle\}$ that satisfies (A.4), its form cannot be known *a priori*; rather, the form of the set $\{|x_m\rangle\}$ uniquely determines the bases into which it can be decomposed.

Before solving for the basis functions of the DKLT, we first make our notation more compact. The original set of random vectors $\{|x_m\rangle\}$ can be formed into a convenient matrix

$$\mathbb{X} \equiv \left(|x_0\rangle\, |x_1\rangle \cdots |x_{M-1}\rangle \right)^\dagger \tag{A.6}$$

This arrangement is commonly known as a data matrix or an embedding matrix [*Mees et al.*, 1987]. Similar matrix arrangements can be made for the basis functions and expansion coefficients

$$\mathbb{A} \equiv \left(|a_0\rangle\, |a_1\rangle \cdots |a_{M-1}\rangle \right)^\dagger \tag{A.7a}$$

$$\mathbb{V} \equiv \left(|v_0\rangle\, |v_1\rangle \cdots |v_{M-1}\rangle \right) \tag{A.7b}$$

Now, from the orthonormality of the set $\{|a_b\rangle\}$ (A.3) and the orthogonality of the set $\{|v_b\rangle\}$ (A.4) we find that

$$\mathbb{A}\mathbb{A}^\dagger = 1 \tag{A.8a}$$

$$\mathbb{V}^\dagger\mathbb{V} = \mathbb{C} \tag{A.8b}$$

where 1 is the identity matrix and $C_{ij} = c_i\delta_{ij}$. Note that $\mathbb{A}$ is unitary only in the special case of square matrices, $M = N$. We can use the matrices (A.6) and (A.7) together with their relations (A.8) to derive matrix expressions analogous to the inverse (A.1) and forward (A.5) Karhunen-Loéve transforms

$$\mathbb{X} = \mathbb{V}\mathbb{A} \tag{A.9a}$$

$$\mathbb{V} = \mathbb{X}\mathbb{A}^\dagger \tag{A.9b}$$

Taking the first of these relations (A.9a) and right multiplying by its adjoint gives

$$\mathbb{X}\mathbb{X}^\dagger = \mathbb{V}\mathbb{A}\mathbb{A}^\dagger\mathbb{V}^\dagger = \mathbb{V}\mathbb{V}^\dagger \tag{A.10}$$

Left and right multiplying (A.10) by $\mathbb{V}^\dagger$ and $\mathbb{V}$, respectively, gives

$$\mathbb{V}^\dagger\mathbb{X}\mathbb{X}^\dagger\mathbb{V} = \mathbb{V}^\dagger\mathbb{V}\mathbb{V}^\dagger\mathbb{V} = \mathbb{C}^2 \tag{A.11}$$

Here we define an auxiliary Hermitian matrix $\mathbb{P} \equiv \mathbb{X}\mathbb{X}^\dagger$ to rewrite (A.11) in compact form as an eigenvalue equation

$$\mathbb{V}^\dagger \mathbb{P}\mathbb{V} = \mathbb{C}^2 \tag{A.12}$$

We note that the Hermitian matrix $\mathbb{P}$ is square, which gives it considerable analytic and computational utility. The solution of the eigenvalue problem is straightforward, and once the coefficients $\mathbb{V}$ are known, we can solve (A.9a) for the basis functions $\mathbb{A}$ as

$$\mathbb{A} = \mathbb{C}^{-1} \mathbb{V}^\dagger \mathbb{X} \tag{A.13}$$

We have then a theoretical machinery developed for solving the DKLT, one which provides us with both the expansion coefficients (A.12) and basis function (A.13). It is also possible to solve an eigenvalue equation directly for the basis functions. We develop the second solution here, and later find a computational motivation for developing two equivalent eigensystem solutions.

Taking the second of the matrix relations (A.9b) and left multiplying by its adjoint gives

$$\mathbb{V}^\dagger \mathbb{V} = \mathbb{A}\mathbb{X}^\dagger \mathbb{X}\mathbb{A}^\dagger \tag{A.14}$$

Again, we define an auxiliary Hermitian matrix, $\mathbb{R} \equiv \mathbb{X}^\dagger \mathbb{X}$, which is proportional to the covariance matrix [*Broomhead and King*, 1986]. We note that $\mathbb{R}$ shares the same square property as $\mathbb{P}$. If the vectors comprising $\mathbb{X}$ are all zero-mean, $\mathbb{R}$ is proportional to the correlation matrix. With it we rewrite (A.14) in compact form as another eigenvalue equation

$$\mathbb{A}\mathbb{R}\mathbb{A}^\dagger = \mathbb{C} \tag{A.15}$$

Once again, the basis functions $\mathbb{A}$ are solved via the eigenvalue problem (A.15), and we have already a solution for the coefficients $\mathbb{V}$ in (A.9b).

The DKLT is unique, in that it is the *only* orthonormal expansion that results in the orthogonality of the coefficient vectors (A.4) [*Therrien*, 1992]. This uniqueness stems from the requirement that the basis functions must be determined using the data directly. The uniqueness of the DKLT can be derived from the optimal property that we develop in the next section. Specifically, it is governed by the information stored in the matrices $\mathbb{P}$ and $\mathbb{R}$. From the equivalent eigensystems, we see that the orthonormal bases are simply the

eigenvectors of the matrix $\mathbb{R}$ (A.15), and the orthogonal coefficient vectors are the eigenvectors of the matrix $\mathbb{P}$ (A.12). Too, the mean squared coefficients (A.4) are encoded in both matrices as the eigenvalues. Note that the eigenvalues of $\mathbb{P}$ and $\mathbb{R}$ are identical[1] — they are the diagonal elements of $\mathbb{C}$.

A.2 Optimal property

In any orthonormal decomposition, we assume that the inverse is true — the decomposed vector can be reconstructed exactly, using all of the expansion terms. In the information theoretic sense, the DKLT expansion (A.1) of a random vector represents the most efficient packing of energy among its expansion coefficients and basis functions [*Akansu and Haddad*, 1992]. The energy contained in the data is defined as the sum of the eigenvalues of the correlation matrix [*Armbruster et al.*, 1994], which we have seen is proportional to $\mathbb{R}$. The uniqueness and optimality of the DKLT stem from the decorrelation of the expansion coefficients in (A.4) [*Rao*, 1973].[2] What this means in the practical sense, is that the DKLT allows us to truncate the expansion and approximate the original vector with the least amount of error. We now show that the truncated Karhunen-Loéve representation is the optimal, in terms of the mean-square error introduced.

Given any of the random vectors comprising $\mathbb{X}$, an approximation $|\check{x}_m\rangle$ can be made by using only the first K of the M basis functions in $\mathbb{A}$. This approximation will introduce some error $|\epsilon_m\rangle$ as

$$
\begin{aligned}
|x_m\rangle &= |\check{x}_m\rangle + |\epsilon_m\rangle \\
&= \sum_{b=0}^{K-1} v_b[m]\,|a_m\rangle + \sum_{b=K}^{M-1} v_b[m]\,|a_m\rangle
\end{aligned}
\tag{A.16}
$$

Using the expectation operator, $\mathcal{E} \equiv \frac{1}{M}\sum_{m=0}^{M-1}$, the mean-square error in making the ap-

---

[1] Actually, only the non-trivial eigenvalues are identical, since $\mathbb{P}$ and $\mathbb{R}$ need not be of the same dimension. This property of the auxiliary matrices is central to the practical computation of the DKLT.

[2] Strictly speaking, the members of the set $\{|v_b\rangle\}$ are uncorrelated only in the case where the vectors to be decomposed $\{|x_m\rangle\}$ are all zero mean. It is sufficient, but not necessary that this condition be met in order to ensure the information theoretic properties of the DKLT. The statistical orthogonality of the expansion coefficients (A.4) is the necessary and sufficient condition for the uniqueness and optimality of the DKLT.

proximation is defined as

$$E \equiv \mathcal{E}\{\langle \epsilon_m | \epsilon_m \rangle\}$$ (A.17)

The mean-square error may be expanded

$$
\begin{aligned}
E &= \mathcal{E}\left\{\left(\sum_b v_b^*[m]\,\langle a_b|\right)\left(\sum_c v_c[m]\,|a_c\rangle\right)\right\} \\
&= \mathcal{E}\left\{\sum_{b,c} v_b^*[m]v_c[m]\,\langle a_b|a_c\rangle\right\} \\
&= \mathcal{E}\left\{\sum_b |v_b[m]|^2\right\}
\end{aligned}
$$ (A.18)

Substituting the forward DKLT (A.5) into (A.18), the mean-square error becomes

$$
\begin{aligned}
E &= \mathcal{E}\left\{\sum_b |\langle a_b|x_m\rangle|^2\right\} \\
&= \frac{1}{M}\sum_b \langle a_b|\,\mathbb{X}^\dagger \mathbb{X}\,|a_b\rangle \\
&= \frac{1}{M}\sum_b \langle a_b|\,\mathbb{R}\,|a_b\rangle
\end{aligned}
$$ (A.19)

We then minimize the error E subject to the orthonormality constraint on the basis functions (A.3), $1-\langle a_b|a_b\rangle = 0$. Using the method of Lagrange's undetermined multipliers, we form the quantity $\mathcal{L}$

$$\mathcal{L} = \sum_b \langle a_b|\,\mathbb{R}\,|a_b\rangle + \sum_b \varphi_b\left(1 - \langle a_b|a_b\rangle\right)$$ (A.20)

Minimization is accomplished by taking the vector gradient with respect to a basis function and setting the result equal to zero. The notation used here, due to *Therrien* [1992], is elegant, compact and equivalent to the standard methods of constrained minimization of a complex, scalar quantity [e.g., *Morse and Feshbach*, 1953; *Arfken*, 1985]. We take the gradient

$$\nabla_{\langle a_b|}\,\mathcal{L} = \mathbb{R}\,|a_b\rangle - \varphi_b\,|a_b\rangle = 0$$ (A.21)

and arrive at an eigenvalue equation for $\mathbb{R}$

$$\mathbb{R}\,|a_b\rangle = \varphi_b\,|a_b\rangle$$ (A.22)

The Lagrange multipliers are thus determined to be the eigenvalues of $\mathbb{R}$. From (A.15) we know that they are simply the diagonal elements of $\mathbb{C}$, c_b. Substituting (A.22) into (A.19), we rewrite the mean-square error as

$$
\begin{aligned}
E &= \frac{1}{M}\sum_b \langle a_b| \mathbb{R}|a_b\rangle \\
&= \frac{1}{M}\sum_b \langle a_b| c_b |a_b\rangle \\
&= \frac{1}{M}\sum_b c_b
\end{aligned}
\tag{A.23}
$$

The minimization for the $\mathbb{R}$-based DKLT is now complete; however, since we have claimed the $\mathbb{P}$-based approach is equivalent, it must also be shown to be optimal in the mean-square sense.

We can write any of the diagonal elements of the matrix (A.12) as

$$
c_b^2 = \langle v_b| \mathbb{P}|v_b\rangle
\tag{A.24}
$$

which allows us to recast the mean-square error (A.18) as

$$
E = \frac{1}{M}\sum_b \frac{\langle v_b| \mathbb{P}|v_b\rangle}{c_b}
\tag{A.25}
$$

Again, we will minimize this quantity, subject to the orthogonality constraint placed on our coefficient vectors (A.4), $1 - \frac{\langle v_b|v_b\rangle}{c_b} = 0$. Using the method of Lagrange's undetermined multipliers, we form the alternate quantity, $\mathcal{L}'$,

$$
\mathcal{L}' = \sum_b \frac{\langle v_b| \mathbb{P}|v_b\rangle}{c_b} + \sum_b \vartheta_b \left(1 - \frac{\langle v_b|v_b\rangle}{c_b}\right)
\tag{A.26}
$$

Minimizing $\mathcal{L}'$ with respect to a coefficient vector and setting the result equal to zero yields

$$
\nabla_{\langle v_b|} \mathcal{L}' = \frac{\mathbb{P}|v_b\rangle}{c_b} - \vartheta_b \frac{|v_b\rangle}{c_b} = 0
\tag{A.27}
$$

which gives us another eigenvalue equation, this time for $\mathbb{P}$

$$
\mathbb{P}|v_b\rangle = \vartheta_b |v_b\rangle
\tag{A.28}
$$

The alternate Lagrange multipliers are now determined to be the eigenvalues of the matrix $\mathbb{P}$. Recall however, that in our development of the DKLT we noted that the eigenvalues of

$\mathbb{P}$ and $\mathbb{R}$ were identical; thus $\vartheta_b = c_b$. Using this, we demonstrate the equivalence of the optimal representation property of both approaches by substituting (A.28) into (A.25), again giving (A.23).

By invoking the singular value decomposition theorem [*Rao*, 1973], it is easy to show that the eigenvalues of $\mathbb{P}$ and $\mathbb{R}$ are positive, semi-definite; we also note that this is guaranteed by our constraint on the expansion coefficients (A.4). Knowing this property of the eigenvalues, we can perform the minimization procedure by inspection. From (A.23) the mean-square error in making an approximate expansion of a vector $|\tilde{x}_m\rangle$, with only the first K basis functions of M available, is proportional to the sum of the last $(M - K)$ eigenvalues associated with the ignored basis functions. So the optimal truncated representation of $|x_m\rangle$ is made using the basis functions associated with the K largest eigenvalues of either $\mathbb{P}$ or $\mathbb{R}$.

A.3 Computation

Given a set of N-dimensional random vectors $\{|x_m\rangle\}$, the problem of interest is to find the matrices $\mathbb{A}$ and $\mathbb{V}$ such that the terms of the orthonormal decomposition (A.1) are known. In principle, either solution — the eigenvalue problem in $\mathbb{P}$ or $\mathbb{R}$ — is adequate; however, a consideration of the properties of the data, or embedding matrix $\mathbb{X}$ used to construct them provides insight as to how to approach the computation efficiently.

Recall that $\mathbb{X}$ is of dimension $[M, N]$, where $M \neq N$, in general. This determines that the auxiliary matrices, $\mathbb{P}$ and $\mathbb{R}$, will be of dimension $[M, M]$ and $[N, N]$, respectively. The rank of a matrix is defined as the number of its non-zero singular values [*Orfanidis*, 1988]. Letting $K \equiv \lfloor M, N \rfloor$ and $K' \equiv \lceil M, N \rceil$, the rank of $\mathbb{X}$ has the property $r \leq K$. It is a simple matter to show that $\mathbb{P}$ and $\mathbb{R}$ each inherit the rank of $\mathbb{X}$, and by (A.12) and (A.15) they must have the same eigenvalues — these are simply the squared singular values of $\mathbb{X}$. The disparate dimension of $\mathbb{P}$ and $\mathbb{R}$ then guarantees that the additional $(K' - K)$ eigenvalues of the larger of the two are equal to zero. The efficacy of current eigensystem routines, virtually all of which are based on the algorithm of *Golub and Reinsch* [1970], go as $\mathcal{O}(K^3)$ operations for a Hermitian matrix of dimension K [*Press et al.*, 1992]. Since the larger of $\mathbb{P}$ and $\mathbb{R}$ contains no more information than the smaller, it makes great computational sense

Case	Auxiliary matrix	A	V
$M < N$	$\mathbb{P} : [M, M]$	$[M, N]$	$[M, M]$
$M \geq N$	$\mathbb{R} : [N, N]$	$[N, N]$	$[M, N]$

Table A.1. Discrete Karhunen-Loéve transform matrix dimensions. Shown are the dimensions of the DKLT auxiliary matrices and expansion matrices possible for an embedding matrix $\mathbb{X}$ of dimension $[M, N]$.

to solve the lesser eigenvalue problem: in $\mathbb{P}$ for $M < N$, or in $\mathbb{R}$ for $M \geq N$. In the event $M = N$, we prefer to solve the eigenvalue problem in $\mathbb{R}$, as most eigensystem packages produce normalized eigenvectors on output. This eliminates a renormalization step for $\mathbb{V}$.

The rank of a matrix can alternately be expressed as the number of its linearly independent rows or columns [*Therrien*, 1992]. For practical data, where additive noise is ubiquitous, the rows and columns of $\mathbb{X}$ are nearly always linearly independent. Thus, to some precision, $r = K$; however, one must be prepared for numerical exceptions. If $r < K$, $\mathbb{C}$ will have at least one diagonal element equal to zero. In this instance, $\mathbb{C}$ is singular and therefore we cannot solve for the basis functions via (A.13). Additional numerical problems can arise if $\mathbb{X}$ is ill-conditioned, but not strictly singular [e.g. *Broomhead and King*, 1986; *Mees et al.*, 1987]; however, we find these cases easy to handle. If the eigenvalue problems (A.12) and (A.15) prove intractable, one can always turn to singular value methods which attack $\mathbb{X}$ directly [*Mees et al.*, 1987]. We typically find that $\mathbb{X}$ has $r = K$, and so solve the lesser of the two eigenvalue problems, (A.12) or (A.15). Even in the face of numerical anomalies — spurious negative or complex eigenvalues, or exact zeros on the diagonal of $\mathbb{C}$— we find our two-pronged eigensystem approach to be very stable and reliable.

Knowledge of the number of terms available in the expansion (A.1), as a function of the dimensions of $\mathbb{X}$, makes it possible to recognize and avoid most numerical difficulties. According to (A.1), for M vectors comprising $\mathbb{X}$ one should have available M basis functions and coefficient vectors. As can be seen in the summary presented in Table A.1, this is only the case when $M < N$. For $M > N$, we have an overdetermined system, one in which the remaining $(M - N)$ eigenvalues may be thought of as zero. Effectively then, any basis function and coefficient vector associated with a zero eigenvalue may be discarded — therein lies our protocol for handling zeros on the diagonal of $\mathbb{C}$.

Bibliography

Ables, S. T., B. J. Fraser, H. J. Hansen, F. W. Menk, and R. J. Morris, Polarisation character-
istics of long period geomagnetic pulsations recorded at Antarctic stations, in *Australian
atmosphereic and space physics research in Antarctica, 1994–1995*, edited by R. J. Morris,
no. 95 in ANARE Research Notes, p. 112, Australian Antarctic Division, Kingston, 1996.

Akansu, A. N., and R. A. Haddad, *Multiresolution Signal Decomposition*, Academic Press,
Boston, Mass., 1992.

Aparicio, B., B. Thelin, and R. Lundin, The polar cusp from a particle point of view: A
statistical study based on Viking data, *J. Geophys. Res., 96*, 14023, 1991.

Arfken, G., *Mathematical Methods for Physicists*, Academic Press, San Diego, Calif., 3rd edi-
tion, 1985.

Armbruster, D., R. Heiland, and E. J. Kostelich, KLTOOL: A tool to analyze spatiotemporal
complexity, *Chaos, 4*, 421, 1994.

Aubry, N., R. Guyonnet, and R. Lima, Spatiotemporal analysis of complex signals: Theory
and applications, *J. Stat. Phys., 64*, 683, 1991.

Baker, K. B., and S. Wing, A new magnetic coordinate system for conjugate studies at high
latitudes, *J. Geophys. Res., 94*, 9139, 1989.

Baker, K. B., J. R. Dudeney, R. A. Greenwald, M. Pinnock, P. T. Newell, A. S. Rodger, N. Mat-
tin, and C.-I. Meng, HF radar signatures of the cusp and low-latitude boundary layer, *J.
Geophys. Res., 100*, 7671, 1995.

115

Bering, E. A., J. R. Benbrook, G. J. Burns, B. Liao, J. R. Theall, L. J. Lanzerotti, and C. G. Maclennan, Balloon measurements above the South Pole: Study of ionospheric transmission of ULF waves, *J. Geophys. Res.*, *100*, 7807, 1995.

Bol'shakova, O. V., and V. A. Troitskaya, The relation of the high-latitude maximum of Pc 3 intensity to the dayside cusp, *Geomag. Aeron.*, *24*, 633, 1984.

Bracalari, M., and E. Salusti, On a nonlinear autoregressive method applied to geophysical signals, *Geophys.*, *59*, 1270, 1994.

Bracewell, R. M., *The Fourier Transform and Its Applications*, McGraw-Hill Electrical and Electronic Engineering Series, McGraw-Hill, New York, 2nd edition, 1978.

Brigham, E. O., *The Fast Fourier Transform*, Prentice-Hall, Englewood Cliffs, N. J., 1988.

Broomhead, D. S., and G. P. King, Extracting qualitative dynamics from experimental data, *Physica D*, *20*, 217, 1986.

Burg, J. P., *Maximum Entropy Spectral Analysis*, Ph.D. thesis, Stanford Univ., Stanford, Calif., 1975.

Carlson, Jr., H. C., and A. Egeland, The Aurora and the Auroral Ionosphere, in *Introduction to Space Physics*, edited by M. G. Kivelson and C. T. Russell, ch. 14, p. 459, Cambridge, New York, 1995.

Chamberlain, J. W., *Physics of the Aurora and Airglow*, Academic Press, New York, 1961.

Chandrasekhar, S., *Hydrodynamic and hydromagnetic stability*, Oxford Univiersity Press, London, 1961.

Chapman, S., Historical introduction to aurora and magnetic storms, *Ann. Géophys.*, *24*, 497, 1968.

Chapman, S., and V. C. A. Ferraro, A new theory of magnetic storms, *Terr. Magn. Atmosph. Elec.*, *36*, 171, 1931.

Chave, A. D., D. J. Thomson, and M. E. Ander, On the robust estimation of power spectra, coherences, and transfer functions, *J. Geophys. Res.*, *92*, 633, 1987.

Chen, L., and A. Hasegawa, A theory of long-period magnetic pulsation, 1. Steady state excitation of field line resonance, *J. Geophys. Res., 79*, 1024, 1974a.

Chen, L., and A. Hasegawa, A theory of long-period magnetic pulsation, 2. Impulse excitation of surface eigenmode, *J. Geophys. Res., 79*, 1033, 1974b.

Chisham, G., D. Orr, T. K. Yeoman, D. K. Milling, M. Lester, and J. A. Davies, The polarization of Pc 5 ULF waves around dawn: A possible ionospheric conductivity gradient effect, *Ann. Geophys., 13*, 159, 1995.

Claerbout, J. F., *Fundamentals of Geophysical Data Processing*, Blackwell Scientific, Palo Alto, Calif., 1985.

Dungey, J. W., Electrodynamics of the outer atmosphere, Report 69, Ion Res. Lab. Penn. State Univ., University Park, Penn., 1954.

Dungey, J. W., *Cosmic Electrodynamics*, Cambridge University Press, New York, 1958.

Dungey, J. W., Interplanetary magnetic field and the auroral zones, *Phys. Rev. Lett., 6*, 47, 1961.

Dungey, J. W., Hydromagnetic waves and the ionosphere, in *Proc. Int. Conference on the Ionosphere*, p. 230, Inst. Physics, London, 1963.

Eather, R. H., Short-period auroral pulsations in λ6300 O I, *J. Geophys. Res., 74*, 4998, 1969.

Engebretson, M. J., C.-I. Meng, R. L. Arnoldy, and L. J. Cahill Jr., Pc 3 pulsations observed near the south polar cusp, *J. Geophys. Res., 91*, 8909, 1986.

Engebretson, M. J., L. J. Zanetti, T. A. Potemra, W. Baumjohann, H. Lühr, and M. H. Acuna, Simultaneous observation of Pc 3-4 pulsations in the solar wind and in the Earth's magnetosphere, *J. Geophys. Res., 92*, 10053, 1987.

Engebretson, M. J., B. J. Anderson, L. J. Cahill, Jr., R. L. Arnoldy, P. T. Newell, C.-I. Meng, L. J. Zanetti, and T. A. Potemra, A multipoint study of high-latitude daytime ULF pulsations, *J. Geophys. Res., 94*, 17143, 1989.

Engebretson, M. J., B. J. Anderson, L. J. Cahill Jr., R. L. Arnoldy, T. J. Rosenberg, D. L. Carpenter, W. B. Gail, and R. H. Eather, Ionospheric signatures of cusp latitude Pc 3 pulsations, *J. Geophys. Res.*, *95*, 2447, 1990.

Engebretson, M. J., J. R. Beck, R. L. Rairden, S. B. Mende, R. L. Arnoldy, L. J. Cahill Jr., and T. J. Rosenberg, Studies of the occurrence and properties of Pc 3–4 magnetic and auroral pulsations at south pole, antarctica, in *Solar Wind Sources of Magnetospheric Ultra-Low-Frequency Waves, Geophys. Mono. Ser.*, vol. 81, edited by M. J. Engebretson et al., p. 345, AGU, Washington, D. C., 1994.

Engebretson, M. J., W. J. Hughes, J. L. Alford, E. Zesta, L. J. Cahill Jr., R. L. Arnoldy, and G. D. Reeves, Magnetometer array for cusp and cleft studies observations of the spatial extent of broadband ULF magnetic pulsations at cusp/cleft latitudes, *J. Geophys. Res.*, *100*, 19371, 1995.

Field, E. C., and C. Greifinger, Transmission of geomagnetic micropulsations through the ionosphere and lower exosphere, *J. Geophys. Res.*, *70*, 4885, 1965.

Fowler, R. A., B. J. Kotick, and R. D. Elliot, Polarization analysis of natural and artificially induced geomagnetic micropulsations, *J. Geophys. Res.*, *72*, 2871, 1967.

Frank, L. A., Plasmas in the Earth's polar magnetosphere, *J. Geophys. Res.*, *76*, 5202, 1971.

Friis-Christensen, E., M. A. McHenry, C. R. Clauer, and S. Vennerstrom, Ionospheric travelling convection vortices observed near the polar cleft: A triggered response to sudden changes in the solar wind, *Geophys. Res. Lett.*, *15*, 253, 1988.

Fu, K. S., *Sequential Methods in Pattern Recognition and Machine Learning, Mathematics in Science and Engineering*, vol. 52, Academic Press, New York, 1968.

Fukushima, N., Generalized theorem for no ground effect of vertical currents connected with Pedersen currents in the uniform-conductivity ionosphere, *Rep. Ionos. Space Res. Jpn.*, *30*, 35, 1976.

Gasiorowicz, S., *Quantum Physics*, Wiley, New York, 1974.

Gaunaurd, G. C., and H. C. Strifors, Signal analysis by means of time-frequency (Wigner-type) distributions — Applications to sonar and radar echoes, *Proc. IEEE, 84*, 1231, 1996.

Glassmeier, K.-H., Reflection of MHD waves in the Pc 4–5 period range at ionospheres with non-uniform conductivity distributions, *Geophys. Res. Lett., 10*, 678, 1983.

Glassmeier, K.-H., On the influence of ionospheres with non-uniform conductivity distribution on hydromagnetic waves, *J. Geophys., 54*, 125, 1984.

Glassmeier, K.-H., ULF pulsations in the polar cap, in *Electromagnetic Coupling in the Polar Clefts and Caps, NATO ASI Ser.*, vol. 278, edited by P. E. Sandholt and A. Egeland, p. 167, Kluwer, Boston, Mass., 1989.

Glassmeier, K.-H., M. Hönisch, and J. Untiedt, Ground-based and satellite observations of traveling magnetospheric convection twin-vortices, *J. Geophys. Res., 94*, 2520, 1989.

Golub, G. H., and C. Reinsch, Singular value decomposition and least squares solutions, *Numerical Mathematics, 14*, 403, 1970.

Greenstadt, E. W., and J. V. Olson, A contribution to ULF activity in the Pc 3–4 range correlated with IMF radial orientation, *J. Geophys. Res., 82*, 4991, 1977.

Greenstadt, E. W., H. J. Singer, C. T. Russell, and J. V. Olson, IMF orientation, solar wind velocity, and Pc 3-4 signals: A joint distribution, *J. Geophys. Res., 84*, 527, 1979.

Greifinger, C., and P. Greifinger, Wave guide propagation of micropulsations out of the plane of the geomagnetic meridian, *J. Geophys. Res., 78*, 4611, 1973.

Heikkila, W. J., The reconnection myth, *Eos Trans. AGU, 78*, 153, 1997.

Heikkila, W. J., and J. D. Winningham, Penetration of magnetosheath plasma to low altitudes through the dayside magnetospheric cusps, *J. Geophys. Res., 76*, 883, 1971.

Huang, N. E., S. R. Long, C.-C. Tung, M. A. Donelan, Y. Yuan, and R. J. Lai, The local properties of ocean surface waves by the phase-time method, *Geophys. Res. Lett., 19*, 685, 1992.

Hughes, W. J., The effect of the atmosphere and ionosphere on long period magnetospheric micropulsations, *Planet. Space Sci.*, *22*, 1157, 1974.

Hughes, W. J., Magnetospheric ULF waves: A tutorial with a historical perspective, in *Solar Wind Sources of Magnetospheric Ultra-Low-Frequency Waves, Geophys. Mono. Ser.*, vol. 81, edited by M. J. Engebretson et al., p. 1, AGU, Washington, D. C., 1994.

Hughes, W. J., and D. J. Southwood, The screening of micropulsation signals by the atmosphere and ionosphere, *J. Geophys. Res.*, *81*, 3234, 1976.

Inoue, Y., Wave polarizations of geomagnetic pulsations observed in high lattitudes on the Earth's surface, *J. Geophys. Res.*, *78*, 2959, 1973.

Jackson, L. B., *Digital Filters and Signal Processing*, Kluwer, Boston, Mass., 3nd edition, 1996.

Jacobs, J. A., *Geomagnetic Micropulsations, Physics and Chemistry in Space*, vol. 1, Springer-Verlag, New York, 1970.

Jacobs, J. A., Y. Kato, S. Matsushita, and V. A. Troitskaya, Classification of geomagnetic pulsations, *J. Geophys. Res.*, *69*, 180, 1964.

Jenkins, G. M., and D. G. Watts, *Spectral Analysis and Its Applications*, Holden-Day, San Francisco, Calif., 1968.

Johnson, J. R., and C. Z. Cheng, Kinetic Alfvén waves and plasma transport at the magnetopause, *J. Geophys. Res.*, *24*, 1423, 1997.

Karhunen, K., Über linearen methoden in der wahrscheinlichkeitsrechnung, *Ann. Acad. Sci. Fennicae, Ser. A*, *37*, 85, 1947, [English translation by I. Selin, Rand Corp., Santa Monica, Calif., Rpt. No. T-131, 1960].

Kato, Y., Y. Tonegawa, and K. Tomomura, Dynamic spectral study of Pc 3–5 magnetic pulsations observed in the north polar cusp region, *Mem. Natl. Inst. Polar Res. Jpn.*, *36*, 58, 1985.

Kivelson, M. G., J. Etcheto, and J. G. Trotignon, Global compressional oscilations of the terrestrial magnetosphere: The evidence and a model, *J. Geophys. Res.*, *89*, 9851, 1984.

Knecht, D. J., and B. M. Shuman, The Geomagnetic Field, in *Handbook of Geophysics and the Space Environment*, edited by A. S. Jursa, ch. 4, p. 4:1, Air Force Geophysics Laboratory, Hanscomb AFB, Mass., 1985.

Krause, T. P., L. Shure, and J. N. Little, *MATLAB Signal Processing Toolbox User's Guide*, The Math Works, Natick, Mass., 1994.

Lacoss, R. T., Data adaptive spectral analysis methods, *Geophys.*, *36*, 661, 1971.

Le, G., and C. T. Russell, Solar wind control of upstream wave frequency, *J. Geophys. Res.*, *101*, 2571, 1996.

Lee, L. C., R. K. Albano, and J. R. Kan, Kelvin-Helmholtz instability in the magnetopause-boundary layer region, *J. Geophys. Res.*, *86*, 54, 1981.

Leonovich, A. S., and V. A. Mazur, Penetration to the Earth's surface of standing Alfvén waves excited by external currents in the ionosphere, *Ann. Geophys.*, *14*, 545, 1996.

Lockwood, M. S., W. H. Cowley, and M. F. Smith, Comment on "B_y fluctuations in the magnetosheath and azimuthal flow velocity transients in the dayside ionosphere" by Newell and Sibeck, *Geophys. Res. Lett.*, *21*, 1819, 1994.

Lundin, R., Acceleration/heating of plasma on auroral field lines: Preliminary results from the Viking satellite, *Ann. Geophys.*, *6*, 143, 1988.

Lyons, L. R., O. de la Beaujardière, and F. J. Rich, Synoptic maps of polar caps for stable interplanetary magnetic field intervals during January 1992 geospace environment modeling campaign, *J. Geophys. Res.*, *101*, 27283, 1996.

Maggs, J. E., and G. J. Morales, Magnetic fluctuations associated with field-aligned striations, *Geophys. Res. Lett.*, *23*, 633, 1996.

Maggs, J. E., and G. J. Morales, Fluctuations associated with a filimentary density depletion, *Phys. Plasmas*, *4*, 290, 1997.

Matthews, D. L., T. J. Rosenberg, J. R. Benbrook, and E. A. Bering III, Dayside energetic electron precipitation over the South Pole ($\lambda = 75°$), *J. Geophys. Res.*, *93*, 12941, 1988.

McHarg, M. G., *The Morphology and Electrodynamics of the Boreal Polar Winter Cusp*, Ph.D. thesis, Univ. of Alaska, Fairbanks, 1993.

McHarg, M. G., and J. V. Olson, Correlated optical and ULF magnetic observations of the winter cusp – boundary layer system, *Geophys. Res. Lett., 19*, 817, 1992.

McHarg, M. G., J. V. Olson, and P. T. Newell, ULF cusp pulsations: Diurnal variations and interplanetary magnetic field correlations with ground-based observations, *J. Geophys. Res., 100*, 19729, 1995.

McIlwain, C. E., Coordinates for mapping the distribution of magnetically trapped particles, *J. Geophys. Res., 66*, 3681, 1961.

McPherron, R. L., Magnetospheric Dynamics, in *Introduction to Space Physics*, edited by M. G. Kivelson and C. T. Russell, ch. 13, p. 400, Cambridge, New York, 1995.

Mees, A. I., P. E. Rapp, and L. S. Jennings, Singular-value decomposition and embedding dimension, *Phys. Rev. A, 36*, 340, 1987.

Meng, C.-I., and M. Candidi, Poiar cusp features observed by DMSP satellites, in *The Polar Cusp, NATO ASI Ser.*, vol. 145, edited by J. A. Holtet and A. Egeland, p. 177, D. Reidel Publishing, Boston, Mass., 1985.

Menk, F. W., and K. Yumoto, Conjgate and neridional phase structure of low latitude ULF pulsations, *Adv. Space Res., 5*, 42⁵. 1994.

Mitchell, C. N., D. G. Jones, L. Kersley, S. Eleri Pryse, and I. K. Walker, Imaging of field-aligned structures in the auroral ionosphere, *Ann. Geophys., 13*, 1311, 1995.

Moler, C. B., *MATLAB Reference Guide*, The Math Works, Natick, Mass., 1992.

Morse, P. M., and H. Feshbach, *Methods of Theoretical Physics*, McGraw-Hill, New York, 1953.

Najmi, A.-H., The Wigner distribution: A time-frequency analysis tool, *J. Hopkins APL Tech. Dig., 15*, 298, 1994.

Narod, B., *Narod Geophysics Ltd. Magnetometer (S-100 Version) Specifications*, Narod Geophysics Ltd., Vancouver, B. C., 1990.

Newell, P. T., and C.-I. Meng, The cusp and the cleft/boundary layer: Low-altitude identification and statistical local time variation, *J. Geophys. Res., 93*, 14549, 1988.

Newell, P. T., and C.-I. Meng, Mapping the dayside ionosphere to the magnetosphere according to particle precipitation characteristics, *Geophys. Res. Lett., 19*, 609, 1992.

Nishida, A., Ionospheric screening effect and sudden commencement, *J. Geophys. Res., 69*, 1861, 1964.

Odera, T. J., Solar wind controlled pulsations: A review, *Rev. Geophys., 24*, 55, 1986.

Olson, J. V., ULF signatures of the polar cusp, *J. Geophys. Res., 91*, 1055, 1986.

Olson, J. V., Poleward propagation of pulsations near the cusp, *Planet. Space Sci., 37*, 775, 1989.

Olson, J. V., and B. J. Fraser, Pc 3 pulsations in the cusp, in *Solar Wind Sources of Magnetospheric Ultra-Low-Frequency Waves, Geophys. Mono. Ser.*, vol. 81, edited by M. J. Engebretson et al., p. 325, AGU, Washington, D. C., 1994.

Olson, J. V., and G. Rostoker, Longitudinal phase variations of Pc 4–5 micropulsations, *J. Geophys. Res., 83*, 2481, 1978.

Olson, J. V., and J. C. Samson, On the detection of the polarization states of Pc micropulsations, *Geophys. Res. Lett., 6*, 413, 1979.

Olson, J. V., and C. A. L. Szuberla, A study of Pc 3 coherence at cusp latitudes, *J. Geophys. Res., 102*, 11375, 1997.

Orfanidis, S. J., *Optimum Sgnal Processing: An Introduction*, Macmillan, New York, 2nd edition, 1988.

Orr, D., and J. A. D. Matthew, The variation of geomagnetic micropulsation periods with lattitude and the plasmapause, *Planet. Space Sci., 19*, 897, 1971.

Pike, E. R., J. G. McWhirter, M. Bertero, and C. de Mol, Generalised information theory for inverse problems in signal processing, *IEE Proc.*, *131F*, 660, 1984.

Pinnock, M., A. S. Rodger, J. R. Dudeney, F. Rich, and K. B. Baker, High spatial and temporal resolution observations of the ionospheric cusp, *Ann. Geophys.*, *13*, 919, 1995.

Preisendorfer, R. W., *Principal Component Analysis in Meteorology and Oceanography, Developments in Atmospheric Science*, vol. 17, Elsevier, New York, 1988.

Press, W. A., S. A. Teukolsky, W. T. Vetterling, and B. P. Flannery, *Numerical Recipes in C*, Cambridge University Press, New York, 2nd edition, 1992.

Prichard, D., J. E. Borovsky, P. M. Lemons, and C. P. Price, Time dependence of substorm recurrence: An information-theoretic analysis, *J. Geophys. Res.*, *101*, 15359, 1996.

Primdahl, F., The fluxgate magnetometer, *J. Phys. E: Sci. Instrum.*, *12*, 241, 1979.

Rao, C. R., *Linear Statistical Inference and Its Applications*, Wiley Series in Probability and Mathematical Statistics, Wiley, New York, 2nd edition, 1973.

Rosenblatt, M., Remarks on some non-parametric estimates of a density function, *Ann. Math. Stat.*, *27*, 832, 1956.

Russell, C. T., and R. C. Elphic, Initial ISEE magnetometer results: Magnetopause observations, *Space. Sci. Rev.*, *22*, 681, 1978.

Sakurai, T., Y. Tonegawa, Y. Kato, K. Makita, M. Ejiri, H. Yamagashi, and N. Sato, ULF waves and magnetic field characteristics in the polar cusp observed at godhaven, *Proc. NIPR Symp. Upper Atmos. Phys.*, *6*, 103, 1993.

Samson, J. C., Pure states, polarized waves, and principal components in the spectra of multiple, geophysical time series, *Geophys. J. R. Astr. Soc.*, *72*, 647, 1983a.

Samson, J. C., The spectral matrix, eigenvalues, and principal components in the analysis of multichannel geophysical data, *Ann. Geophys.*, *1*, 115, 1983b.

Samson, J. C., and J. V. Olson, Some comments on the descriptions of the polarization states of waves, *Geophys. J. R. Astr. Soc.*, *61*, 115, 1980.

Samson, J. C., and J. V. Olson, Data-adaptive polarization filters for multichannel geophysical data, *Geophys.*, *46*, 1423, 1981.

Samson, J. C., J. A. Jacobs, and G. Rostoker, Latitude dependent characteristics of long-period geomagnetic micropulsations, *J. Geophys. Res.*, *76*, 3675, 1971.

Samson, J. C., T. J. Hughes, F. Creutzberg, D. D. Wallis, R. A. Greenwald, and J. M. Ruohoniemi, Observations of a detached, discrete arc in association with field line resonances, *J. Geophys. Res.*, *96*, 15683, 1991.

Sandholt, P. E., J. Moen, and D. Opsvik, Periodic auroral events at the midday polar cap boundary: Implications for solar wind-magnetosphere coupling, *Geophys. Res. Lett.*, *19*, 1223, 1992.

Schwartz, S. J., D. Burgess, and J. J. Moses, Low-frequency waves in the Earth's magnetosheath: Present status, *Ann. Geophys.*, *14*, 1134, 1996.

Sibeck, D. G., A model for the transient magnetospheric response to sudden solar wind dynamic pressure variations, *J. Geophys. Res.*, *95*, 3755, 1990.

Sibeck, D. G., Transient events in the outer magnetosphere: Boundary waves of flux transfer events, *J. Geophys. Res.*, *97*, 4009, 1992.

Sibeck, D. G., Transient and quasi-periodic (5–15 min) events in the outer magnetosphere, in *Solar Wind Sources of Magnetospheric Ultra-Low-Frequency Waves, Geophys. Mono. Ser.*, vol. 81, edited by M. J. Engebretson et al., p. 173, AGU, Washington, D. C., 1994.

Silverman, B. W., Choosing the window width when estimating a density function, *Biometrika*, *65*, 1, 1978.

Singer, H. J., D. J. Southwood, R. J. Walker, and M. G. Kivelson, Alfvén wave resonances in a realistic magnetosphere magnetic field geometry, *J. Geophys. Res.*, *86*, 4589, 1981.

Smith, M. F., and M. Lockwood, The pulsating cusp, *Geophys. Res. Lett.*, *17*, 1069, 1990.

Smith, M. F., and M. Lockwood, Earth's magnetospheric cusps, *Rev. Geophys.*, *34*, 233, 1996.

Southwood, D. J., The hydrodynamic stability of the magnetospheric boundary, *Planet. Space Sci.*, *16*, 587, 1968.

Southwood, D. J., Some features of field line resonances in the magnetosphere, *Planet. Space Sci.*, *22*, 483, 1974.

Stellmacher, M., K.-H. Glassmeier, R. L. Lysak, and M. G. Kivelson, Field line resonances in discretized magnetospheric models: an artifact study, *Ann. Geophys.*, *15*, 614, 1997.

Stewart, B., On the great magnetic disturbance which extended from August 2 to September 7, 1859 as recorded by photography at the Kew Observatory, *Phil. Trans. Roy. Soc. Lond.*, *11*, 407, 1861.

Stockwell, R. G., L. Mansinha, and R. P. Lowe, Localisation of the complex spectrum: The S transform, *J. Assoc. Expl. Geophys.*, *17*, 99, 1996.

Storey, L. R. O., An investigation of whistling atmospherics, *Phil. Trans. Roy. Soc.*, *246*, 113, 1953.

Streltsov, A., and W. Lotko, Influence of the finite ionospheric conductivity on dispersive, nonradiative field line resonances, *Ann. Geophys.*, *15*, 625, 1997.

Symons, L. P., Analogue data aquisition system for ANARE stations, in *Australian atmosphereic and space physics research in Antarctica, 1994–1995, ANARE Research Notes*, vol. 95, edited by R. J. Morris, p. 168, Australian Antarctic Division, Kingston, 1996.

Szuberla, C. A. L., M. G. McHarg, W. F. Denig, and J. V. Olson, Characteristic magnetic signatures of the cusp region, *Suppl. Eos Trans. AGU*, *75*(44), 555, 1994.

Takahashi, K., and R. L. McPherron, Harmonic structure of Pc 3-4 pulsations, *J. Geophys. Res.*, *87*, 1504, 1982.

Taylor, J. R., *An Introduction to Error Analysis*, University Science Books, Mil Valley, Calif., 1982.

Theiler, J., S. Eubank, A. Longtin, B. Galdrikian, and J. D. Farmer, Testing for nonlinearity in time series: The method of surrogate data, *Physica D*, *58*, 77, 1992a.

Theiler, J., B. Galdrikian, A. Longtin, S. Eubank, and J. D. Farmer, Using surrogate data to detect nonlinearity in time series, in *Nonlinear Modeling and Forecasting, SFI Studies Sci. Complexity*, vol. XII, edited by M. Casdagli and S. Eubank, p. 163, Addison-Wesley, Menlo Park, Calif., 1992b.

Therrien, C. W., *Discrete Random Signals and Statistical Signal Processing*, Prentice Hall, Englewood Cliffs, N. J., 1992.

Tonegawa, Y., H. Fukunishi, L. J. Lanzerotti, C. G. Maclennan, L. V. Medford, and D. L. Carpenter, Studies of the energy source for hydromagnetic waves at auroral latitudes, *Mem. Natl. Inst. Polar Res. Jpn.*, *38*, 73, 1985.

Troitskaya, V. A., ULF wave investigations in the dayside cusp, *Adv. Space Res.*, *5*(4), 219, 1985.

Troitskaya, V. A., and O. V. Bol'shakova, Diurnal latitude variation of the location of the dayside cusp, *Planet. Space Sci.*, *25*, 1167, 1977.

Troitskaya, V. A., T. A. Plyasova-Bakunina, and A. V. Gul'elmi, Relationship between Pc2-4 pulsations and the interplanetary field, *Dokl. Aka. Nauk. SSSR*, *197*, 1313, 1971.

Vallance Jones, A., *Aurora*, D. Reidel Publishing, Boston, Mass., 1974.

Walker, A. D. M., J. M. Ruohoniemi, K. B. Baker, R. A. Greenwald, and J. C. Samson, Spatial and temporal behavior of ULF pulsations observed by the Goose Bay HF radar, *J. Geophys. Res.*, *97*, 12187, 1992.

Waters, C. L., J. C. Samson, and E. F. Donovan, The temporal variation of the frequency of high latitude field line resonances, *J. Geophys. Res.*, *100*, 7987, 1995.

Welch, P. D., The use of the fast Fourier transform for the estimation of power spectra: A method based on averaging over short, modified periodograms, *IEEE Trans. Audio Electroacoust.*, *AU-15*, 70, 1970.

Wolfe, A., R. D. Kelman, S. E. Warren, C. G. Maclennan, and L. J. Lanzerotti, Hydromagnetic frequency spectra in the high latitude quiet magnetosphere, in *Solar Wind Sources*

of Magnetospheric Ultra-Low-Frequency Waves, Geophys. Mono. Ser., vol. 81, edited by M. J. Engebretson et al., p. 375, AGU, Washington, D. C., 1994a.

Wolfe, A., L. J. Lanzerotti, C. G. Maclennan, and R. L. Arnoldy, Simultaneous enhancement of Pc 1, Pc 4, and Pc 5 hydromagnetic waves at AGO-P2, Antarctica, *Suppl. Eos Trans. AGU, 75*(44), 550, 1994b.

Yagodkina, O. I., and V. G. Vorobjev, Daytime high-latitude pulsations associated with solar wind dynamic pressure impulses and flux transfer events, *J. Geophys. Res., 102, 57*, 1997.

Yamauchi, M., The first EGS Alfvén Conference, *Eos Trans. AGU, 78*, 125, 1997.

Yumoto, K., Generation and propagation mechanisms of low-latitude magnetic pulsations – A review, *J. Geophys., 60*, 79, 1986.

Zhou, X.-W., and C. T. Russell, The location of the high-latitude polar cusp and the shape of the surrounding magnetopause, *J. Geophys. Res., 102*, 105, 1997.

Zhou, X.-W., C. T. Russell, G. Le, and N. Tsyganenko, Comparison of observations and model fields at high-altitudes above the polar caps: POLAR initial results, *Geophys. Res. Lett., 24*, 1451, 1997.

Ziesolleck, C. W. S., Q. Feng, and D. R. McDiarmid, Pc 5 ULF waves observed simultaneously by GOES 7 and the CANOPUS magnetometer array, *J. Geophys. Res., 101*, 5021, 1996.